University of Stavanger

Faculty of Science and Technology

MASTER'S THESIS

Study program/ Specialization: Master in constructions and materials / Offshore Construction	Spring semester, 2011 Open
Writer: Ole Vegar Moldesæther	…… (Writer's signature)
Faculty supervisor: Vikas Arora External supervisor(s): Harald Ramfjord (Beerenberg Corp. AS)	
Title of thesis: Utilization of synthetic diamonds for cutting purposes in explosive atmospheres	
Credits (ECTS):	
Key words: Thermal modeling, Hot Surfaces, Ignition of explosive atmospheres, Wire Cutting	Pages: 91 + enclosure: 29 Stavanger, 08.07.11 Date/year

Abstract

Modifications in the process industry are quite common. For many of these modifications cutting of existing equipment and structure will be a central activity. The abrasive diamond wire cutting technology is adopted from the stone cutting industry, and has proven to cut cross-sections of steel quite efficient. However, as for any machining process, there will be heat generated from friction and a spark emission.

Since most of the process plants are regarded as a hazardous zone, in terms of potentially explosive atmospheres, there will always be a risk increase when performing work which produces potential ignition sources. The ATEX Directive was founded for allowing free trade of explosion proof equipment within the European Union. Thus the requirements found within the ATEX Directive are established to reduce the risk of ignition for the relevant equipment which fulfills the requirements stated therein.

In this thesis the theory of diamond wire is established by adopting central elements from conventional abrasive technology. This theory is then used as a basis for a thermal model, usable for numerical simulations. The model is partially validated against measured temperatures. However, when adding coolants the model would over-estimate the temperatures.

The results obtained showed that diamond wire cutting most likely would be safe, in terms of hot surfaces, if adequate cooling is applied. When regarding sparks no conclusions could be obtained of either ignition potential or temperature.

Contents

List of figures and tables

Preface

The master thesis marks the final part of my master degree. When conducting the work under this thesis some problems were encountered. When encountered with the fact that grinding forces were determined experimentally for each individual set up it was discovered that the original method (as seen in appendix E) could not be conducted as planned. Thus, it was suggested to perform experiments with the relevant equipment. However, due to lack of time and availability this was also discarded. Instead the theory of specific grinding energy related to the melting energy of the work piece, as proposed by Malkin and Guo, was adopted. This is the reason for the inconsistency between the enclosed synopsis report and the Scope of Work section found within this thesis.

I would like to use this opportunity to thank Baste Tveito and Harald Ramfjord for allowing me to perform this study.

I would also use this opportunity to thank my guidance supervisor, Vilas Arora, for his support, and special thanks go to Geir Pedersen at GexCon and Geir Harris at Beerenberg for their invaluable technical support.

Problem definition

When performing modifications, such as cutting, on process equipment or structural members in a hazardous zone it is usual to take extraordinary measures to reduce the potential for an accident. An accident is here referred to as a situation of fire or explosion caused by ignition of hydrocarbons by sparks from the modification activities.

For a hydrocarbon processing plant, offshore or onshore, the possibility of presence of hydrocarbons in the atmosphere will be possible as long as the plant is in operation. Therefore a process plant will be characterized as a hazardous zone when it's operating. This is due to the high possibility for leaks in valves, flanges and other connections.

As a result of a process plant being a hazardous zone there is a strict control of all sources of ignition. This means that all activities that will generate a source of ignition will be assessed individually to ensure that correct measures are being implemented to compensate for the addition of ignition source.

These extraordinary measures are usually rather expensive. Reducing the risk of a potential accident can be obtained by either remove the presence of hydrocarbons or remove the source of ignition.

Cutting activities are conventionally characterized as "Hot Work", which means it generates a source of ignition. The main objective of this thesis is to document that cutting by DW will not produce high energy sparks, and hence document that cutting by DW can be characterized as "Cold Work" e.g. does not produce ignitions sources in an explosive atmosphere.

Scope of work

In this thesis the following objectives will be performed:

- Study of abrasive processes
- Thermal modeling of diamond wire process
- Study of explosive atmospheres
- Study of ATEX Directive and harmonized standards
- Comparison of results from thermal model with requirements in relevant standards

1 Introduction to material removal processing

1.1 Available technologies for heavy duty cutting purposes on site

Heavy duty cutting operations are quite common in the oil and gas industry. Usually when a modification is to be performed, removal of existing equipment is the first step of the actual work. Also, the decommissioning phase of an oilfield is becoming more and more relevant as the installations reach their end of production. Through this chapter a brief introduction to some of the available technologies will be given. These technologies include; wire sawing, abrasive water jet and hydraulic scissors.

1.1.1 Abrasive water jet

Abrasive water jet is a method that combines ultra high pressures and abrasive grains. It is very much similar to the process of sandblasting which is used for surface treatment. The shearing medium is the abrasive grains and the transporting medium is the pressurized water.

Figure 1.1 shows a principal sketch of the water jet method. It's seen that the abrasives are added through an ejector where the abrasives are mixed with the high pressure and high velocity water stream. The water stream will accelerate the abrasives and the abrasives will erode the work piece and hence remove the material.

Figure 1.01 Abrasive water jet [F1]

This method has its advantages in its ability to cut a large variety of material in an effective matter while not producing any heat affected areas. The aspect of pollution combined with abrasive water jet cutting is more or less negligible in terms of environmental damage since there are no chemicals involved in the operation. However, an abrasive water jet cutting operation will cause a severe mess around the cutting area since the material removed along with the abrasive stream will squirt in several directions. Any excess abrasive stream will also be a potential hazard to any obstacles it meets, hence cover up of adjacent equipment might be challenging since the possibility of the abrasive stream destroying the temporal shields is high. At this point it should also be noted that this operation, on the mentioned basis, is a serious hazard threat for human injury.

The set up of an abrasive water jet is a detailed operation were a lot of elements needs to be addressed. Abrasive water jet is a remotely operated tool which versatility is due to that the whole tool is consistent of a lot of individual parts, this allows the tool to be customized for extremely large varieties of geometries. The mobilization of the tool will then include building a guiding trajectory for

the water jet to move along. This guiding trajectory may be complicated to build and therefore quite time consuming.

For a successful execution of a cut by abrasive water jet then needs extensive planning and adaption of the environment to the hazards involved. When compared to abrasive wire cut the abrasive water jet will require a more extensive preparation process due to the elements mentioned above. Effective cut time is somewhat identical, but preparation time is more extensive for abrasive water jet. Nevertheless, the abrasive water jet method has a wider acceptance in the oil and gas industry. It is assumed that this is due to the low heat generation in the cut surface and that spark emission is more or less negligible.

The spark emission from abrasive water jets will be addressed in chapter 4.

1.1.2 Hydraulic scissors

Hydraulic scissors are utilized in extremely heavy duty decommissioning operations. This method involves extreme plastic deformation of the work piece and hence is not applicable for operations where precision, to some extent, is preferable. Demolition of large buildings is often executed by either dynamite or hydraulic scissors or a combination of these two methods.

Utilization of hydraulic scissors requires vast energy, due to the extreme plastic deformation, and hence it is not regarded as a rival technology to the other two technologies presented in this chapter.

1.1.3 Abrasive wire cutting

Wire cutting is a rather new technology for offshore applications topside. For operations where heavy duty cutting is involved abrasive water jet has been the chosen technology. However, wire cutting has been utilized in the mining industry since the late 1940's where it replaced the gang saw [I1]. The reason for the wire saw to gain market was its ability to process a large variety of geometries without extensive modification to the equipment along with higher removal rate, higher precision and less noise. However, the wire proved to have a rather short life expectancy and often the wire would break during a cut. To reduce the effects of this problem an extremely long wire was used to distribute the wear over a larger wire area and thus reducing the risk of wire failure during a cut. After some time abrasive wire cutting was replace by rotating grinding wheels. The reason for this exchange was the invention of grinding wheels with replaceable cutting bits, thus decreasing operational costs since it was no longer necessary to replace the same amount of equipment. For the mining industry the full versatility of the wire saw was never needed as the cutting equipment often was stationary equipment.

For offshore applications wire cutting has an advantage in being easy to mobilize as well as being usable for cutting in almost any material. A detailed description of the abrasive wire cutting operation will be given in the following chapters.

1.2 Basics of material removal

The whole process of manufacturing includes a variety of processes. The dictionary defines manufacturing as processing raw material into a finished product, especially for large-scale industrial operations. For a tidier explanation manufacturing can be divided into two main categories, processing operations and assembly operations. Processing operations include all the processes needed to shape a starting material into a usable part. Assembly operations include all the operations needed to build a finished product.

The processing operations can also be divided into under-groups. These could consist of shaping operations, property enhancement and surface treatment. Shaping processes consist of all operations performed for shaping the work piece. This includes casting, extrusion, rolling and material removal processes among others.

Material removal processes represent the group of processes where the aim is to remove excess material to gain the desirable shape. This category includes a wide range of different operations, all dependent on work piece shape and size, and the desirable grade of roughness in the output part.

The scope of this thesis is concerned with cutting operations, especially wire cutting for modification and decommissioning purposes. The majority of the available theory for cutting operations is mainly concerned with the manufacturing processes found in workshops. However, there is little difference in the physics of a cutting process whether it's executed in a workshop for manufacturing purposes or at an offshore installation performed for modification purposes. Hence it’s found reasonable to adapt some parts of manufacturing theory to the scope of this thesis.

1.2.1 Definition of cut

Cutting operation is a under group of material removal processes. The basic of material removal processes is removal of any excessive material to leave the desired geometry. The different material removal processes include the following:

- Conventional processes
  This group includes process like turning, drilling and milling
- Abrasive processes
  This group includes processes like grinding and sawing with abrasive wire
- Non-traditional processes
  Modern techniques like chemical and thermal machining is part of the non-traditional processes

The main focus of this thesis is the abrasive processes, so the remaining processes will only be treated superficial. However, the fundamentals of a cutting operation, in terms of course of events, will be somewhat identical for the mechanical processes and the abrasive processes.

A cut is a process where a sharp tool removes material from the work piece by forming chips. Figure 1.2 [F2] shows a generalized cutting operation performed by abrasive grains (grinding)

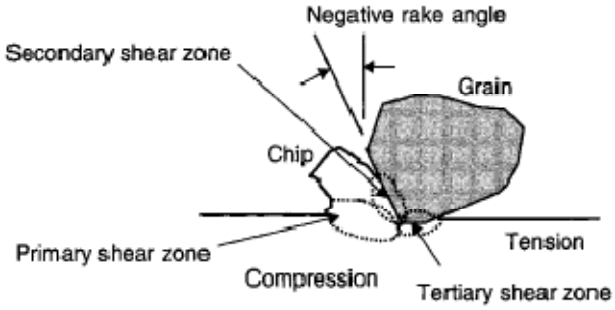

Figure 1.02 Grinding grain [F2]

In a cutting process there are a number of parameters which can be investigated and a few presumptions to obtain a cut. These features will be present regardless of which technique that is being analyzed.

Presumptions to obtain a cut are:

- There is a tool present that interacts with the work piece. This can be related to a displacement which is called “in-feed”. For conventional machining processes this displacement is discrete, i.e. the same in-feed is applied to the whole work piece before it is reset and applied to the whole work piece again. In grinding the in-feed can be treated as continuously, this mainly applies to work processes where the aim is to cut in the cross sectional direction or producing conical surfaces.
- The tool/work piece interaction is controlled by at least two independent movements. In grinding and milling the tool will rotate around its own axis. The second movement is a lateral movement between the tool and the work piece. Hence, this can be obtained by movement of either the work piece or the tool, or in some cases both. This latter movement is commonly known as the feed. In more precise literature it is referred to as the cross feed.

Most metallic materials are considered as relatively hard materials. Carbon steel has a Brinell hardness in the range of 150 to 300 while aluminum, which is considered to be rather soft, will have a hardness ranging from 50 to 100 approximately. The result of this fact is that shearing will only occur in a concentrated zone where the tool interacts with the work piece. This region is usually referred to as the tool/chip-interface.

Features of a cutting process are:

- High speeds/feeds
- Elevated temperatures in work piece and tool together with the chips
- Extreme pressures

1.2.2 Mechanics of cutting processes

The two processes of conventional and abrasive machining can easily be compared in terms of mechanics. To explain the mechanics in this process it’s more convenient to assess an idealized model than an actual model. Cutting processes are 3-dimensional, but some processes can be treated as 2-dimensional. Turning and grinding are examples of the latter.

In figure 1.3 [F.3] the basics of a cutting process, in terms of mechanics, are described. It’s shown as the tool moves along the work piece there will be a plastic deformation ahead of the tool. This deformation occurs mainly in the plane which is noted “Shear Zone/plane”, there will be other deformations as well, but these will be addressed later. The presentation principle of this figure is

called “deck of cards”, this is because it shows the chip divided into segments. An actual cutting process of a ductile material will produce more or less continuous chips, and also the shear plane will be moving continuously not discrete as shown in the figure.

The term shear plane is misguiding to some extent. If a shear plane, with no thickness, should appear in a cutting process it would mean that the deformation would occur instantaneously over the plane. This is highly unlikely and therefore it’s more convenient to refer to shear zones where the deformations will evolve over time, the time span however is very narrow. For mathematical purposes experiments has shown that the uncertainty increase by treating the shear zone as a shear plane is negligible [3].

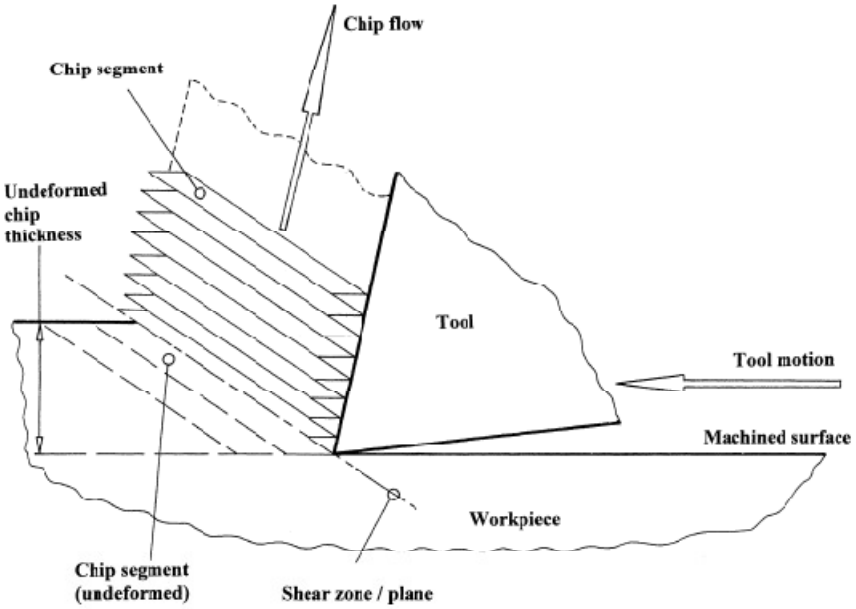

Figure 1.03 Sketch of conventional cutting by turning [F3]

As figure 1.3 suggest one single shear plane there is not described any deformations except for the deformation in this plane. This needs to be modified since the chip will be deformed by the rake face of the tool and the work piece will undergo some deformations at the machined surface. These deformations will be related to the secondary and tertiary shear zones.

A generalized description of metal cutting is then consisting of deformations in three zones, primary, secondary and tertiary. Figure 1.4 [F4] shows the orientation of these zones in a turning operation.

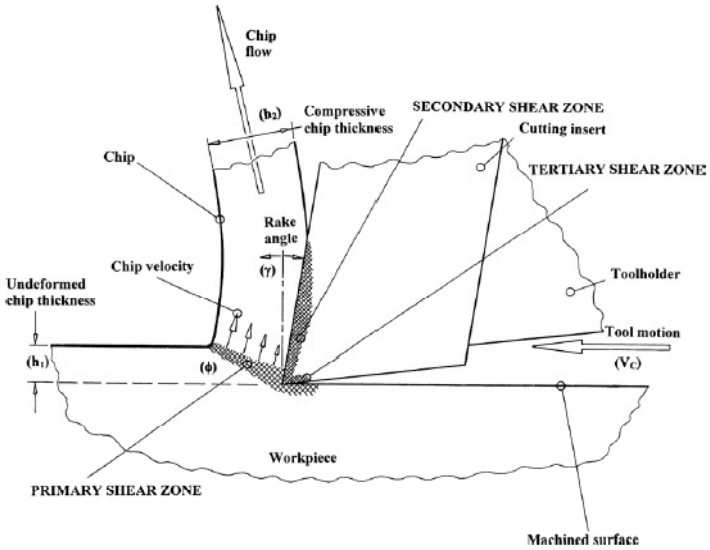

Figure 1.04 Orientation of shear zones [F4]

1.2.3 Cutting in abrasive processes

For abrasive processes the principles are mainly the same, but since both the rake and relief angle differ quite a lot the stress distribution and energy consumption will have different characteristic values than conventional machining. The tool in an abrasive process will be an abrasive grain. For traditionally grinding processes, it's common to use a rotating grinding wheel which is mainly built out of abrasive grains and bonding material. As the grinding wheel is rotating the work piece passes at the periphery of the wheel as shown in figure 1.5. This will create both tangential and normal forces. A cut with an abrasive process is obtained by three stages; rubbing, plowing and cutting (chip formation) as seen in figure 1.6.

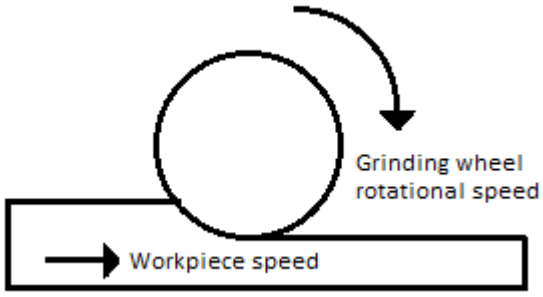

Figure 1.05 Description of grinding.

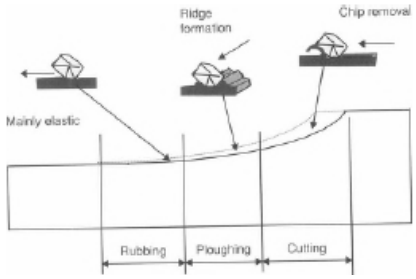

Figure 1.06 Stages of grinding [F5]

The total energy consumed during grinding or cutting with abrasives will be a combination of the energy contribution from all of these stages:

$$u = u_{rubbing} + u_{plowing} + u_{chip\ formation} \tag{1-1}$$

Rubbing stage

As the grain, as shown in figure 1.6, initiates contact with the work piece the rubbing stage will initiate. At the rubbing stage (also called sliding stage) the grain will not penetrate the material nor will it cause any plastic deformation of the work piece, thus the deformation will be elastic. Hence, at this stage the work piece will undergo a temperature rise due to the friction between the work piece and the grinding tool without any material removal being present.

As no material removal is obtained at the sliding stage, this stage will be an energy consumer which is unwanted except for the contribution to reduce the specific chip formation energy. This feature will be explained along with the theory for specific chip formation energy in chapter 1.3.

Rubbing energy is directly dependent on wear flats. Wear flats is a measure of the tool's dullness, and is shown in figure 1.7.

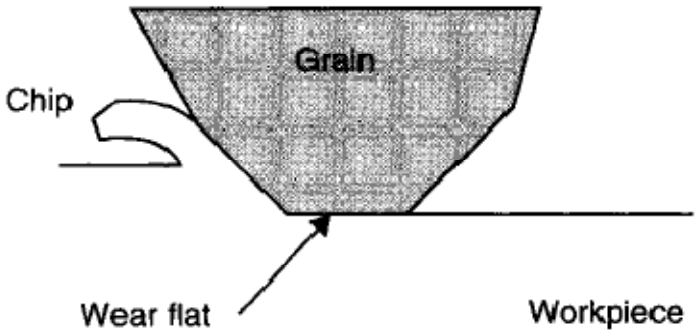

Figure 1.07 Sketch of wear flat in abrasive processes [F6]

As the wear flat area increase the grinding forces will also increase. Malkin and Guo have performed a series of test on the effect of wear flats [1]. Their experiments concluded that by maintaining the average contact pressure constant they found a linear dependence of the grinding forces and the wear flat area. They then expressed the grinding forces as a combination of cutting forces and sliding forces:

$$F_t = F_{t,c} + \mu \bar{p} A_a \quad (1\text{-}2)$$
$$F_n = F_{n,c} + \bar{p} A_a \quad (1\text{-}3)$$
$$A_a = b l_c A \quad (1\text{-}4)$$

In the above equations subscripts t and n denote tangential and normal respectively. The wear flat area, A_a, is the product of the contact length, l_c, the width of the contact length, b, and the portion of the grains which are wear flats. The latter expressions in equation (1-2) and (1-3) represent the sliding components to the grinding forces.

The obtained results from Malkin and Guo are presented below:

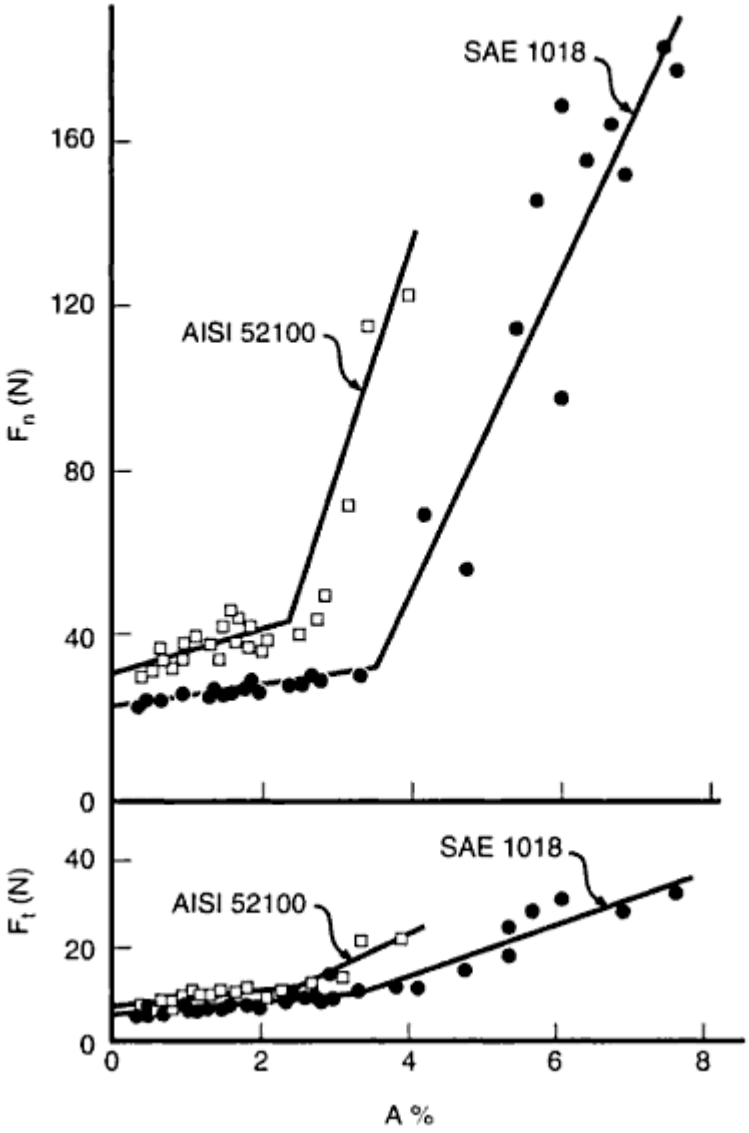

Figure 1.08 Force components in grinding and wear flats [F7]

Figure 1.8 shows that the proposed relationships are linear to a certain point where the gradient dramatically increases. The breaking point is the limit for work piece burn.

By regarding the cutting forces in eq. (1-2) and (1-3) as constant it is easily understood that work piece burn will occur by either applying to much pressure or by the grain's inability to re-sharpen itself. Equations (1-2) and (1-3) implies that if the tool is perfectly sharp there will be no rubbing effects, this will never occur in reality as the grain will have a contact zone with the processed surface even though it will be infinitesimal this at the same time implies that there will always be a contact pressure present at grinding. The friction coefficient, μ, will be dependent on the work piece material and the tool material. It should be noted that it is not unusual to apply cutting fluids to reduce the friction coefficient, and that this purpose is often the main objective with applying cutting fluids rather than just cooling of the work piece.

As presented, rubbing energies are directly affected by wear flats which will be dependent on the cutting tool characteristics. The features of wear flats, and its generating mechanisms will be addressed in chapter 1.4.

Plowing stage

With reference to figure 1.6 the stage following rubbing is plowing. This stage initiates when the deformation changes from elastic to plastic. At this stage the grain will not penetrate the work piece but it will cause a ridge build-up in front of the grain as well as some build-up to the sides. Plowing will not be limited to the stage preceding chip formation since the interface between the grain, work piece and chip will undergo some plastic deformation. However, the amount of energy consumed by plowing during chip formation is assumed to be negligible.

The amount of work performed in the plowing stage will be independent of the cut depth, when neglecting plowing during chip formation. This is because as the grain passes the grinding zone in the rubbing stage the deformation will be elastic, as mentioned above, when the deformation changes to plastic the grain will create a path into the work piece and when this depth has reached a critical value, h', cutting will initiate as shown in figure 1.9.

The plowing stage is relevant for surface and fine grinding where the operation is characterized by low cut depths and high number of passes. For heavy duty cut operations with high material removal rates and large cut depths the magnitude of plowing energies will be negligible.

Chip formation

Up to this point the described stages does not remove any material. The chip formation stage will succeed the plowing stage at that point where the grain reaches the critical cut depth, h', until the chip is removed from the work piece as shown in figure 1.9.

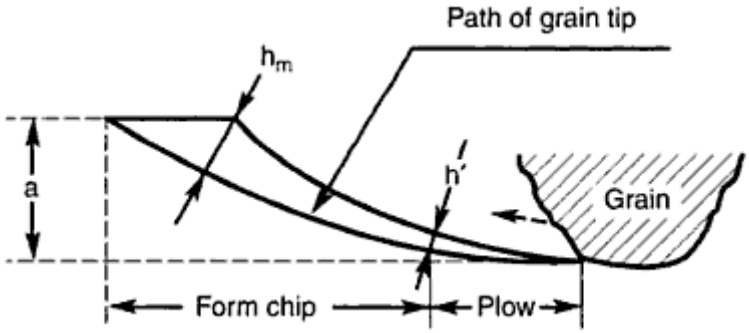

Figure 1.09 Sketch of critical cut depth [F8]

When the grain reaches the critical depth the actual material removal will occur. At this point the work piece will undergo intense plastic deformation at the cutting path. Even though figure 1.9 is extremely exaggerated it shows a large difference in the depth, a, and the uncut chip max depth, h_m. This is due to the grain moving at much higher speed than the work. The analytical expression for the uncut chip depth would be:

$$h_m = a_e \frac{v_w}{v_s} \tag{1-5}$$

Where a_e refers to the actual cut depth and subscripts w and s refers to work piece and wheel respectively. The uncut chip thickness is a measure of the max depth a single grain can penetrate the work piece and hence it is easy to mistake it for the measure a_e which is the initial cut depth corrected for deflections in the tool and work piece.

Usually the wheel speeds are much higher than the work piece speeds, thus the chip will undergo a large plastic deformation as the grain will carve the material along the cutting path. This deformation will happen at high rates and thus implying the process to be adiabatic. This is questionable as the chips are in direct contact with the work piece and will undergo a serious temperature rise before being detached from the work piece. But treating the process as nearly adiabatic has proven to give proper results as will be seen in the next chapter.

The amount of chip formation per unit time is measured by the material removal rate (MRR). The analytical expression for MRR is as follows:

$$Q = b_w a_e v_w \tag{1-6}$$

Where Q denotes the MRR, a_e is the actual in-feed (cut depth), b_w is the width of the tool and v_w is the work piece speed.

Comparison between conventional grinding and wire sawing

The theory discussed up to this point has been concerned with grinding and conventional machining. Wire sawing will be somewhat different. However, the differences between grinding and wire sawing with an abrasive is mainly the tool holder geometry i.e. for grinding the tool holder will be a grinding wheel while for wire sawing the tool holder will be the wire itself. The core mechanics of material removal by grinding will be identical, wire sawing will also undergo the three stages which are presented above and the energy consumption and thermal aspects will be identical on a microscopic scale.

For example In figure 1.9 a conventional grinding process with a circular grinding wheel is presented, this is slightly different for wire cutting as the arc of the grinding path will curve in the opposite direction and its radius will be a lot larger. However, the abrasive theory will be similar as for grinding.

1.3 Chip formation energy

According to Malkin the energy required to remove material during a grinding process consist of three individual components. These components are related to the three different stages of material removal which are chip formation, plowing and rubbing. All of these sub-processes are described under basics of material removal section.

For a process of surface grinding all of these components will affect the total energy consumption in a significant matter. This is due to the low in-feed rates, which also implies low material removal rates. The plowing and sliding contributions to the total energy consumption are not dependent on the actual material removed for each passing. Bearing this in mind it would be acceptable to treat these components as constant. When considering the cutting energy versus the material removal rate the energy will be very high for smaller removal rates, and as the removal rate increases the cutting energy will converge against the quantity known as the chip formation energy.

The figure below shows experimental results from Malkin and Guo [F9]. It emphasizes that the cutting energy per unit material removed will decrease with increasing material removal rate and that the cutting energy will converge towards the chip formation energy.

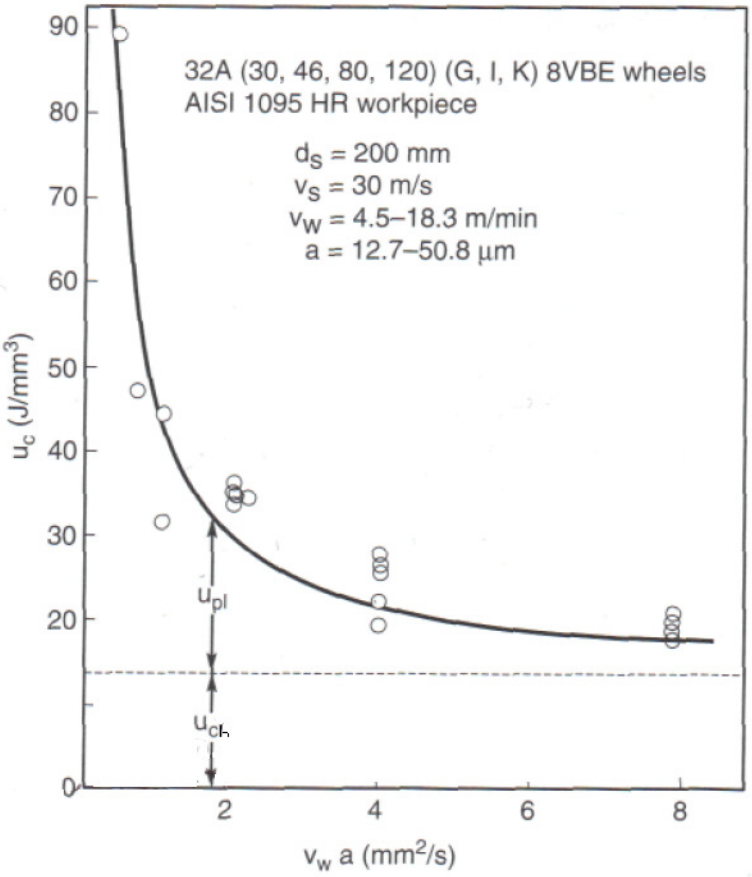

Figure 1.10 Specific cutting energy VS volumetric removal rate per unit width for plunge grinding [F9]

The sliding effect is not included in the above shown graph. Sliding energies are highly dependent on the amount of wear flats on the grinding wheel. By assuming that the grinding wheel is perfectly sharp this effect would be somewhat non-existing. However, this effect should be included to some extent as all abrasive processes will include some sliding effects at the initial state of cutting, before the plowing effects initiates.

Machining processes like turning will have a specific cutting energy in the range of 1,6-2,2 [J/mm^3]for cutting of carbon steel [3]. This implies that the cutting energy would be almost ten times higher for cutting by grinding than for cutting by turning when regarding a grinding process which is optimal e.g. the effects of plowing and sliding are negligible and the chip formation energy would be 13,5 [J/mm^3]. It's evident that the different processes have huge differences in cutting energy, this might seem surprising given that the output, in terms of machined work piece, could be regarded as identical. The key factors to be investigated when comparing grinding with conventional machining are the actual contact area and the rake angles.

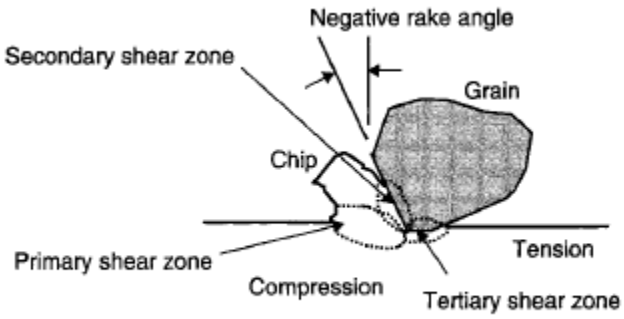

Figure 1.11 Rake angle grinding [F2]

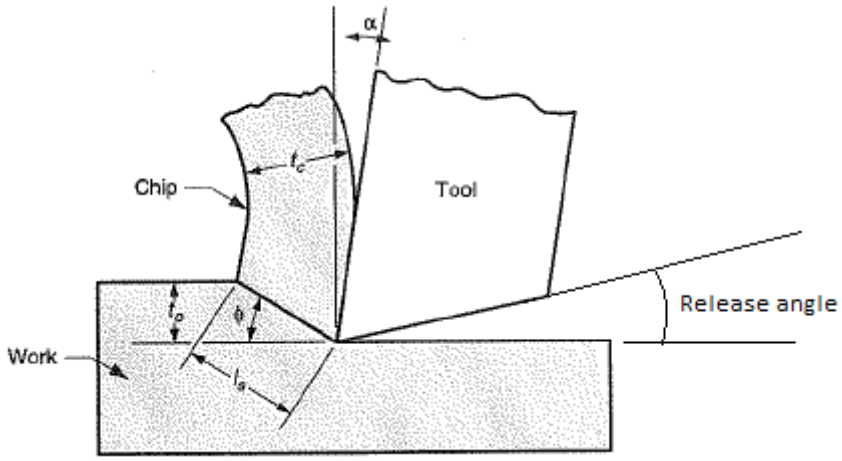

Figure 1.12 Rake angle conventional machining [F10]

It can be seen from the figures 1.11 and 1.12 that conventional machining is a much more precise operation than grinding. Positive rake angles (noted as α in figure 1.12) will provide the possibility for a continuous chip formation, and a proper release angle will decrease the friction between the tool and the processed surface. There will be some friction between the chip and tool but the main work is done in the primary shear zone which is located along the line l_s. In this plane the chip will be separated from the work piece and plastically deformed. Actual contact area for separation thus will only be the tip of the tool and it will be extremely small. When the bonds between the atoms are broken plastic deformation will initiate. It is obvious that the specific cutting energy for a conventional machining process will be limited by the energy consumed in plastic deformation. The actual shearing energy, in terms of fraction of total chip formation energy, will be decreasing towards zero with increasing material removal rate and thus it will be negligible at some stage.

Abrasive processes, like shown in figure 1.11, will evolve in a slightly different matter. Due to the negative rake angles the chip formation will be limited to a significant extent, and thus requiring additional energy to break the bonds in the chip. As figure 1.11 shows, the process of abrasion will be brutal and as it is presented it would be more convenient to regard cutting by abrasion as a plowing technique than actual shearing.

The above mentioned characteristics and differences between the processes in question is assumed to account for the vast differences in specific cutting energy between the conventional machining process by turning and an abrasive process.

1.3.1 Determining the chip formation energy in grinding

The total energy consumption during cutting by abrasion will be dependent on the contribution from the three stages; rubbing, plowing and chip formation. The energy contribution from the sliding stage will be addressed under the wear flats section, plowing energies are more or less neglected since the process to be investigated has a high removal rate ref. chapter 1.2.3.

As mentioned previous, chip formation in abrasive processes can be regarded as near adiabatic. By doing this it is possible to determine the highest energy level it is possible to obtain in a chip by comparing the chip formation by the melting energy for the relevant work piece material.

Past experimental studies has shown the specific cutting energy to be approximately identical for different types of steel grades [1]. In terms of material strength, this might seem very surprising. However, past studies has shown that the specific chip formation in grinding of various types of steel converges towards a constant value of approximately 13,8 J/mm^3 [1]. By assuming that 75% of the specific chip formation is spent by actual shearing and the remaining 25% to be consumed by grain-chip interface frictions, the shearing energy would correspond to 10,4 J/mm^3. This value is near the melting energy for iron.

Malkin and Joseph has also performed test on other materials with results that support the statements above [16]. They measured the specific energy for grinding in several materials and tested these result against the melting energies for each material. The results are shown in Figure 1.13. As can be seen from this figure is that there is a relation between the minimum cutting energy and the melting energy.

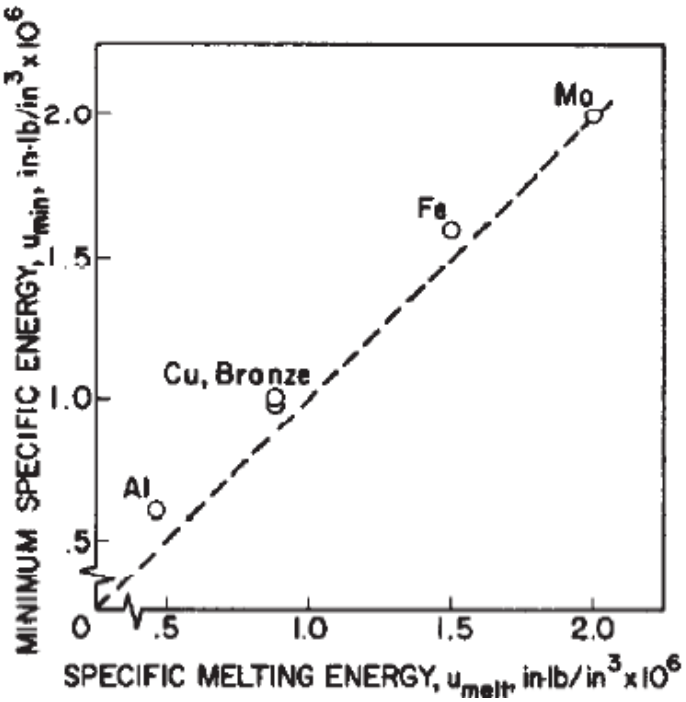

Figure 1.13 Minimum specific energy VS specific melting energy [16]

By accepting that the specific chip formation energy is dependent on the melting energy of the relevant work piece, the unaffected chip formation due to different strength characteristics may be explained. Steel is an alloy which consists of mainly iron, different strength characteristics are obtained by different alloying products or heat treatment. Heat treatment will have no effect on the heat capacity or the latent heat of fusion, hence will the melting energy remain unchanged after tempering or hardening. Alloying will have an effect on the melting energy as the process changes the chemical composition. However, the fraction of steel that corresponds to alloying members is so small that it is negligible in terms of defining melting energy.

Figure 1.10 shows the specific cutting energy for a given process of grinding. In this experiment the rubbing energy is not included and the remaining energy should be the combination of plowing and chip formation. The chip formation energy is assumed to be constant and thus it is evident that the plowing energy levels are extremely high with low removal rate, this is consistent with previously mentioned characteristics of the plowing stage. As the removal rate is increasing a decrease towards the chip formation energy is experienced.

Specific cutting energy can be obtained from the following relationship:

$$u_c = \frac{F_{t,c} v_s}{b v_w a_e} \tag{1-7}$$

Where the following quantities are included:
$F_{t,c}$ – Tangential cutting force
v_s – Grinding wheel speed
b – Width of cutting zone
v_w – Work piece speed (in feed)
a_e – Depth of cut

Utilization of equation (1-7) demands knowledge of either the cutting energy or the tangential cutting force. It should be noted that the cutting energy in this equation includes all the three stages of material removal by abrasive grains and thus calculation of tangential cutting force on the basis of the chip formation energy will be an under estimation.

1.3.2 Calculation of chip formation energies

By following the line of reasoning which is presented in this chapter, chip formation energies are calculated for 4 different materials. The melting energies are calculated as follows:

$$u_{melt} = \rho c_p \Delta T + L_f \rho \tag{1-8}$$

Where;
ρ – Density [Kg/m^3]
c_p – Heat capacity [J/KgK]
ΔT – Temperature difference between ambient and melting point [K]
L_f – Latent heat of fusion [J/Kg]

When utilizing equation (1-8) it is important to account for the changing heat capacity by temperature. Heat capacity is the materials ability to contain energy at a specific temperature level.

Thus the heat capacity will be zero at zero degrees Kelvin, and vary towards the melting point. The heat capacities which are used for this calculation are presented in Appendix 1.

By assuming that 75% of the chip formation energy is consumed in actual shearing the following results were obtained:

Material	Melting point (K)	Density [kg/m^3]	Melting energy [J/mm^3]	Chip formation energy [J/mm^3]
Steel	1800	7854	10,40	13,86
Stainless steel 304	1670	7900	9,57	12,76
Titanium	1953	4500	6,49	8,65
Aluminum pure	933	2702	2,75	3,66

Table 1Calculation of chip formation energies

Table 1 show obtained results which correspond well with the results presented by Malkin and Guo. For calculation purposes specific heat capacities for iron were used for calculation of steel properties.

1.3.3 Connection between chip formation energy and surface temperature

Malkin and Guo have studied the nature of temperature distribution in both surface grinding and abrasive cut-off operations [1]. Diamond wire cutting would be of the latter category. During such an operation the following expression is proposed for the maximum temperature rise:

$$\theta_m = \theta_{ad}\left[\left(1+\frac{\tau}{2}\right)erf\left(\frac{\sqrt{\tau}}{\pi}\right)-\frac{\tau}{2}+\frac{\sqrt{\tau}}{\pi}e^{-\frac{\tau}{4}}\right] \quad (1\text{-}9)$$

The main bracket in equation (1-9) will be increasing until it reaches unity, thus it represent the transient effect of the process. For cut-off operations the steady-state of equation 1-9 will be reached rather quickly, hence the maximum temperature rise will be estimated from:

$$\theta_m = \theta_{ad} = \frac{\epsilon u}{\rho c} \quad (1\text{-}10)$$

Equations (1-10) represent the adiabatic temperature rise due to the uniform heating by the cutting energy entering the work piece. In equation (1-10) the variable u refers to the cutting energy. For abrasive cut-off operation the material removal rates are high and thus the energy consumed in cutting can be approached as the chip formation energy, under the assumption of cutting with a perfectly sharp tool (rubbing energy is neglected).

Energy partition to the work piece will be determined from:

$$\epsilon = \frac{u_{rubbing}+u_{plowing}+0{,}55u_{chip\ formation}}{u} \quad (1\text{-}11)$$

And since:

$$u = u_{chip\ formation}$$

Then:

$$\epsilon = 0{,}55$$

Calorimetric experiments have concluded with the above mentioned results [1]. However, the effects of applying coolants will influence this energy partition to a great extent. For some cases the energy partition experienced a decrease from 60% to 20% [17].

The application of fluids and their effects on the temperature distribution would be highly dependent on the type of fluid and the flow across the cut path.

1.4 Wear flats and friability

1.4.1 Grain wear

As mentioned in the rubbing stage section the rubbing energy is dependent on the amount of wear flats in the abrasive tool. As this effect is of a more unwanted character studying of the tool wear mechanisms are important to b able to avoid this feature.

When cutting with abrasive grains there will always be a wearing effect on the surfaces, initially the grains are preferably coarse to reduce friction against the processed surface. As the grains carves the chip from the work piece there are three main types of wearing that will arise.

The first type of wearing to be addressed is wear flats which is dullness of the grain. This kind of wheel wear is the least wanted type as it will contribute to extensive friction and heat generation. Figure 1.14 shows a sketch of grain dullness:

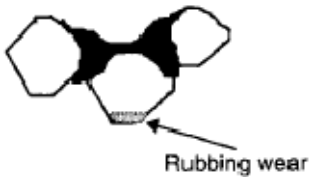

Figure 1.14 Sketch of grain dullness [F12]

Grain dullness is usually arises as the stresses imposed on each singular grain is low and the tips of the grain is just rubbing the surface of the work piece material. With reference to the section about the rubbing stage and figure AAA the effects of grain dullness is described. It should be noted that applying extreme pressures in the normal direction during cutting with an abrasive the flexibility in both the tool and work piece will cause the contact length to increase and thus creating wear flats without the grain actually being dulled. This can easily be experienced by applying intense force to an angle grinder while grinding, then it is quickly seen that the temperature rise in the work piece is a lot more severe without the material removal rate being increased with an equivalent magnitude.

The effect of rubbing wear can be reduced by applying cutting fluids which reduce the friction between the grain wear flat and the work piece. However, these fluids could have a negative effect on the bond strength. Bond strength will be addressed at the end of this chapter.

Fraction of the grains is the second kind of grain wear. This mechanism occurs at high stresses on the individual grains. In terms of wheel wear this would be the most preferable mechanism, this is due to

the re-sharpening effects this mechanism will provide. Rowe separates between two types of grain fracture, micro and macro as shown in figure 1,15:

Figure 1.15 Grain fracture [F12]

Whether a grain fracture propagates to a macro fracture or remains a micro fracture is not revealed in the fundamental literature. Malkin and Guo choose not to divide grain fracture into sub groups. It is assumed that Rowe's intention is to emphasize that micro fracture is the preferable mechanism as this mechanism will provide a slow wear rate on the abrasive tool without creating wear flats. It should also be noted that grain fracture is dependent on the crystalline structure of the singular grains and thus this alone might be the reason for the sub grouping of the fracture mechanism.

The term friability is correlated to the grains ability to fracture under certain loading. A high friability grain will fracture at lower stress level than a grain of low friability. High friability then counteracts wear flats and re-sharpens itself at a higher rate.

Bond fracture is the third wearing mechanism. As the name implies bond fracture arises when the bonds between the grains break causing the grain to leave the abrasive tool. This mechanism is more likely to succeed grain dullness as the grain then will undergo pressures over a larger area thus generating grater forces in the bonding between the grains. Bond fracture is shown in figure 1.16:

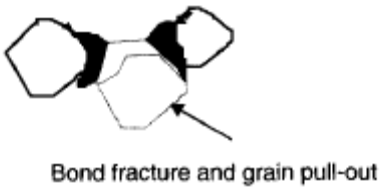

Figure 1.16 Bond fracture [F12]

The main cause of bond fracture is high pressure. Bond material strength then will be of significant interest when addressing bond fracture. The bond material strength might be affected by several characteristics arising during grinding. Temperature might soften the binder material and thus impelling grain pull-out. Coolants will contribute to reduce this effect, however the chemical composition of the coolants might have an eroding effect on the binder and thus reducing its strength [1].

1.4.2 Wear resistance

Since the amount of wear flats will determine, to some extent, the cutting energy and thus the temperature generation due to cutting it is of utter most interest to keep the generation of wear flats as low as possible. The wear resistance in an abrasive grain thus is an interesting characteristic.

In terms of toughness diamond grains will be the superior available abrasive grain, if this characteristic alone would describe the abrasive grain wear resistance ability diamond would easily be the preferred abrasive grain. However, Malkin and Guo state that rubbing wear of an abrasive grain is both a mechanical and chemical process. The chemical reactions that will arise in the grain to work piece interaction will be numerous, including combinations of reactions between air, work piece metal, coolant and abrasive grain among others.

Diamond as abrasives when cutting low carbon metals has a disadvantage in being carbon rich. Low carbon steels will be unsaturated in carbon and their affinity for carbon will cause the diamond abrasives to degrade into graphite. The effect of this reaction is similar to the effect of clogging which is seen when grinding ferrous metals with aluminum oxide. Clogging arises as the metal particles with fresh surfaces reacts and bonds with the abrasives. The latter phenomenon is relevant for cutting with diamond abrasives in stainless steel. [Diamond cutting in nuclear industry]

Rapid diamond wear effects are thus apparent in cutting of ferrous material and the wear resistance of diamond can be regarded as low. However, re-sharpening of the wire by cutting through concrete has proven to reverse the above mentioned effects at least to a useable extent. By following the procedure of re-sharpening as necessary the hardness of the diamond grains can be utilized to its full extent and thus support the diamond abrasive as a tool of high wear resistance.

1.4.3 Concluding remarks

Grain wear is an important feature of cutting with an abrasive, the preferable type of wear is fraction with absence of wear flats. The presence of wear flats will influence the cutting parameters noticeably in terms of larger forces and higher temperatures. It's assumed that the amount of wear flats can evolve to amount for 8% of the effective contact surface before eventually fracture or pull-out [2].

Solutions for counter of wear flats effect and clogging of tool is proposed with applying cutting fluids and re-sharpening by cutting concrete respectively.

1.5 In depth review of cutting by diamond wire

1.5.1 Introduction

Diamond wire cutting (DWC) is a remotely operated operation where hydraulic power is the power source. The necessary equipment needed to perform this operation is:

- Hydraulic power unit (HPU)
- Sawing machine
- Diamond abrasive wire

In the following section an introduction to the equipment will be given subsequent to a description of the cutting process and the characteristic features of the DWC characteristics.

1.5.2 Hydraulic power unit

A HPU's purpose is to convert electrical power to hydraulic power. In the oil and gas industry hydraulic power has been the preferred energy carrier for performing heavy duty work by remote control, this can be seen in cranes and subsea remotely operated vehicles among others.

The power source in a HPU is usually an electrical motor which is indirectly connected to a closed hydraulic loop through a hydraulic pump. It is not necessary that the power source should be electrical, the main criteria is that the power source can provide energy to the hydraulic pump by a translational or rotational movement depending on the hydraulic pump.

The hydraulic loop in a HPU consists of at least a hydraulic pump, hydraulic oil reservoir, directional valve and a consumer. In addition to this it is usual to include pressure safety valves, instrumentation, oil filters and an accumulator. For diamond wire cutting there is no need for an accumulator as the sawing machine is active continuously after cutting is initiated. Accumulators are necessary where the consumer is activated at a more random pattern, manipulators on a subsea remotely operated vehicle is an example of such an operation. Figure 1.17shows a sketch of a simple HPU, in this sketch the cylinder is the consumer.

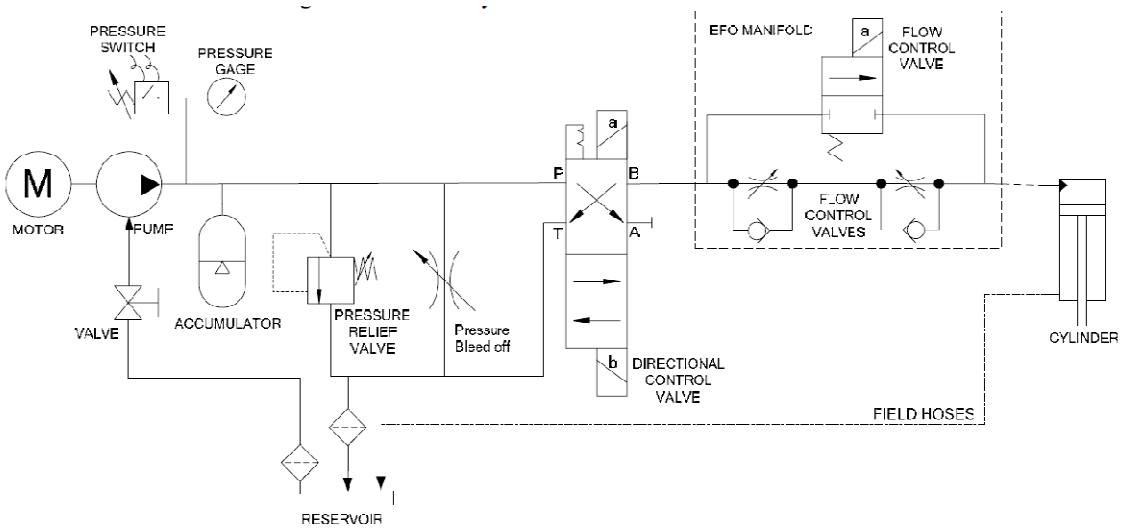

Figure 1.17 Flow chart HPU [F13]

The working principle for the HPU in figure 1.17 is quite simple. When the pump is being engaged by the electrical motor it will transport oil from the reservoir to the accumulator. The HPU will operate after a constant pressure principle, so any energy not consumed will be stored in the accumulator. When the energy amount in the accumulator has reached a certain limit it will stop the electrical motor. This also allows the consumer to perform work without engaging the electrical engine. The control valve allows the operator to allow or shut down the oil flow to the consumer.

It's assumed that the total degree of efficiency for most HPUs is in the range of 0,8-0,9.

A flow chart diagram for the Hydro stress RD-SRC power unit is shown in appendix B.

1.5.3 Sawing machine

The main purpose of the sawing machine is to convert the hydraulic energy into usable cutting energy. From the section on basic material removal it is known that there will be need for displacements in at least two directions to obtain a cut. For diamond wire the directions of the displacements will be along the wire and perpendicular to the wire, the first displacement will be controlled by a hydraulic motor causing the wire to run and the second displacement will b controlled by a hydraulic cylinder which applies tension to the wire. Figure 1.18 shows a principal sketch of a sawing machine:

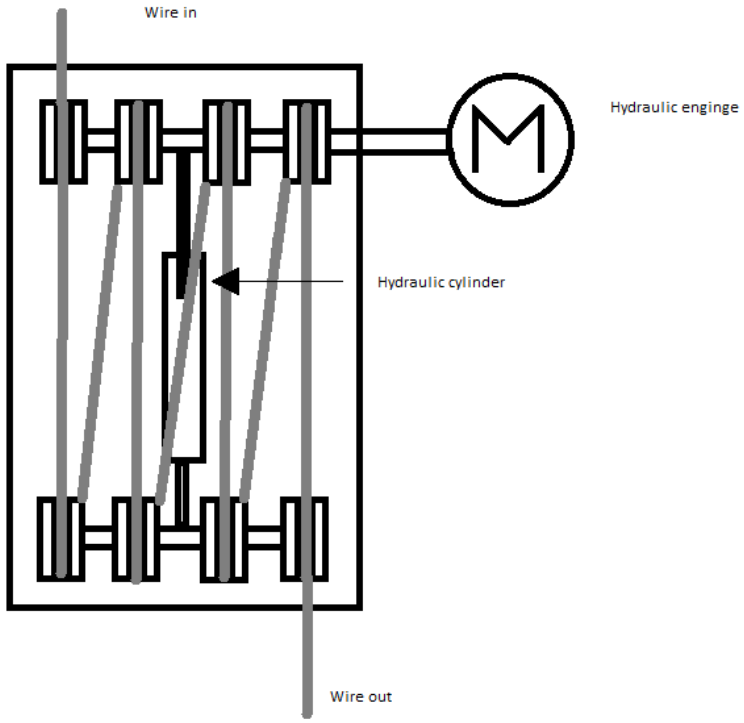

Figure 1.18 Principal sketch of a sawing machine

As seen in figure 1.18 the hydraulic motor is connected to a set of drive pulleys, these are fixed to the frame of the sawing machine. The deflection pulleys are fixed to a hydraulic cylinder which allows the set of deflection pulleys to move in the height direction thus altering the distance between the set of drive pulleys and the set of deflection pulleys. This movement will then cause the tension in the wire to increase with the increasing distance between the pulleys. In addition to the mentioned and observed pulleys in figure 2, there will be additional swiveling pulleys to control the angles of attack for the cutting wire.

A proper drawing of the Tyrolit Hydrostress SB35 is shown in appendix B

1.5.4 The diamond wire

The design of a typical diamond wire is shown in figure 1.19:

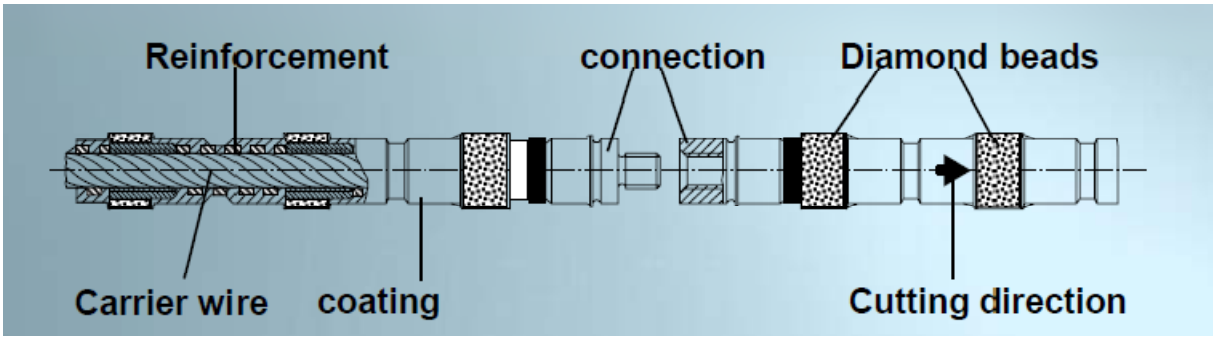

Figure 1.19 Outline of diamond wire design [F14]

As seen in figure 3 the structure of a diamond wire is consistent of several parts. The basis for the diamond wire is the steel carrier wire, this wire will have a high strength to be able to resist the high stresses which arise during cutting. On top of the carrier wire a reinforcement spring is installed. This spring will function as a spacer for the diamond beads and hence prevent a disarrangement of the diamond beads as well as absorbing the stress peaks which will be generated when encountering particles with higher cutting resistance. The diamond beads are the actual cutting medium, these are installed between the reinforcement springs. On top of the reinforcement springs a coating layer is applied, usually this layer is made of rubber. The intention of applying the coating layer is to prevent corrosion as well as fixing the diamond beads and reinforcement springs to the carrier wire.

The structure of the diamond beads is subject for further explanation. Figure 4 shows an outline for the most common diamond beads:

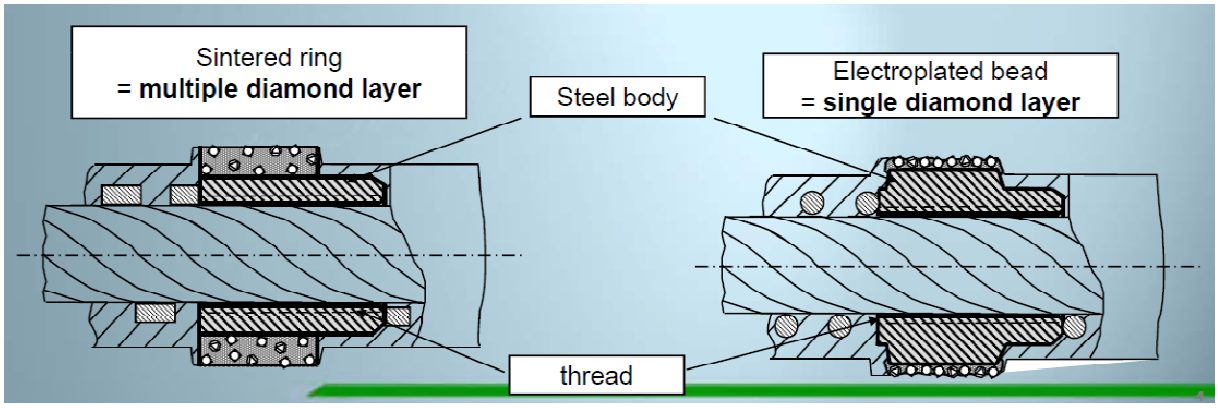

Figure 1.20 Outline of diamond beads [F14]

The diamond beads consists of an annular steel body which is threaded at the inside providing a tighter fit to the carrier wire. On top of the steel body is the diamond layer applied, as seen in figure 1.20, there are two main types of diamond layers.

Sintered bead are made by combining diamonds with bronze, iron or nickel at its powder form. The composition is then applied to the steel body and the entire part is heated to allow the powder to bond thus making it a solid. With the use of this technology several layers of diamonds are applied and then implying a long life wire.

Electroplating is a method where the diamonds are deposited on the beads electrolytically. The bonding material is usually nickel. Since the diamonds are applied in one layer only it is possible to reduce the bonding materials cover up of the diamonds and then creating a larger free surface of

every single diamond. Electroplated diamond wires are commonly known for being sharper and more robust, but due to the single layer it wears out at an earlier stage than sintered diamond wire.

There is also a third kind of diamond beads, this method is assumed as relatively new to the market as the available literature on abrasive machining does not refer to this method. In this method diamonds are adhered to the steel body by vacuum brazing, which is an active welding method. The manufactures claims this type of diamond beads to be even more wear resistant and sharper than the above described types. [19]

1.5.5 The cutting operation

Cutting with diamond wire is described by numerous parameters. The main parameters are:

- Wire speed
- Wire tension
- Positioning of the swivel pulleys

These are the directly controlled parameters, in addition the characteristics of the work piece and diamond wire will have significant effect on the output parameters of a cutting process in terms of material removal rate, temperature distribution and cutting energy among others.

Determining the cut path

The basic procedure to a set up is to lay the wire around the work piece, tighten the wire and start up the machine. After the pretension of the wire, the wire will have an initial length, the rate at which the wire decreases in length will be the in-feed speed. The positioning of the swivel pulleys are important as any sharp angles in the cutting path will cause a rapid wear of the wire and the probability for the wire to break will be high. When determining the cutting path it is important to choose a path that will distribute the pressure over an even area during the entire cut. It also follows that the path should not create sharp angles (equivalent with extremely small radius curves) nor creating too large contact areas as the distributed stress will be too low. The positioning of the swivel pulleys will be a significant parameter in this assessment. In figure 5 an example of a diamond wire is sketched:

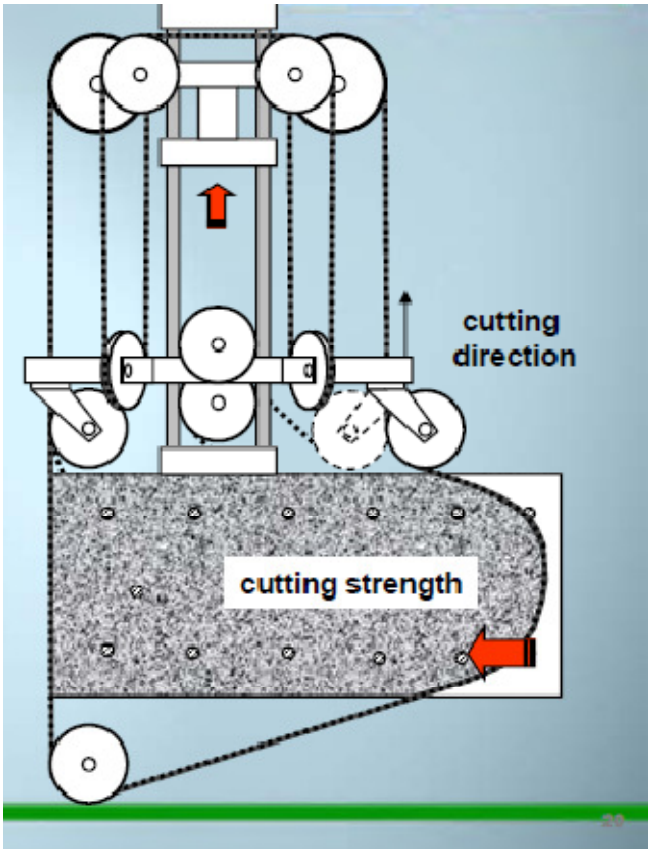

Figure 1.21 Sketch of diamond wire set up [F14]

In figure 1.21 an additional pulley is installed to reduce the contact area between the wire and work piece. It's also seen that the cutting path is creating an arc without any sharp angles. The problem of sharp angles is more relevant for cutting of non-homogeneous cross sections, such as I and H beams. If a cut is set up by placing the beam's centerline at the line of symmetry for the wire path a sudden decrease in contact area will be experienced after cutting through the flange thus creating a sharp angle and intense pressures on both the wire and the web. Applied pressure to the wire is a limiting factor. A sharp angle is indicated in figure 6, where the red line represents the cutting wire.

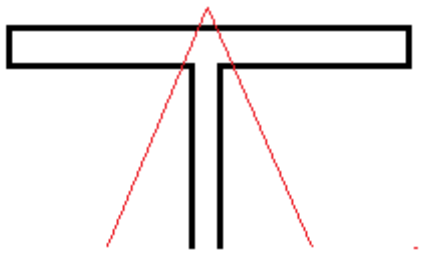

Figure 1.22 Sketch of sharp cutting angles

The problem outlined in figure 1.22 is usually solved by adding wood pieces in such a manner that it would increase the cutting length and then also increasing the radius of the curvature of the wire.

Twisting of wire

When installing the wire in the sawing machine it should be twisted around its own axis. This will prevent uneven wear as the whole surface of the diamond beads will be utilized.

The kinematics of the twisting implies that the wire will contain an up-righting torsion component and thus it will also rotate after engaging in the work piece. This will then force the cutting grains to move along a helical path instead of straight forward path.

The main reason for twisting the wire, as mentioned above, is to prevent uneven wear of the diamond beads. However, twisting of the wire will also have positive synergy effects on the removal of chips as the twisting movement will transport chips to the free surface. An un-twisted wire will cause the chips to build up ahead of the grains and thus forcing the grains to cut already removed chips. Twisting of the wire will then allow the energy input to be more focused on the actual material removal from the work piece.

Another synergy effect of wire twisting arises when applying coolants or lubrication fluids. Due to the rotational motion of the wire, around its own axis, fluids will be transported into the cut surface in a more efficient matter and thus obtaining a better utilization of the relevant fluids.

When a cut is performed with small contact lengths the probability for uneven wear will increase. As the wire is in a finite length and the wire speed remains constant, this combined with the assumption of the wire rotating around its own axis is constant after some time will imply that the grain will encounter the work piece at same place at each passing. It the rate of rotation is too small this would imply that there might be some grains that never encounter the work piece, or at least at lower frequency than other grains.

Operation of the sawing machine

As mentioned in the section on basic material removal, a cut is obtained by at least to movements creating an interaction between the tool and the work piece. For diamond wire cutting these two movements would be the wire speed and the in-feed speed. The wire speed is obtained by the rotation from the hydraulic motor while the in-feed speed is controlled by the hydraulic cylinder and the tension it will impose on the wire.

The cutting operation will be performed by constant wire speed and manually operated wire tension. The operator will reduce the wire length by increasing the distance between the drive and deflection pulleys.

Diamond wire cutting as reviewed in this thesis is a remotely operated process. This allows the operator to monitor the operation at a safe distance. Safe distance is referred to as two times the free running wire length, at this distance the operator should not be in danger of being whipped by a broken wire.

Vibrations in wire

During a cutting operation the wire will undergo vibrations along its main axis. These vibrations will arise due to the loading from the cutting operation. The loading from the cutting operation will fluctuate as the surface in the cutting path will be uneven by the changing density of cutting ridges.

This will create movements in the normal direction to the wire and thus transmitting vibrations over the wire's free span.

To obtain an optimal cutting operation it is important to keep the vibration frequency as low as possible also maintaining the amplitude of vibration as low as possible. Frequency and amplitude will affect the wire's possibility to maintain a constant connection with the work piece.

Unwanted vibrations are compensated for by altering wire speed or wire tension or both.

1.5.6 Cutting fluids

For most cutting operations it is common to add cutting fluids. These are applied to enhance the cutting parameters and to reduce temperature development in the work piece. The most common cutting fluid is water, this cutting fluid will be categorized as a coolant as the cutting enhancement obtained by adding water is only a reduction of the temperature development. The other category of cutting fluids are the lubricants, these fluids will reduce the friction between the grains and the work piece and thus reducing the necessary energy input. Lubricants are usually oil-based or synthetically produced. This resulting in that many of them might be pollutive and thereof should be handled with care. Diamond wire cutting is usually performed in open environments and controlling the used cutting fluids is regarded as problematic, hence the common cutting fluid for diamond wire is water as water will impose any considerable environmental threat. The purpose of using water as a cutting fluid when cutting with diamond wire, is to prevent temperature development as well as to obtain a more efficient removal of chips.

2 ATEX

2.1 Introduction

Hazardous atmospheres in industry became a challenge as the need for coal expanded during the industrial revolution in the 18th century. Methane gas, which is absorbed by coal, was released while mining. This led to a series of unfortunate events as the gas, which is lighter than air, rose to the top of the mine and initiating contact with the miners thus, creating explosions. The first solution to this problem was to hire special miners to ignite the gas pockets on a daily basis, of course this solution would be short lived as the miners most likely would die by occupational hazard or refuse to execute when realizing the risks involved. As a result of the miners' refusal to execute this operation, convicts from local penitentiaries were recruited but, under the same reasons for the miners, this solution never gained approval as being viable solution. The next step in the evolution of securing hazardous areas was to equip different animals with candles, or some kind of ignition source, and send them through the mines.

The problem with the miners' solution was that they attacked the problem from the wrong angle. They realized that they were operating in a hazardous environment and mobilized all their creativity to reduce the potential hazard in the atmosphere itself. Being cynic in definitions one would not characterize an atmosphere with methane gas as hazardous in itself, but in combination with an ignition source, would be a lethal scenario. The miners' realized this and in 1815 the first ATEX secured torch light was invented [25].

After the invention of the invention of the secured torchlight the next milestone appeared when utilization of electrical equipment became usual in coal mines. To account for the added risk, all electrical equipment was enclosed to contain the explosions and shield them from the surrounding atmosphere.

The need for explosion protection was mostly a challenge for the mining industry up to around 1920 when the use of cars and airplanes increased significantly. The increased use of hydrocarbons as fuel then increased the amount of hazardous areas as processing plants, bunkering terminals and similar became necessary. This led to the classification known as Division 1 by the American authorities. Under this area classification subgroups for different hazardous atmospheres were later introduced. The sub grouping was characterized by the gases explosive pressure, flame transmission and ignition temperature.

The classification of Division 1 would not allow for different safety measures for different hazard levels within an installation. Thus, in 1956 the Division 2 classification was introduced along with the intrinsic safety philosophy. This allowed for the use of less secured equipment in zones with a reduced potential hazard adjacent to zones with a higher potential hazard.

The first European classifications were observed in Germany around 1935. This introduces the marking of equipment with the symbol "Ex" as a certificate for fulfilling the criteria's established by the German standard.

One of the reasons for founding of the European Union was to ensure a free trading zone within the borders of the participants' areas. This led to a merger of the relevant standards and practices used by the different participants. The merger then introduced the Zone classification which is still utilized

in the different industries today. In 1975 the first EU directive was established as the “Explosion Protective Directive” this was later renamed to the ATEX directive. In 1978 the first European standard covering protection of personnel and equipment in hazardous areas was published.

The European Union founding led to two independent markets within securing hazardous areas as the evolution in the North America had been independent of the evolution in Europe. This led to a lengthy debate in the North America of whether to classify the hazardous areas as Zones or as Divisions. At some time the North American authorities choose to adapt the Zone classifications, but their standards differ slightly from the European standards within the zones by having different names for gas grouping.

2.2 ATEX directive and harmonized standards

The ATEX directive intention is to provide the paramount requirement for placing equipment, intended for use in hazardous areas, on the European Union market. The responsibility for implementation and enforcement lies within each member state or any other who wishes to implement the requirements of the directive [I4]. Each state would be responsible for naming a Notified Body, whose assignment is to assure that equipment in question are in compliance with the ATEX directives. In Norway, DNV (Det Norske Veritas) is recognized as a Notified Body.

The two ATEX directives are:

1) Directive 94/9/EC Equipment and protective systems intended for use in potentially explosible atmospheres
2) Directive 1999/92/EC Minimum requirements for the safety and health protection of workers potentially at risk from explosible atmospheres

For this thesis the first of the above mentioned directives would be relevant. The Directive 94/9/EC would be the governing requirements for a set of “Harmonized Standards” creating a hierarchy which can be visualized as follows:

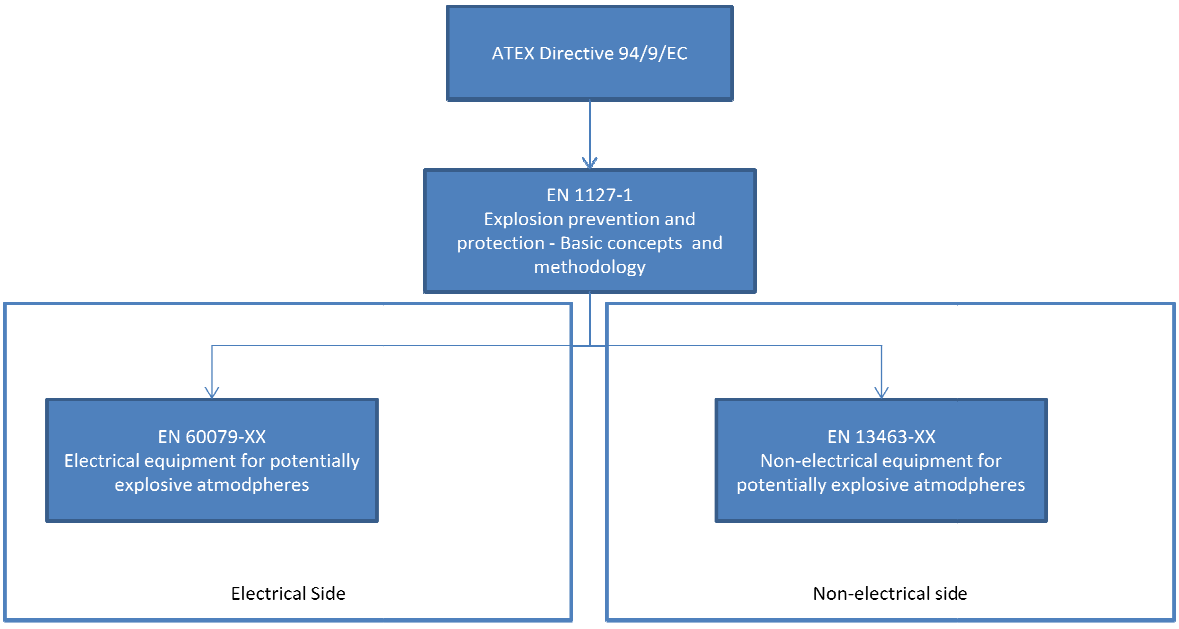

Figure 2.01 Hierarchy for standards

The standards below the ATEX Directive in the hierarchy seen in figure 2.1, states the actual technical requirements for the equipment.

The process of evaluating equipment can be visualized as follows:

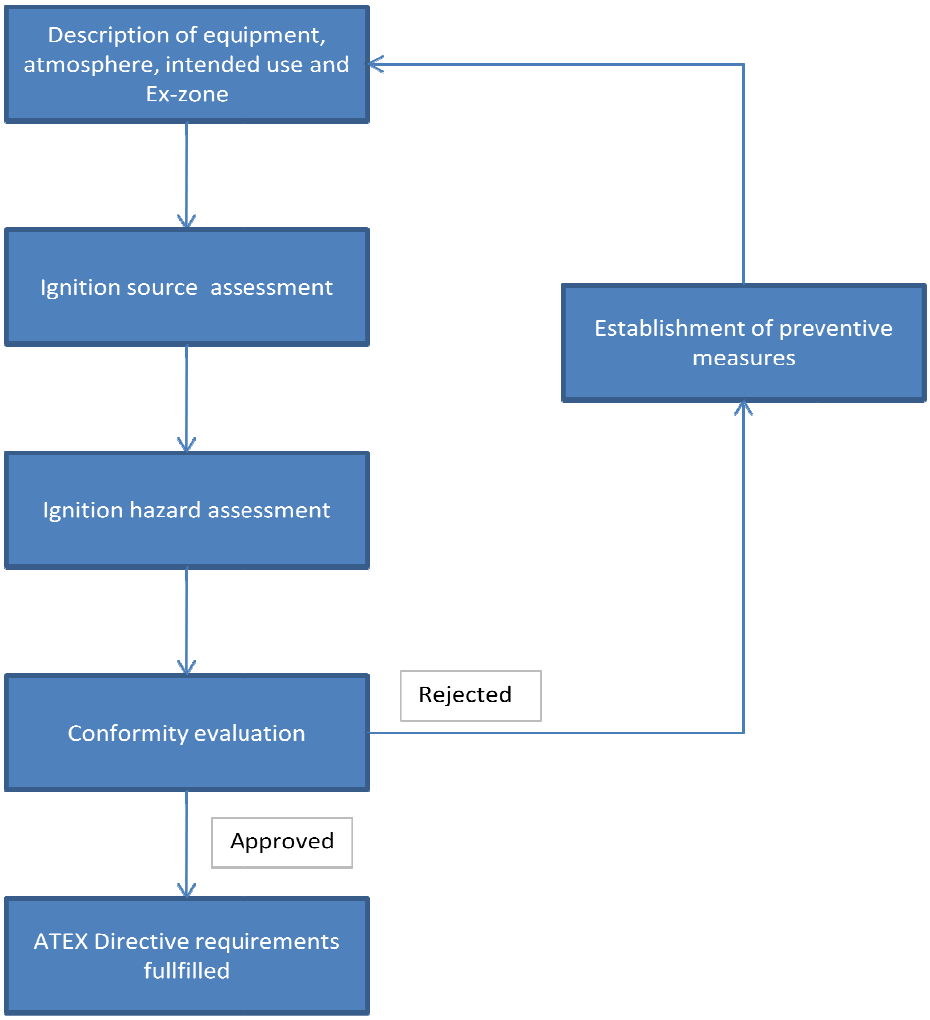

Figure 2.02 Evaluating process for equipment [F15]

The scope of this thesis is to evaluate the ignition hazard for cutting with diamond wire at offshore installations. The ignition hazard to be evaluated is restricted to the ignition sources from hot surfaces and spark emission. The elements in figure 2.2 to be evaluated under this thesis are then:

- Description of equipment, atmosphere, intended use and Ex-zone
- Ignition hazard assessment

In addition the preventive measures will be discussed to some extent.

2.3 Application of ATEX Directive and Harmonized Standards

The Directive 94/9/EC mainly constitutes the formal requirements in an approval process and the responsibility which lies within the state, Notified Body and manufacturer. In addition it defines the following expressions [25]:

Explosive atmospheres
Mixture with air, under atmospheric conditions, of flammable substances in the form of gases, vapors, mists or dusts in which, after ignition has occurred, combustions spread to the entire unburned mixture.

Potentially explosive atmosphere
An atmosphere which could become explosive due to local and operational conditions.

Equipment groups and categories
Equipment group 1 applies to equipment intended for use in underground parts of mines, and in those parts of surface installations of such mines, liable to be endangered by firedamp and/or combustible dust.

Equipment group 2 applies to equipment intended for use in other places liable to be endangered by explosible atmospheres.

For each group of equipment there will be sub-categories for the level of protection found within the equipment. Equipment group 1 is only relevant for mining industries, and thus it is not relevant for the scope of this thesis. The sub-categories are defined in Annex 1 to Directive 94/9/EC:

- Category 1 comprises equipment designed to be capable of functioning in conformity with the operational parameters established by the manufacturer and ensuring a very high level of protection.
- Category 2 as for category 1, but ensuring a high level of protection
- Category 3 as for category 2, but ensuring a normal level of protection

The protection levels are defined such that a very high level of protection will maintain sufficient protection if the equipment has two independent malfunctions of the protection barriers. Protective barriers could be cooling of parts which undergo heating during normal operation or similar. The high protective level demands safe operation with one malfunction, while normal level of protection demands safe operation under normal operation.

The determination of equipment category relies in what zone of explosible atmosphere it is intended used. When referring to zones of explosible atmosphere it is the frequency of presence of an explosible atmosphere which is of interest. EN 1127-1 Annex B classifies the zones as follows:

Zone 0 – Atmosphere consisting of air mixed with flammable substances which is present continuously, over long periods of time or frequently e.g. inside of vessels, pipes etc.

Zone 1 – Atmosphere consisting of air, mixed with flammable substances, which is likely to occur under normal operations occasionally.

Zone 2 - Atmosphere consisting of air, mixed with flammable substances, which is not likely to occur under normal operation but, if it occurs, it will only persist for a short period of time.

An offshore installation will contain a lot of equipment as stated under Zone 0 and thus the immediate vicinity would be classified as Zone 1 [28]. According to EN 1127-1 Annex C equipment category for use in Zone 1 would be either category 2 or category 1.

2.4 Ignition sources

The common ignition sources are listed in EN 1127-1:

1) Hot surfaces
2) Flames and hot gases
3) Mechanically generated sparks
4) Electrical apparatus
5) Stray electric currents
6) Static electricity
7) Lightning
8) Radio frequency, electromagnetic waves from 10^4 Hz to 3 x 10^{12} Hz
9) Electromagnetic waves from 3 x 10^{11} Hz to 3 x 10^{15} Hz
10) Ionizing radiation
11) Ultrasonic's
12) Adiabatic compression and shock waves
13) Exothermic reactions, including self-ignition of dusts

From the problem definition only two of the listed ignition sources will be evaluated, hot surfaces and mechanically generated sparks.

In terms of ignition source control, the ATEX Directive, which contain the superior requirements, states that equipment of category 2 equipment group 2 should be designed as to prevent ignition sources arising, even in the event of frequently occurring disturbances or equipment operating faults.

2.4.1 Hot surfaces

EN 13463-1 determines the final requirement for maximum surface temperatures as:

The maximum surface temperature should not exceed the auto ignition temperature of the gas for which the equipment is intended used within.

For offshore installations the potentially hazardous atmosphere will mainly consist of natural gas and hence natural gas would be the target for the assessment in this thesis. Composition of natural gas varies to some extent, but the main components are Methane, Ethane, Butane and Pentane.

The auto ignition temperatures for these gases lie within 243 degrees Celsius (Butane) to 537 degrees Celsius (Methane) [25]. Hence target surface temperature would be 243 degrees Celsius.

2.4.2 Mechanically generated sparks

EN 1127-1 5.3.4 [24] defines the hazard due to mechanical sparks as follows:

"As a result of abrasive processes, such as grinding, particles can become separated from solid materials and become hot owing to the energy used in the separation process. If these particles consist of oxidizable substances, such as steel or iron, they can undergo an oxidation process, thus reaching even higher temperatures. These particles (sparks) can ignite combustible gases."

The requirements of EN 1127-1 6.4.4 [24] for category 2 equipment states the following:

“If hazards due to mechanically generated sparks have been identified, dependent on the type of explosible atmosphere the following requirement for equipment of category 2 shall be complied with:

Sparks shall be excluded in the case of normal operation and in the case of malfunction.”

2.4.3 Testing of equipment

Clause 8 of EN 13463-1 states the requirements to the necessary tests. For determining the maximum surface temperature under operation measuring should be done with recognized measuring devices such as thermometers, thermocouples or IR camera etc. Where direct measurement is not possible other methods, like calculations, can be applied.

For testing of the ignition potential in mechanically generated sparks full scale test in an atmosphere of 6,5 – 7% methane and 25-26% oxygen in nitrogen [25].

2.4.4 Approval system

The results from relevant testing of the criterions presented in this chapter will be part of the technical file which would be the documentation which declares the equipments category and level safety for use in hazardous areas. The management of technical file is a responsibility belongs to the Notified Bodies.

Other parts of this documentation include description of equipment and intended use along with necessary technical data sheets etc. The tests will be performed on the outcome of the ignition hazard assessment report.

The final part of an evaluation process will be the conformity evaluation, as seen in figure 2.2. In this evaluation the results from the ignition hazard assessment, along with necessary test results will be compared against the target criteria’s and the possible declaration of conformity will either be approved or rejected. If rejected it would be possible to add preventive measure and test the equipment for conformity again.

The instances able to perform the whole evaluation are either a Notified Body, or other parties approved by the Notified Body. These rules applies for both electrical and non-electrical equipment intended for use in Zone 0, but for Zone 1 the manufacturer, or operator, of the equipment, if non-electric, can declare its conformity by following the procedure mentioned in this chapter. For electrical equipment in Zone 1 the same rules as for Zone 0 applies.

2.5 Summary and comments for further work

In this chapter a brief introduction to the ATEX Directive, and the requirements established on its basis, is presented.

It’s seen that a lot of considerations needs to be taken account for when approving equipment in accordance with the requirements stated by the ATEX directive an thus the assignment of declaring equipment will be a rather extensive task.

The direct requirements to be tested in this thesis are:

- The maximum surface temperature shall not exceed 243 degrees Celsius, even if the equipment experiences malfunction.

- The equipment should not emit any sparks when operating in an explosive atmosphere

The test requirements will not fulfill the requirements stated in EN 13463-1 and thus their validity as a part of an ignition hazard assessment have to be evaluated by a Notified Body or others approved by a Notified Body

The elements stated to be addressed in this thesis, as mentioned in section 2.2 will be assessed in the following sections:

- Intended use addressed in problem definition
- Description of equipment addressed in chapter 1
- Explosive atmosphere and Ex-Zone addressed in this chapter
- Ignition hazard and preventive measures will be addressed in the following chapters

3 Thermal analysis model

3.1 Introduction

For this thesis it is of interest to study whether a diamond wire cutting process will be classified as an ignition source when performing this process in an explosible atmosphere. The process of diamond wire will include high temperatures and spark emission, so initially it would be logically to characterize this process as an ignitions source. Bearing this in mind, it is of great interest to study the compensating measures, and their effect on the process. In addition to this the two following statements are to be explored:

1) The temperature distribution during cutting of stainless steel will be higher than when cutting conventional construction steel
2) The material removal rate will be significantly lower for cutting of stainless steel than for cutting conventional steel

These statements were uttered by people known for their expertise in the relevant fields.

The chosen method for determining the above mentioned problems will be thermal analysis. Published research usually base their thermal simulation on either moving heat source theory as proposed by Jaeger [21, 22] or by finite element simulation [20]. However, both these methods, as presented in the respective papers, are concerned with surface grinding. Diamond wire will be slightly different, mainly because it is a cut off operation. Apart from the type of operation the geometries in the cut will be quite different as the contact length will be vastly larger in wire cutting than in cutting with grinding wheel. The geometrical difference was the main reason for discarding the proposed methods, also since the derivation of the moving heat source theory was not explained in detail, an adoption of this theory to diamond cutting failed. Instead of the complex proposed method analysis with conventional transient thermal analysis will be performed.

3.2 Transient thermal analysis theory

Heat conduction through a plane wall with different surface temperatures will transport heat according to Fourier's law:

$$\mathrm{q} = -\kappa \, dydz \, \frac{dT}{dx} \tag{3-1}$$

By integration this equation, and some manipulation, the temperature distribution is obtained:

$$T(x) = T_1 - \frac{T_1 - T_2}{L} x \tag{3-2}$$

And the heat conduction equation for one dimensional analysis would be:

$$\frac{\partial}{\partial x}\left(\kappa \frac{\partial T}{\partial x}\right) = 0 \tag{3-3}$$

By considering a slab with an initial uniformly distributed temperature suddenly exposed to a temperature source it is evident that the slab will not have temperature distribution equal to equation (3-2) instantly. Equation (3-2) will herby be referred to as the equilibrium distribution or steady-state distribution. The distribution in the time region between the exposure and equilibrium state will be determined by transient thermal analysis.

To be able to account for time effects of conduction it is necessary to apply heat diffusion theory. By considering an infinitesimal volume element and applying the theory of conservation of energy:

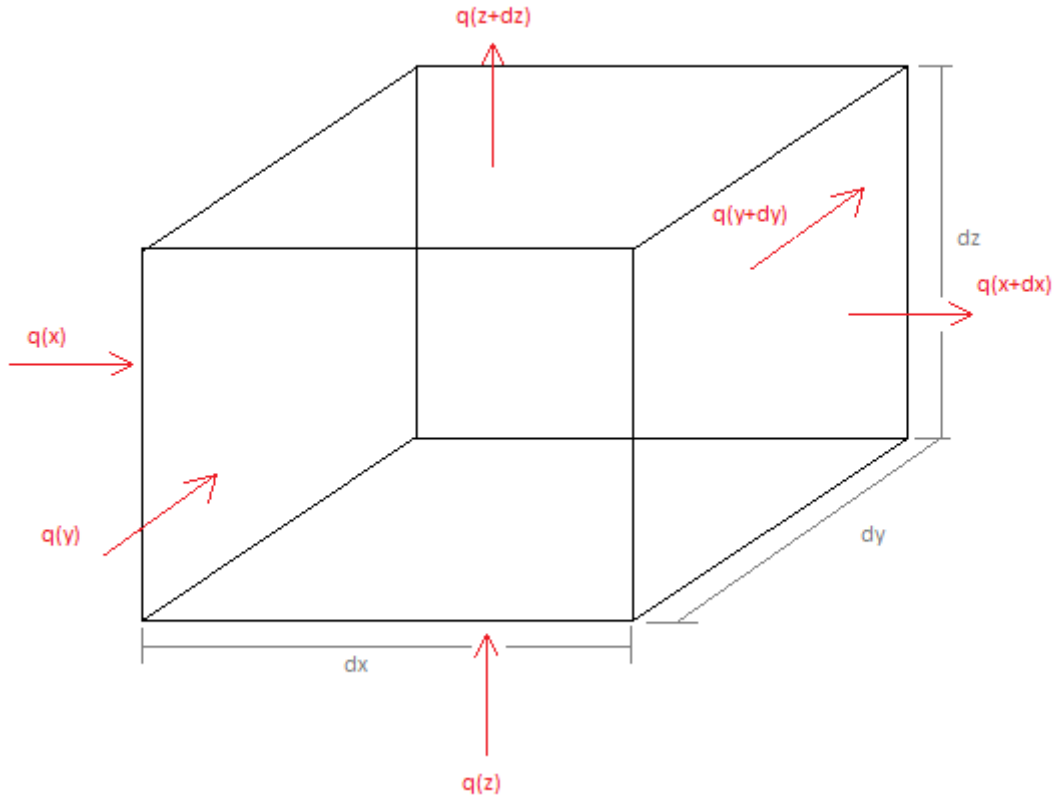

Figure 3.01 Infinitesimal volume

Assuming the material in figure 3.1is homogeneous the heat rates at the opposite sides can be found by Taylor expansion and linearizing:

$$q(x+dx) = q_{x+dx} = q_x + \frac{\partial q_x}{\partial x}dx \tag{3-4a}$$

$$q(y+dy) = q_{y+dy} = q_y + \frac{\partial q_y}{\partial y}dy \tag{3-4b}$$

$$q(z+dz) = q_{z+dz} = q_z + \frac{\partial q_z}{\partial z}dz \tag{3-4c}$$

Equation 3-4 refers to the heat rates which flow through the volume element, in addition there might be a source within the element that generates heat, and this is expressed by:

$$\dot{E_g} = \dot{q}dxdydz \tag{3-5}$$

In equation (3-5) q refer to the amount of heat generated pr unit volume. In addition to the heat generated internally the last thing to account for is the change of energy amount stored within the element:

$$\dot{E_{st}} = \rho c_p \frac{\partial T}{\partial t}dxdydz \tag{3-6}$$

By conserving of energy principle, on the rate form:

$$\dot{E}_{in} + \dot{E}_g - \dot{E}_{out} = \dot{E}_{st} \tag{3-7}$$

Substituting equations (3-4), (3-5) and (3-7) into (3-8) and simplifying:

$$-\left(\frac{\partial q_x}{\partial x}dx + \frac{\partial q_y}{\partial y}dy + \frac{\partial q_z}{\partial z}dz\right) + \dot{q}dxdydz = \rho c_p \frac{\partial T}{\partial t}dxdydz \tag{3-8}$$

Dividing equation (3-8) by the volume and substituting for Fourier's law:

$$\frac{\partial}{dx}\left(\kappa\frac{\partial T}{\partial x}\right) + \frac{\partial}{dy}\left(\kappa\frac{\partial T}{\partial y}\right) + \frac{\partial}{dz}\left(\kappa\frac{\partial T}{\partial z}\right) + \dot{q} = \rho c_p \frac{\partial T}{\partial t} \tag{3-9}$$

Then:

$$\frac{\partial^2 T}{\partial x^2} + \frac{\partial^2 T}{\partial y^2} + \frac{\partial^2 T}{\partial z^2} + \frac{\dot{q}}{k} = \frac{1}{\alpha}\frac{\partial T}{\partial t} \tag{3-10}$$

$$\frac{1}{\alpha} = \frac{\rho c_p}{\kappa} \tag{3-11}$$

The alpha term in equation (3-11) will be the thermal diffusivity of the material. Equation (3-10) is commonly known as the heat conduction equation, by setting the right side equal to zero the expression for steady-state conduction is obtained.

For the scope of this thesis the equation (3-10) will be applied in one and two dimensions, assuming no internal heat generation, leaving the following governing equations:

$$\frac{\partial^2 T}{\partial x^2} = \frac{1}{\alpha}\frac{\partial T}{\partial t} \tag{3-10a}$$

$$\frac{\partial^2 T}{\partial x^2} + \frac{\partial^2 T}{\partial y^2} = \frac{1}{\alpha}\frac{\partial T}{\partial t} \tag{3-10b}$$

Solutions for these two partial differential equations are proposed in the following chapters.

3.2.1 Analytical solution

Analytical solution for the transient thermal problem is obtained only for the one dimensional problem. The discussion for this decision will follow in the next chapters. When solving the partial differential equation it suitable to change the notation of the temperature distribution from T to u since the suggested solution will contain an alternative T, thus governing equation and suggested form of solution:

$$u_{xx} = \frac{1}{\alpha}u_t \tag{3-11}$$

$$u(x,t) = X(x)T(t) \tag{3-12}$$

Derivating and substituting equation (3-12) into (3-11), rearranging and introducing the separation constant:

$$\frac{X''}{X} = \frac{1}{\alpha}\frac{T'}{T} = -\lambda \tag{3-13}$$

Then the following ordinary differential equations are obtained:

$$X'' + \lambda X = 0 \tag{3-13}$$

$$T' + \alpha\lambda T = 0 \tag{3-14}$$

Solving equations (3-13) and (3-14) requires a set of boundary conditions and an initial condition. Solutions of the transient heat conduction with homogeneous boundary conditions are obtained by solving the above listed ordinary differential equations. The problem defined with homogeneous boundary conditions implies a steady-state condition with a temperature distribution of zero degrees over the entire model. However, the solutions for the transient thermal problem with non-homogeneous boundary conditions will be analogous to the transient thermal problem with homogeneous boundary conditions.

Homogeneous boundary conditions:

$$u(0,t) = 0 \tag{3-15a}$$

$$u(L,t) = 0 \tag{3-15b}$$

The initial condition can be represented by a function of x, describing the temperature at each point in the model:

$$u(x,0) = f(x) \tag{3-16}$$

Addressing equation (3-13) it's seen that this is an eigenvalue problem, solutions then are:

$$X_n = \sin\left(\frac{n\pi x}{L}\right) \tag{3-17}$$

And the accompanying eigenfunctions:

$$\lambda_n = \left(\frac{n\pi}{L}\right)^2 \tag{3-18}$$

Substituting equation (3-18) for the separation constant in equation (3-14) and neglecting proportionality coefficients it's assumed that the solution will be on the form:

$$T_n(t) = \exp\left(\frac{n^2\pi^2\alpha t}{L^2}\right) \tag{3-19}$$

Then the boundary conditions are met, the remaining initial condition will be fulfilled by representing the solution as a series where choosing coefficients to meet the initial conditions, thus:

$$u(x,t) = \sum_{n=1}^{\infty} c_n \exp\left(\frac{n^2\pi^2\alpha t}{L^2}\right)\sin\left(\frac{n\pi x}{L}\right) \tag{3-20}$$

The coefficient c in equation (3-20) will be determined by:

$$u(x,0) = \sum_{n=1}^{\infty} c_n \sin\left(\frac{n\pi x}{L}\right) = \mathrm{f(x)} \tag{3-21}$$

$$c_n = \frac{2}{L}\int_0^L f(x)\sin\left(\frac{n\pi x}{L}\right)dx \tag{3-22}$$

When addressing the transient thermal problem with non-homogneous boundary conditions the steady-state condition in equation (3-2) needs to be accounted for. Assuming the total temperature distribution will be a combination of the steady-state distribution, v, and the transient distribution, w. The thermal problem will then be redefined as:

$$u(x,t) = v(x) + w(x,t) \tag{3-23}$$

$$(v(x) + w(x,t))_{xx} = \frac{1}{\alpha}(v(x) + w(x,t))_t \tag{3-24}$$

The steady-state condition is linear and only dependent on x as seen in equation (3-2). Thus the problem in equation (3-24) reduces to equation (3-11) and the solution will be carried out analogous to the solution derived above.

The final solution will be somewhat different as the steady-state condition needs to be represented, thus:

$$u(x,t) = T_1 - \frac{T_1 - T_2}{L}x + \sum_{n=1}^{\infty} c_n \exp\left(\frac{n^2\pi^2\alpha t}{L^2}\right)\sin\left(\frac{n\pi x}{L}\right) \tag{3-25}$$

And the coefficient c:

$$c_n = \frac{2}{L}\int_0^L \{f(x) - (T_1 - \frac{T_1 - T_2}{L}x)\}\sin\left(\frac{n\pi x}{L}\right)dx \tag{3-26}$$

Thus the mathematical foundation for modeling the thermal distribution, by the analytical solution, during diamond wire is explained. As seen in equations (3-25) and (3-26), there will be a vast number of calculations to apply this form for the solution sought. By this reason, the solution for the two dimensional problem will not be sought.

As calculations often get quite extensive there are numerical methods which simplifies the problem some, these will be explained in the next chapters.

3.2.2 Numerical solution by FDM

Within the field of heat transfer the finite difference method is particularly popular. This is a numerical method where the body, to be investigated, is divided into nodes. Figure 3.2 shows a graphical sketch of an area divided into nodes.

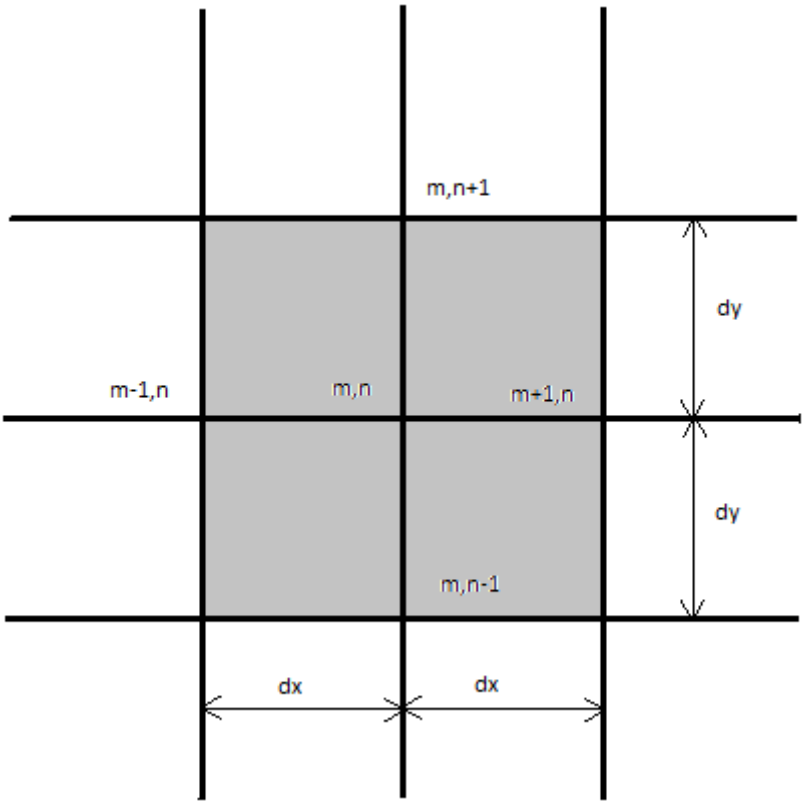

Figure 3.02 FDM representation of area

In the finite difference method the temperature gradients are treated as linear thus by numerical derivation (dx and dy represents the lengths in figure 3.2):

$$\frac{\partial T}{\partial x}\Big]_{m+1/2,n} \approx \frac{T_{m+1,n}-T_{m,n}}{dx} \tag{3-27a}$$

$$\frac{\partial T}{\partial x}\Big]_{m-1/2,n} \approx \frac{T_{m,n}-T_{m-1,n}}{dx} \tag{3-27b}$$

$$\frac{\partial T}{\partial y}\Big]_{m,n+1/2} \approx \frac{T_{m,n+1}-T_{m,n}}{dy} \tag{3-27c}$$

$$\frac{\partial T}{\partial y}\Big]_{m,n-1/2} \approx \frac{T_{m,n}-T_{m,n-1}}{dy} \tag{3-27d}$$

$$\frac{\partial^2 T}{\partial x^2}\Big]_{m,n} \approx \frac{\frac{\partial T}{\partial x}\Big]_{m+1/2,n} - \frac{\partial T}{\partial x}\Big]_{m-1/2,n}}{dx} = \frac{T_{m+1,n}+T_{m-1,n}-2T_{m,n}}{dx^2} \tag{3-27e}$$

$$\frac{\partial^2 T}{\partial y^2}\Big]_{m,n} \approx \frac{\frac{\partial T}{\partial y}\Big]_{m,n+1/2} - \frac{\partial T}{\partial y}\Big]_{m,n-1/2}}{dy} = \frac{T_{m,n+1}+T_{m,n-1}-2T_{m,n}}{dy^2} \tag{3-27f}$$

For a steady state problem the heat flow into an element would be equal to the heat flow out of an element and thus by assuming constant conductivity equation (3-10) expanded for two dimensions would have its solution by substituting for equation (3-27e) and (3-27f).

For a transient analysis the right hand side of equation (3-10) needs to be approximated. This is done by:

$$\frac{\partial T}{\partial t} \approx \frac{T_{m,n}^{p+1} - T_{m,n}^{p}}{\Delta t} \tag{3-28}$$

Then by substituting equation (3-28), (3-27e) and (3-27f) into equation (X3-10b) the following expression will be obtained (if dx = dy):

$$T_{m,n}^{p+1} = \frac{\alpha \Delta t}{dx^2}\left(T_{m+1,n}^{p} + T_{m-1,n}^{p} + T_{m,n+1}^{p} + T_{m,n-1}^{p}\right) + [1 - \frac{4\alpha \Delta t}{dx^2}]T_{m,n}^{p} \tag{3-29}$$

The superscripts, p and p+1, refers to the time increment.

Introducing the Fourier number:

$$Fo = \frac{\alpha \Delta t}{dx^2} \tag{3-30}$$

Equation (X-36) is the mathematical basis for modeling a transient thermal problem with the finite difference method. This equation will give the temperature of the interior points at selected time increments. It should be noted that a negative sum of the last bracket in equation (3-29) would break the second law of thermodynamics. Hence the Fourier number will be limited upwards at 0,25 for a two dimensional analysis. This also shows the limitations of the method. To obtain a high accuracy a high number of distance increments are needed. By limitation of the Fourier number, the maximum time interval becomes determined. Thus large amount of distance increments demands small time intervals. The result of this is that modeling with FDM might create programs which are very time consuming.

Despite the limitations of this method, it is capable of handling boundary conditions with ease. Especially changing boundary conditions will be difficult to handle with the analytical solution, this however is treated quite easy with the finite difference method. Convection is an example of complex to model boundary condition. In addition to being complex to handle, the accuracy in the established theories is given with +/-20% [7]. This implying that modeling with convection will always be an estimate as the knowledge of convection is limited.

Boundary conditions in finite difference method

For the finite difference method two different boundary conditions will be treated, this being convection and insulated lines or points.

Insulated lines or points

Insulated lines refer to a thermal barrier which allows no heat transfer trough the line. Modeling such a line is done by symmetry. If the barrier is located at m, the nodes at m+1 would disappear from equation (X-36) and the nodes at m-1 would be multiplied by two to obtain symmetry.

Convection

The empirical relationship for convection is known by Newton's law of cooling:

$$q = hA(T_w - T_\infty) \tag{3-31}$$

Here the variable, h, refers to the heat transmission coefficient, subscript w refers to wall and infinity refers to the surroundings. Equation (3-31) will have to equal the amount of heat conducted from the relevant body, and hence:

$$-kA\frac{\partial T}{\partial x}\Big]_{wall} = hA(T_w - T_\infty) \tag{3-32}$$

The finite difference approximation will be (setting the node m+1 equal to wall):

$$-\kappa\frac{\Delta y}{\Delta x}(T_{m+1} - T_m) = h\Delta y(T_{m+1} - T_\infty) \tag{3-33}$$

By setting the amount of energy conducted into the node, and the energy convected into the node equal to the internal energy of the node the following expression is obtained after some rearranging:

$$T_{m,n}^{p+1} = \frac{\alpha\Delta t}{dx^2}\left\{2\frac{hdx}{\kappa}T_\infty + 2T_{m-1,n}^{p} + T_{m,n+1}^{p} + T_{m,n-1}^{p} + \left[\frac{dx^2}{\alpha\Delta t} - 2\frac{h\Delta x}{\kappa} - 4\right]T_{m,n}^{p}\right\} \tag{3-34}$$

Thus the theory for modeling the temperature distribution during diamond wire cutting is presented.

3.2.3 Finite element method

Finite element method is a numerical method which is growing popular in several fields, also within the field of heat transfer. However, it seems that finite difference methods are more commonly used as the textbooks on heat transfer consistently uses finite difference methods [7, 10, 9].

Cook, Malkus, Plesha and Witt has proposed a formulation for using the finite element method in transient thermal analysis [14]. This method is at its core similar to the finite difference method, but instead of placing all the heat at nodes, FEM allow the heat to be distributed over the element. Accuracy then should be better, but the formulation will also increase in complexity. The proposed formulation is:

$$\left(\frac{1}{\Delta t}[C] + \beta[K_T]\right)\{T\}_{n+1} = \left(\frac{1}{\Delta t}[C] + (1-\beta)[K_T]\right)\{T\}_n + (1-\beta)[R_T]_n + \beta[R_T]_{n+1} \tag{3-35}$$

This method will also have limitations on the size of time step, this is based on the method of direct integration. This will be dependent on the value of beta in equation (3-35). If this variable is set equal to zero the method will be based on a forward difference, this is also seen from the equations as the heat vector for the next time increment is cancelled from the equation. The finite difference method proposed above is also based on a forward difference, at the same principles the finite element method will have limitations for stability on the same basis as the finite difference method. However, by setting the variable beta equal to one, the method will be based on a backward difference. Backward difference method have no limitations on size of time step, it is unconditionally stable.

Similar to the finite difference method applying boundary conditions in the finite element method should be an easy operation. As for the finite difference method this will be the main advantage.

Utilization of equation (3-35) can be done by hand, however it is usually a vast number of calculations to be performed so computer software is highly recommended. For the finite element method Matlab is a commonly used software, in terms of user friendliness ANSYS might be a better alternative as the graphical interface and the built in features allows utilization without being significantly trained.

3.2.4 Concluding remarks and reason for selection of method

In this chapter the relevant methods for analysis is presented. All of these methods have their limitations and advantages. The analytical solution is presented without the convective boundary condition, this condition will be presented at a later chapter and it will be seen that the convective boundary condition will limit the use of the analytical solution. Even if the formulation of the analytical solution seems rather elegant, it is obvious that the amount of calculation within is quite extensive. This is also the reason for the two dimensional problem is not considered.

The finite difference method has its main advantage in being extremely easy to use regardless of boundary conditions, the problem with the presented forward finite difference method is it s limitations due to the Fourier number. This can be compensated for by using the backward difference method and it still would be able to treat boundary conditions without problems. However, the syntax of the calculation would be completely different as the nodal temperatures would be calculated simultaneously by Gaussian reduction or similar. Thus implying the user friendliness is compromised.

The finite element model will be discarded for modeling in this thesis due to lack of available literature and the strong position the finite difference method hold in the field of heat transfer.

The final temperature distribution will be modeled by a 2-dimensional FDM with forward difference. Initially it was assumed that it would be possible to use the one dimensional analytical approach for the cut path and then apply the distribution from this analysis as the initial temperatures for a two dimensional FDM analysis with increased distance increments. This will be argumented for in the following sections and the analytical approach will also be presented in detail.

3.3 Assumptions made in idealization of the model

The aim in this thermal analysis is to determine whether diamond cutting can be safely executed in the presence of an explosible atmosphere. The key factor for this chapter is to determine the surface temperatures obtained during cutting.

In the previous chapters both the physical expressions, in terms of maximum temperatures generated, and the mathematical expressions, in terms of thermal conduction theory, is explained. This theory is the basis for a simulation of the cutting process.

The model needed for this simulation is explained as follows:

By considering a slab of rectangular cross-section, the diamond wire will cut through this slab as shown in figure 1.21, sketch of a diamond wire set up. The arc of the wire will be extremely difficult to recreate, and thus the model will by idealized by assuming the cut path to be perfectly straight.

Also, the in-feed velocity for diamond wire cutting will be constant. For modeling purposes this motion will be discretisised. Discretisation is a source of error as the heat source then will be modeled as stationary instead of moving. The distance increments are chosen to be quite small, which would compensate to some extent for the discretisation of the moving heat source and provide a higher confidence level within the model.

3.3.1 The initial approach

The one dimensional cut sequence will be modeled by the analytical approach. The heat conduction to the sides will be equal to the heat conduction straight ahead of the diamond wire cutting direction (This will be proven in the next chapter).

Discretisation of the in-feed velocity will be performed by setting the in-feed velocity equal to the distance increments, thus one passing of the wire will be done in one second.

After each pass the model will be redefined by removing one distance increment. The temperature distribution from the thermal analysis will then be used as initial condition for the next time increment. This also means that the integral from equation (3-26) will not be evaluated analytically as the functional expressions are not obtained.

The boundary conditions are modeled by keeping the side, at which the wire is present at, at the maximum temperature generated by chip formation. The opposite side will be calculated by Newton's law of cooling. Steady-state conduction will then be treated as a linear function between the boundaries.

The first initial condition will equal the ambient temperatures for all nodes except for that node representing the diamond wire.

After the analytical approach has been used to simulate a cut the results will be used as initial conditions for a two dimensional analysis performed according to the presented forward difference FDM technique in the previous chapter. To compensate for the stability requirements the distance increments will be chosen to obtain a stable calculation with a time increment of 1 second.

3.3.2 The final approach

The convection effects and its effect on the analytical calculation led to a discarding of this method, this will be shown in the following sections. This led to utilization of the FDM approach for the entire simulation. The assumptions made for this operations are identical to those made above, except for the increasing of the distance increments, thus simulations became quite time consuming.

3.4 Validation of assumptions

3.4.1 Two-dimensional analysis reduced to one-dimensional analysis

Figure 3.3 shows a representation of a diamond wire cutting process in the cross section of a slab.

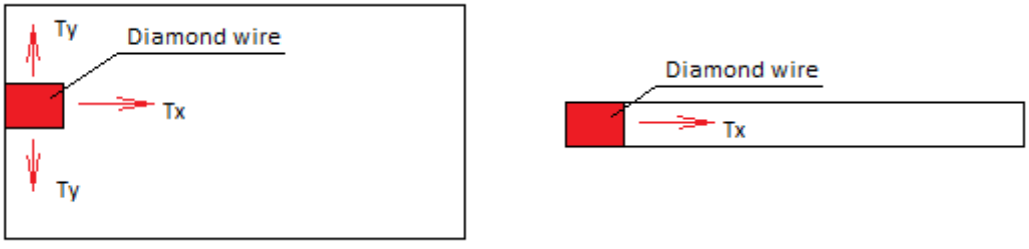

Figure 3.03 2-dimensional representation of cut and 1-dimensional representation of cut.

The red cube representing the diamond wire is modeled as a uniform heat source containing the maximum temperature as calculated in appendix A. For the one dimensional model the horizontal boundaries will be treated as insulated lines, i.e. there will be no heat flow through these sides. Since this is a poor estimation of the reality compensating measures will be applied.

The whole idea of modeling in one dimension instead of two is that proposed model for two dimensional analysis is time consuming to a non-satisfactory extent. This is quite the opposite for most other applications as a numerical method is usually applied to reduce computing time. This however, is not the case for abrasive cut-off operations.

Hence two dimensional analysis is performed to calculate the steady-state loading of a diamond wire cutting process. The proposed expression for temperature rise needs to be investigated, along with the proposed energy partition.

By the use of FDM, a 200X200 node grid was established. Instead of revising the equations, the theory of symmetry was applied. For the initial condition the uniform adiabatic temperature rise was used. This temperature was then calculated by the energy partition proposed by Malkin and Guo and stated under equation (1-11).

The diamond wire supplier estimated the material removal rate for cutting in conventional steel to be 0,15 m^2/h for a diamond wire with a 13mm cross section. This is including into the model by setting the distance increment equal to the material removal rate in the x direction, and then applying the number of distance increments needed to correspond to the diamond wire diameter. The area in the model which corresponds to the diamond wire will then be modeled as a rectangle instead of a circle, which is the form it actually obtains, this will be a source of error and could possibly be reduced by reducing the height of the area.

As the distance increments are set the time increments are already determined by the Fourier number. This leads to a vast number of iterations to display one second of heat transfer.

The cutting sequence is then modeled as follows, the area in question is heated to the uniform adiabatic temperatures. The heating is modeled as a sudden temperature increase. After heating the area will cool off over the material removal rate interval which is set to one second. When the area has been cooling off for one second the actual material removal initiates. This method then implies high temperatures at the initial states of each cut, sometimes higher than the melting point. It should be noted that this is due to the backward heat generation assumed in the model.

After cooling for 1 second the temperature distribution in the cutting area is logged before applying the uniform heating of the cutting area over again. Re-applying the uniform heating will represent a new cut.

After executing this procedure for a number of times the temperature distribution will converge and the steady-state temperature is obtained.

The energy partition is then to be investigated. The uniform adiabatic temperature rise is dependent on the energy fraction entering the work piece. By performing the analysis as stated above, the energy partition which is associated with the steady state temperature should, if combined with the adiabatic energy fraction, result in the chip formation energy. Thus;

$$\left((T_{melt} - \bar{T})c_p + L_f\right)\frac{\rho}{0{,}75} = \epsilon u_{chip\ formation} \qquad (3\text{-}36)$$

In equation (3-36) the temperature difference corresponds to the difference between the melting point and the mean measured value calculated as stated above.

Solving of equation (3-36) requires iteration as both temperature difference and energy partition is unknown. After running the model stated above the following results were obtained:

Material	Steady state temperature [C]	Mean heat capacity [J/KgK]	Energy conducted to work [J/mm^3]	Energy partition
Steel	350	700	10,62	0,73
Stainless steel	726	614	6,90	0,54
Titanium	783	626	5,88	0,68
Aluminum	70	1000	3,56	0,97

Table 2 Steady state temperatures in cutting

These results were obtained by assuming a contact length of 0,1 meter and a material removal rate of 0,15 m^2/h for a 13mm diamond wire. Stainless steel however is calculated with a reduced material removal rate corresponding to 75% of the material removal rates for the remaining work pieces. This has a correlation with the statements in the introduction to this chapter were it is stated that the removal rate for stainless steel is less than for steel. Table 2 does not verify this statement, rather on the contrary it supports that stainless steel will have a much higher removal rate. Based on this no conclusions towards the removal rate will be based on the above shown results, hence material removal rates for titanium and aluminum was set equal to the removal rate of steel. The steady temperatures in table 2 supports the first statement as the steady state temperature for cutting in stainless steel is significantly higher than for cutting in conventional steel. The convergence of the temperatures is shown in figure 3.4. The Matlab program for calculating these values are enclosed in appendix C.

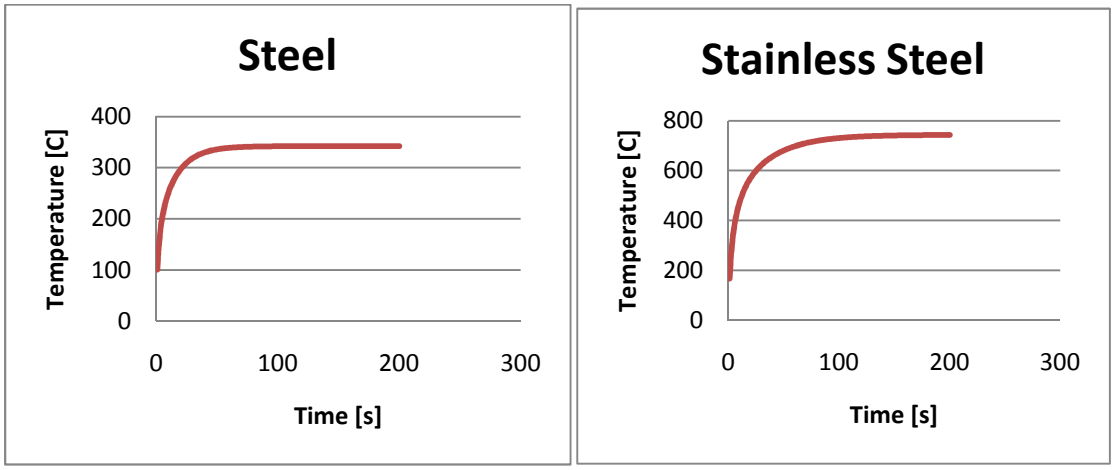

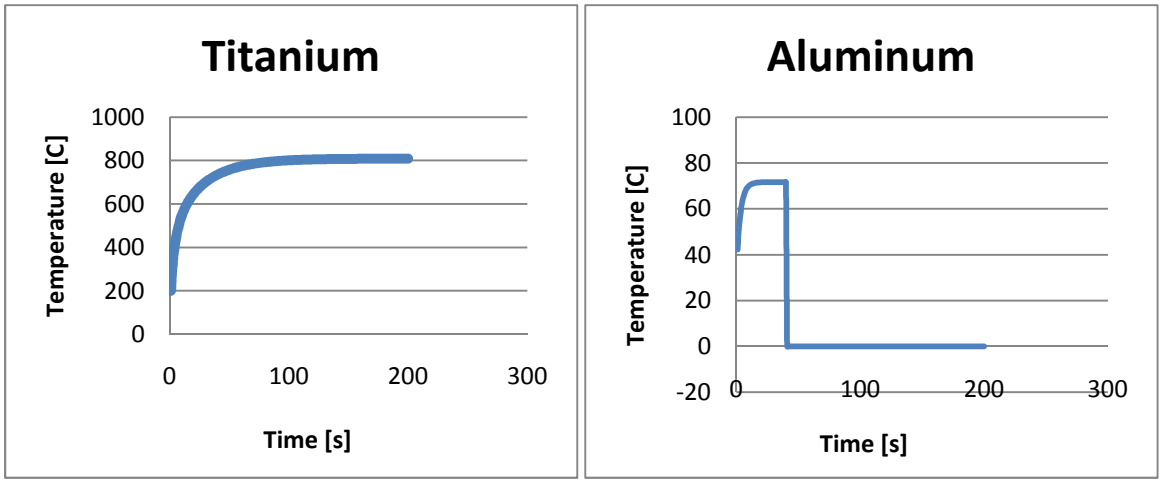

Figure 3.04 Convergence of steady state temperatures

In terms of energy partition the obtained results differ quite from the value proposed by Malkin and Guo and listed in equation (1-11). However, their work was mainly concerned with high speed abrasive cut-off. Diamond wire will also be such a technology, however, due to the thickness of the wire and the contact lengths it will be regarded as slow in terms of in-feed compared with conventional high stock removal grinding processes. Nevertheless diamond wire has a material removal rate approximately 5 times the material removal rate for conventional high stock removal grinding.

A high stock removal process with material removal rate of 600mm^2/s over a 2mm wide cut and a contact length of 0,1 meters was investigated by the procedure stated above and the following results were obtained:

Material	Steady state temperature	Mean heat capacity	Energy conducted to work	Energy partition
Steel	843	700	7,73	0,53

Table 3 Steady state temperatures in high stock removal grinding

The results from table 3 shows a rather good correlation with the values proposed from Malkin and Guo.

Table 2 shows the steady state temperatures for cutting in steel to be of a rather low temperature, at least compared to conventional abrasive techniques. However, it shows an alarmingly high energy partitioning value. This means that the amount of material surrounding the cut zone will be of high interest when assessing temperatures in diamond wire cutting. This phenomenon will be investigated further in the next chapter along with convection effects.

For modeling in one dimension the calculated steady state temperature should be used as the initial temperature. It should be noted that the contact length will have great influence on the steady state temperatures. Based on the next section, this effect is not obtained in this thesis.

The accuracy in performing a heat analysis like stated above is not demonstrated in this thesis. For most fields in engineering numerical methods are adapted with great confidence, for an operation like diamond wire cutting little research has been performed on temperature development. The

method proposed is applied to a great extent in other fields of engineering, and hence it is assumed to be reliable. However, the input fluxes in diamond wire are more complex compared to uniform heating of a slab. The reason for this complexity is its continuous transfer inwards in the work piece combined with a longitudal movement.

Actually the heat loading should have been modeled at even smaller increments. This was not performed in this analysis as the method as executed already is quite time consuming. This also is the main concern by applying the FDM with a forward difference. On the other side, Malkin and Guo emphasizes that the chip formation energy is the main heat source, and when material removal rates are high the other contributions in terms of rubbing and plowing are negligible.

3.4.2 Convection effects

The phenomenon of convection has been subject for research for many years. However, specialists within the field of heat transfer claims that present knowledge of convection still has an amount of uncertainty corresponding to ±20% [7].

Regardless of the uncertainty the convective boundary condition is possible in both analytical and numerical approaches. In this chapter the convective boundary condition will be modeled for both approaches and compared against each other, at the same time this will also give a comparison of the two approaches in general.

The boundary condition is expressed in equation (3-32) and the nodal expression for one dimensional analysis is obtained from equation (3-33) after some rearranging:

$$T_{m+1} = \frac{T_m + \frac{h\Delta x}{\kappa} T_\infty}{1 + \frac{h\Delta x}{\kappa}} \tag{3-37}$$

The model chosen for comparison is from Applied Thermodynamics by Eastop and McConkey [9], the problem is as follows:

Cooling of a large steel plate, initially at 800 ^oC, in air at 25 ^oC. Assume heat convection coefficient of 125 W/m^2 K.

This problem is easily modeled in Matlab producing the listed result in the Eastop and McConkey experiment. Modeling the same problem with the analytical approach involves some modifications to the proposed approach in the previous chapter.

By following the approach as described by Incropera, DeWitt, Bergman and Lavine in Fundamentals of heat and mass transfer the governing equations (3-10a) will be nondimensionalized. This leads to the introduction of the following parameters:

$$\theta^* = \frac{T - T_\infty}{T_i - T_\infty} \tag{3-38}$$

$$x^* = \frac{x}{L} \tag{3-39}$$

$$t^* = \frac{\alpha t}{L^2} \tag{3-40}$$

The problem is modeled with the theory of symmetry about the line at the half width of the plate, thus L in the equations above is set equal to the half width. Equation (3-38) represents the ratio between the temperature difference and the maximum possible temperature difference. The non-dimensionalized time variable is identical to the Fourier number as presented in the previous chapters.

The modified governing equation then becomes:

$$\frac{\partial^2 \theta^*}{\partial x^{*2}} = \frac{\partial \theta^*}{\partial t^*} \tag{3-41}$$

With the modified initial condition:

$$\theta^*(x^*, 0) = 1 \tag{3-42}$$

The boundary condition at the centerline of the slab:

$$\left.\frac{\partial \theta^*}{\partial x^*}\right]_{x^*=0} = 0 \tag{3-43}$$

And the boundary condition at the surface of the slab:

$$\left.\frac{\partial \theta^*}{\partial x^*}\right]_{x^*=1} = -Bi\theta^*(1, t^*) \tag{3-44}$$

Equation (3-44) introduces a new variable, the Biot number, Bi. This value represents the ratio between the temperature difference within the solid and the temperature difference between the surface and the surroundings. Having a plane wall with temperatures T_1 and T_2 at the boundaries the relationship for the Biot number will be:

$$\frac{T_1 - T_2}{T_2 - T_\infty} = \frac{hL}{k} = Bi \tag{3-45}$$

In the above expression variable h represents the heat transfer coefficient and the variable k represents the thermal conductivity of the solid. This variable will prove to be of high importance later on in this chapter.

The modified governing equation will be solved in the same procedure as described for the original governing equation in the previous chapters and the solution would be, as proposed by Incropera, DeWitt, Bergman and Lavine [Fundamentals of heat transfer]:

$$\theta^* = \sum_{n=1}^{\infty} c_n \exp(-\zeta_n^2 \mathrm{Fo}) \cos(\zeta_n \mathrm{x}^*) \tag{3-46}$$

Where:

$$c_n = \frac{4 \sin \zeta_n}{2\zeta_n + \sin(2\zeta_n)} \tag{3-47}$$

And the values of ζ_n are the roots of the following transcendental equation:

$$\zeta_n \tan \zeta_n = Bi \tag{3-48}$$

The last equation proves that modeling a transient thermal problem with convective boundaries by an analytical approach is a detailed operation. Even though the increase for each root will converge towards π there may be a lot of roots which will have to be calculated manually by iteration. It should also be noted that the increase between two preceding roots converges more rapidly with low Biot numbers, thus implying that heat conduction over a long solid will require more calculations than a short solid.

The example stated earlier in this chapter is modeled by the method described above. The FDM approach was initially modeled with the amount of increments equal to the text book, in addition another analysis were also performed this time with 100 distance increments. By assuming that the analytical solution is the correct solution, the ratio between the numerical solution is then calculated for the 6 points which was displayed in the textbook. The following results were obtained.

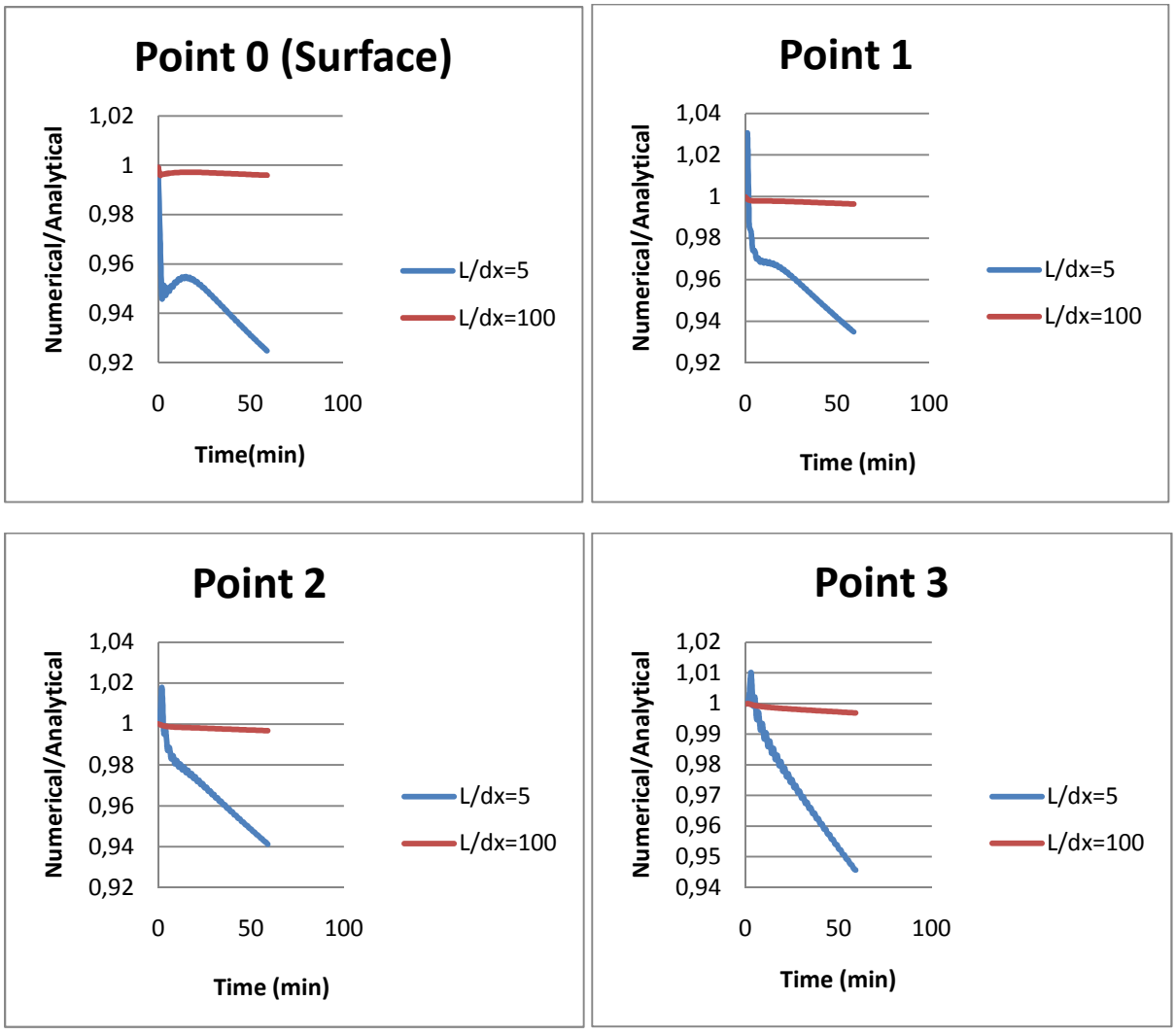

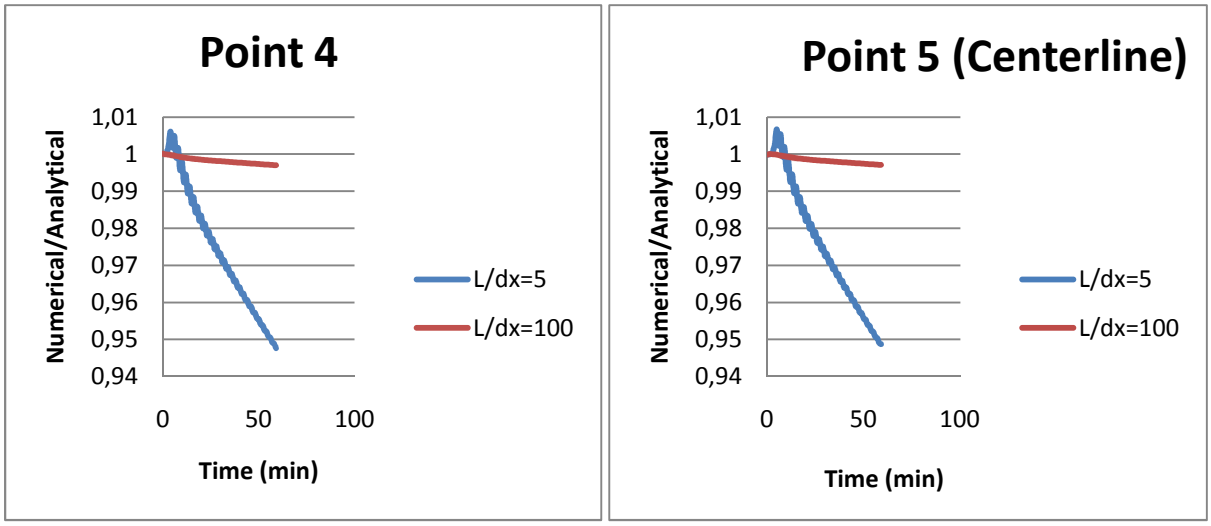

Figure 3.05 Temperature distributions in steel slab

From the results it's evident that there is an agreement between the analytical solution and the numerical solution when 100 distance increments are applied. This chapter also reveals a quite disturbing aspect of using the analytical approach. For the problem investigated the analytical approach is applied with a moderate level of complexity, this is due to the manual calculation required for the eigenvalues of the Biot equation. The technology under investigation in this thesis has a moving boundary condition, thus the Biot number will vary continuously.

Approximate values have been tried for the eigenvalues, resulting in nothing but an unstable solution. It's quite remarkable how accurate the values need to be to obtain a reliable solution. It's assumed that this problem can be solved by programming a numerical iteration syntax for finding the roots of the transcendental equation. This is not performed in the scope of this thesis.

Despite this, this chapter actually proves the reliability of the numerical solution. Of course, this is dependent on the choice of distance increments. As seen in figure 3.5, it is evident that a high number of increments are needed.

The Matlab code for determining the values displayed in Fig. 3.5 is found in appendix C.

3.4.3 Numerical stability in FDM

As stated in previous chapters the key factor to successfully modeling with the finite difference method with a forward difference is the Fourier number. Based on this, the forward difference method will be conditionally stable. The finite difference method based on a backward difference would be unconditionally stable, but the effort in calculations would be much more time consuming for this method.

For every numerical method the amount of increments would play a significant role in assuring accuracy. By choosing very small increments, as for cutting with diamond wire, the numerical stability criteria would also provide accuracy to a great extent.

Comparing the backward and forward difference methods is not performed in detail in this thesis. However, in terms of computational effort, it is assumed that the two methods would be rather

similar as the reduced computational time for forward difference is lost due to the large number of time increments relative to the backward difference approach.

There exists a correlation between the second law of thermodynamics and the numerical stability criteria in the forward difference method. The key outline of the second law of thermodynamics is that no heat can flow from a cold spot to a hot spot. By evaluating the expression for the interior points in a FDM analysis eq.(3-29) it's seen that the criterion is actually that the sign of the node to be assessed at the previous time increment cannot be negative.

By investigating the components of the Fourier number it's plausible to say that it is a comparison of an approximate temperature wave, given by the materials diffusivity constant, over the time increment against the distance increment [7]. Comparing this against the expression (3-29) it is seen that choosing the Fourier number to be 0,25, the previous node (in time) will have no effect on the node being assessed. This implies that the amount of heat contained within this node at the previous time increment would already be transferred to the surrounding nodes (in space). Thus overstepping the limits of the Fourier number would actually create a vacuum, in terms of temperature, in the heat transfer analysis as the above mentioned temperature wave will have propagated beyond the borders of the next distance increment.

Hence the Fourier number is constrained by the second law of thermodynamics indirectly, by the formulation of the finite difference method.

3.5 Description of thermal model

In the previous chapters the features of transient thermal modeling is presented. The outline of the thermal analysis is to successfully simulate the effects of a moving heat source with convection on all sides.

The philosophy is as follows:

The chip formation energy is represented by an instant temperature rise corresponding to the adiabatic temperature rise. This is a theoretical value since in reality the temperature would raise until the energy input would be equal to the chip formation energy.

After instant temperature rise the un-removed chip will "cool down" in the surrounding material until the material removal rate is obtained. This procedure will then be repeated until the wanted cut time or cut length is obtained.

In nature conductivity, density and heat capacity would vary with temperature, thus will also thermal diffusivity change with time. This then would imply a non-linear analysis. This feature is not available in the FDM with forward difference, at least not with the author's abilities and knowledge within the field of heat transfer and Matlab programming.

For finite element analysis the feature of non-linear analysis is available [14]. However, for this analysis these variables are treated as constant.

3.5.1 Analytical approach

By following the same philosophy as mentioned above the analytical approach will be based on performing a series of analysis. The total analysis will be divided into a single analysis for each in-feed increment.

The flow chart for the calculation is shown in figure 3.7. The associated Matlab code is found in appendix C.

In this approach the convection effect is not included at all. The proposed approach where it was assumed it would be possible to include this feature by revising the steady-state condition was discarding after analyzing the FDM approach. The reason is that heat will accumulate in front of the wire as it cuts through the material. This means that it will be an upward rise in the temperature ahead of the wire before it descends towards the boundary. If an analysis where to be performed by the analytical approach with the proposed modification of the boundary condition this feature would be discarded as well. Hence this approach is only included to emphasize the challenges it generates.

It is assumed that the analytical approach can be utilized for the problem in question, but the procedure should then be based on the non-dimensionalizing of the variables as shown in section 3.4.2.

This is initial an analytical approach, however the utilization in this relation would be more like a numerical solution since the time variable is treated as constant. This also means there are some conditions to regard to obtain stable solutions. For this approach this condition is to obtain consistency between the initial condition, steady-state condition and the Fourier coefficient integral.

Figure 3.07 Flow chart analytical approach

3.5.2 FDM approach – simple model

Modeling with FDM was initially performed according to the flow chart shown in figure 3.8. The associated Matlab program is found in appendix C. For this model the convection to the created sides were not included. However, it serves well for indication of the scenarios that arises with convection and the scenarios that arises when there is a small amount of material to conduct the heat away.

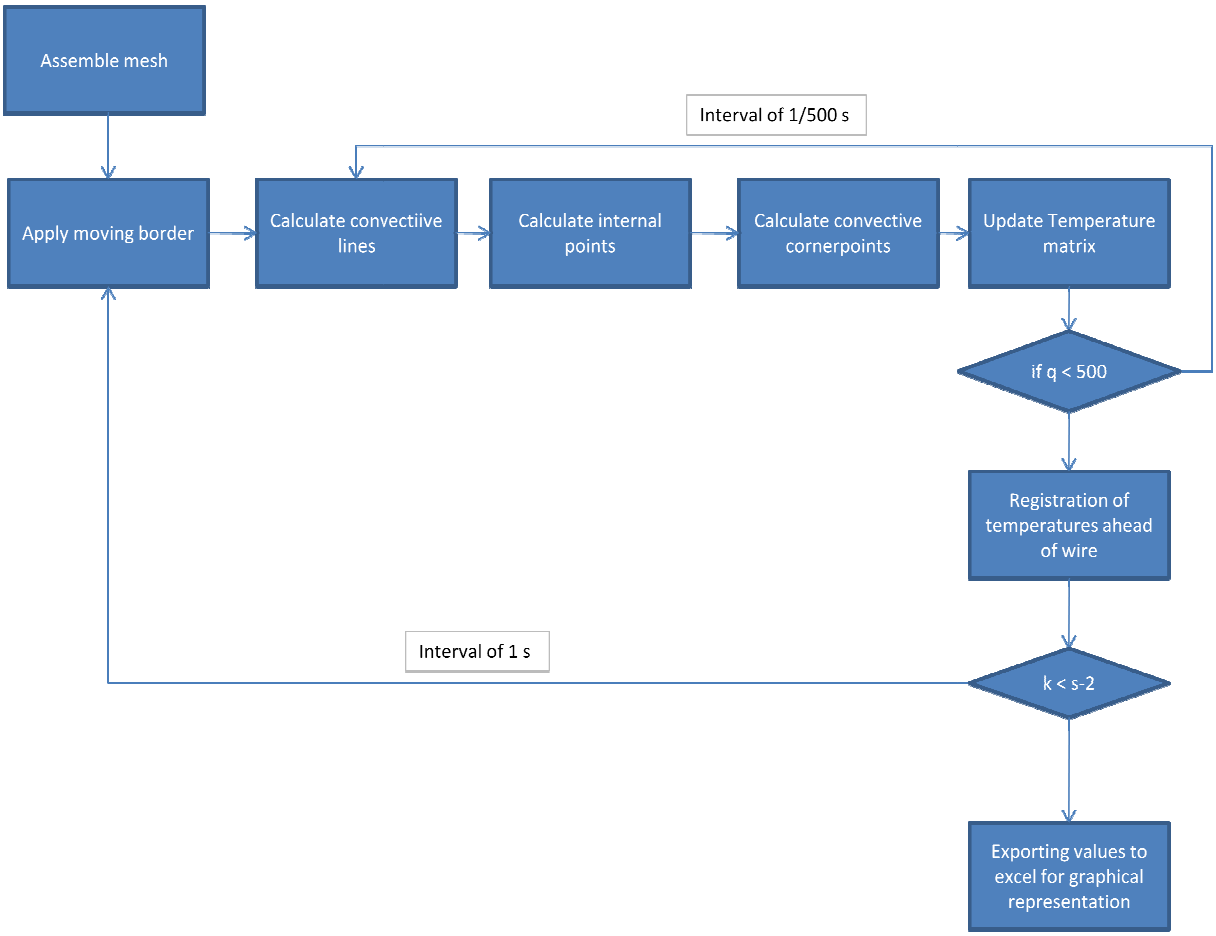

Figure 3.08 Flow chart FDM approach without convection to created surfaces

In figure 3.8 the variable k represents real time while the variable s represents the size of the work piece in increments. The variable q represents the time increments thus this program is more time consuming then real time. The obtained results for the temperature are shown in figure 3.9-3.12. For these simulations a heat convection coefficient of 125 W/m^2 K is applied, similar to the example in section 3.4.2. This coefficient is assumed to represent convection to air with movement.

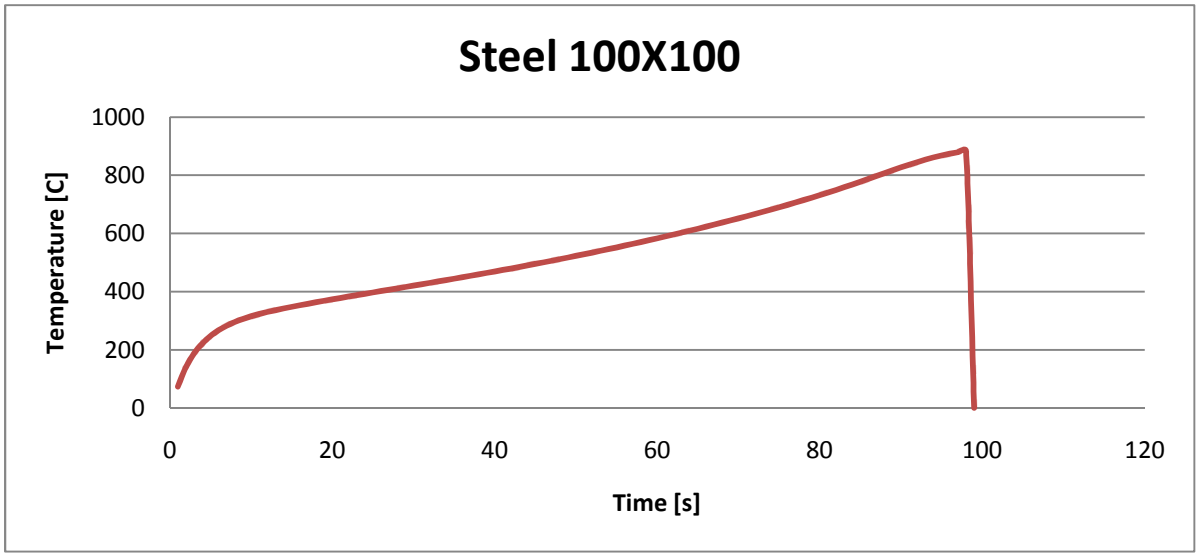

Figure 3.09 Temperature ahead of wire when cutting steel with cross section 40X40 mm (100X100 increments)

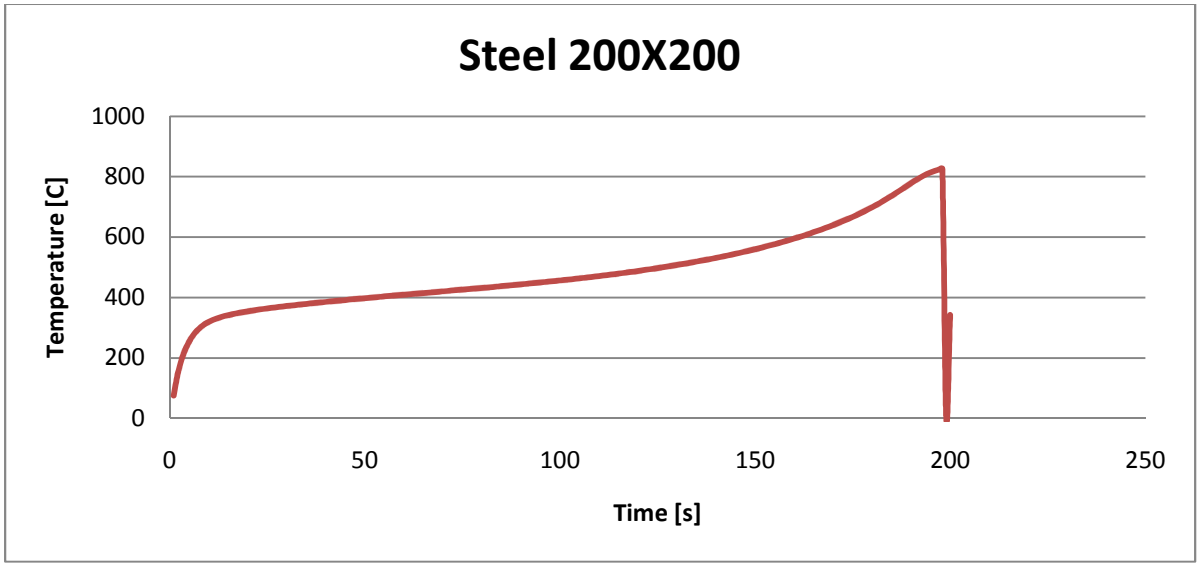

Figure 3.10 Temperature ahead of wire when cutting steel with cross section 80X80 mm (200X200 increments)

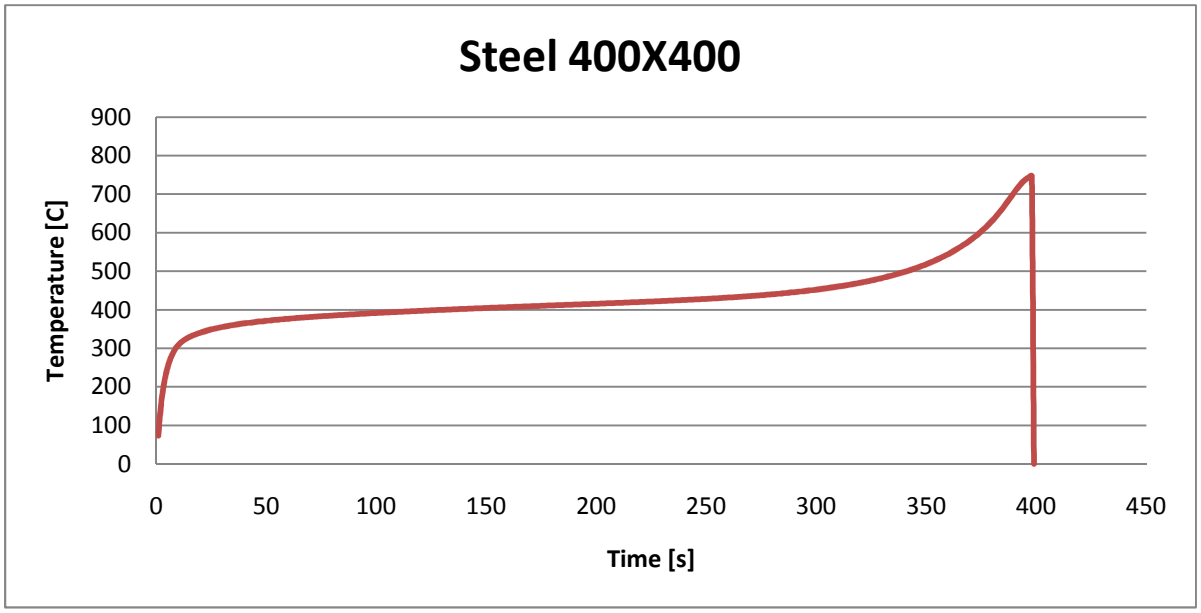

Figure 3.11 Temperature ahead of wire when cutting steel with cross section 160X160 mm (400X400 increments)

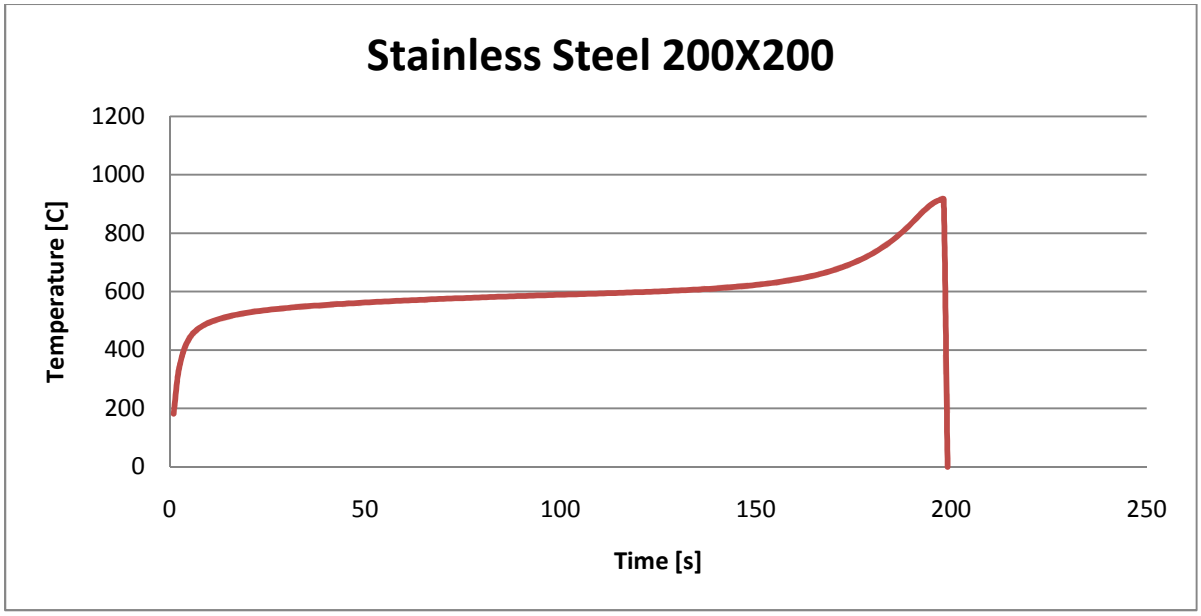

Figure 3.12 Temperature ahead of wire when cutting steel with cross section 80X80 mm (200X200 increments)

The trends are obvious in the temperatures shown in the previous figures. As there are small amounts of surrounding material the temperatures will rise as there are reduced possibilities for heat conduction. It shows that the steady state condition will not be obtained in very small cross sections as there will be a continuous temperature rise. For the largest cross section (Fig. 3.11) the steady state temperature is clearly identified. This figure shows a higher temperature than figure 3.4. The

reason for this is that the model used for calculating is developed to indicate the temperature where the work piece is unaffected by convection i.e. it represents a model where convection is absent.

From figure 3.12 it is seen that the temperature development when cutting stainless steel is somewhat different from cutting conventional steel. In addition to having a higher steady state and maximum temperature it also obtains the steady state quicker. When modeling stainless steel the material removal rate is reduced to 75% of the material removal rate used for cutting steel.

3.5.3 FDM approach – Extended model

Modifying the model in figure 3.8 to include the effects from convection from the created surfaces that arise during cutting requires some effort in programming. The model in figure 3.8 is quite easy to establish since the borders are constant during the operation. First off, the theory of symmetry needs to be applied to keep calculation time as low as possible and reducing the programming effort needed. The proposed Matlab is represented by the flow chart in figure 3.13.

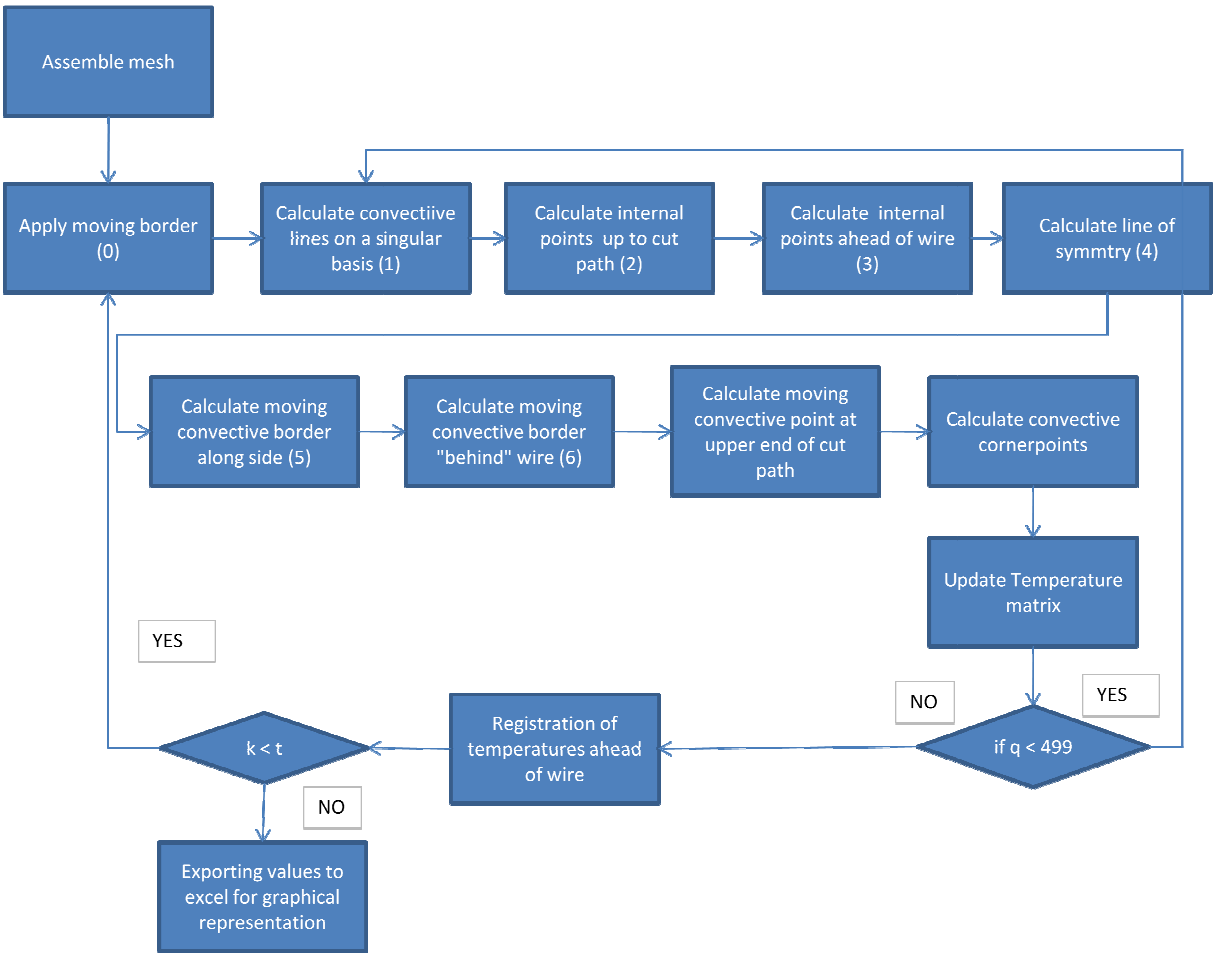

Figure 3.13 Flow chart FDM approach with convection to created surfaces

The numbers within the parenthesis in figure 3.13 corresponds to the numbering in the sketch of the work piece found in figure 3.14. The associated Matlab is found in appendix C.

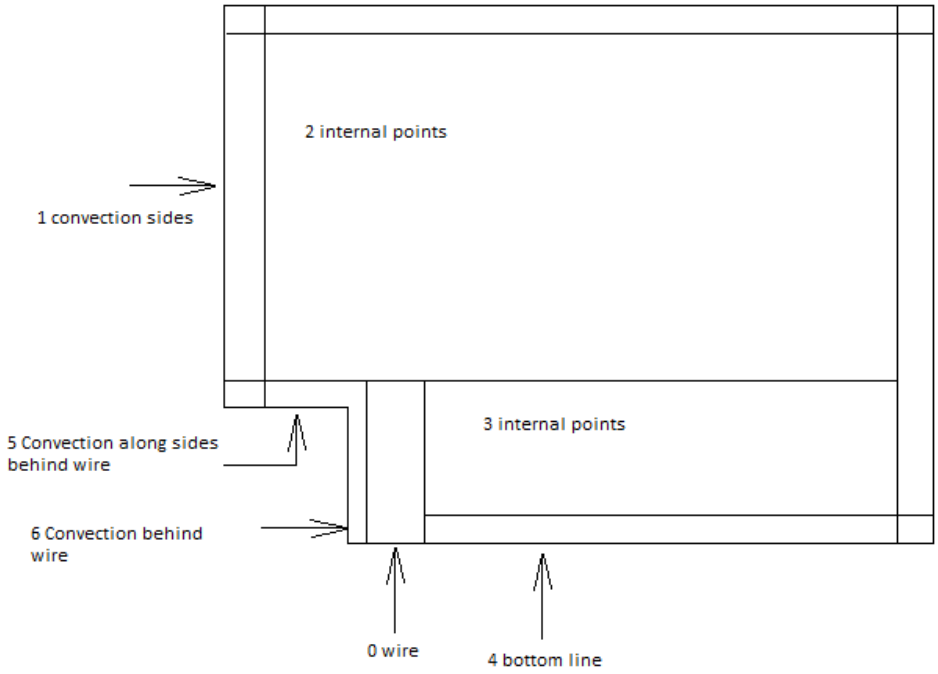

Figure 3.14 Representation of work piece for FDM analysis

The main difference between the model in figure 3.14 and 3.8 is a slightly more difficult geometry. Even small changes like this geometry difference would change the syntax of the program in a considerable matter. Instead of being able to calculate the interior nodes and the convective lines in two single loops each convective line needs their own loop as well as the interior points needs two be calculated by two loops to obtain the desired geometry.

The obtained result by using the extended FDM model is shown in figure 3.15. By comparing against figure 3.10 it's seen that the temperature will be slightly lower until the wire approaches the end. At approximately 175 s the temperature distribution in figure 3.15 will undergo a steeper increase. This is due to the added convection effects. In figure 3.9-3.12 there is no heat loss to the surroundings from the cut path, this will allow heat to be conducted into the area which in reality is removed. Since the thermal resistance in conduction is less than for convection the heat accumulation ahead of the wire will increase when including convection to created surfaces.

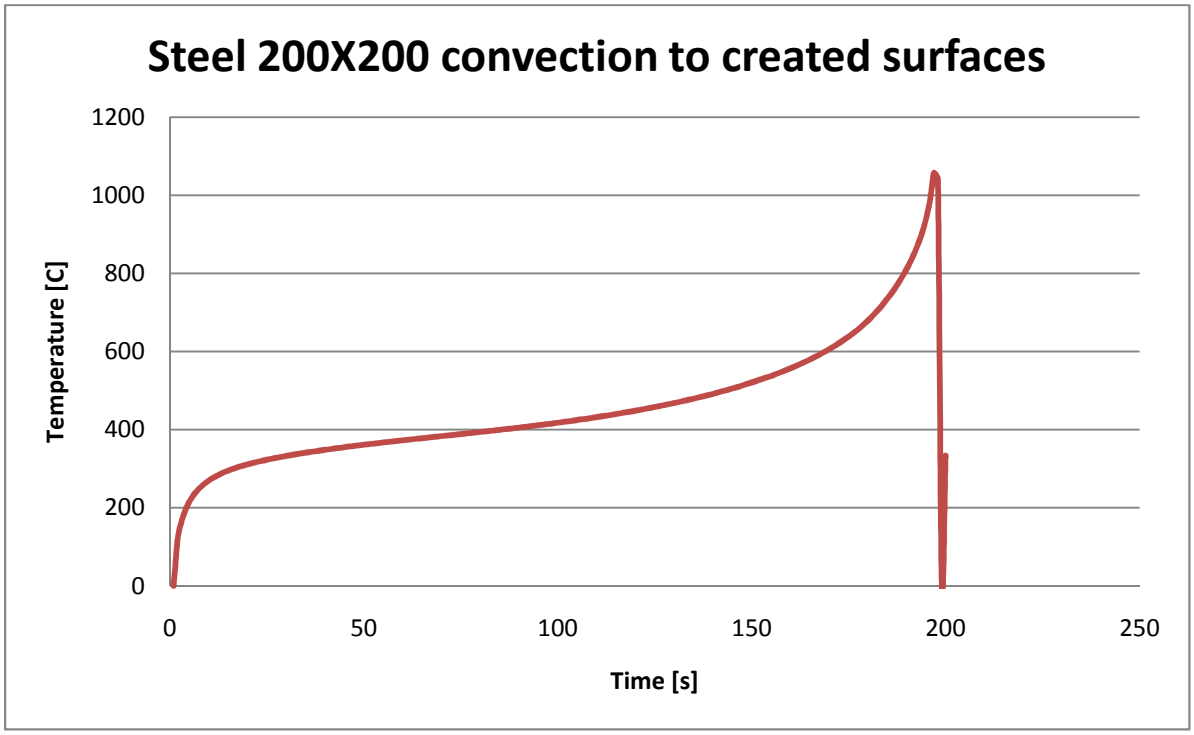

Figure 3.15 Temperature ahead of wire when cutting steel with cross section 80X80 mm (200X200 increments) and convection to all sides

3.6 Additional features to be regarded

3.6.1 Effects of water as coolant

Coolants main purpose is to reduce the temperature rise in the work piece by reducing the energy partition. The side effect of reducing the temperature is that the positive synergy effects of preheating are also lost. Hence reducing the energy partition would increase the required input energy to perform a cutting operation.

By using the model proposed in section 3.5.3 the effects of water cooling was studied by applying to different heat convection coefficients. The coefficient proposed previous for air was applied to the external sides, while a new heat convection was introduced to represent the heat carried away with water. This coefficient was applied to the created surfaces from cutting. The heat convection coefficient was chosen to be 6000 W/m^2 K, this value was found in examples from Fundamentals of heat and mass transfer [10]. Other sources claim this coefficient will be in the range of 500-10 000 W/m^2 K [I3].

The results for the average temperature ahead of wire are shown in figures 3.16-3.19.

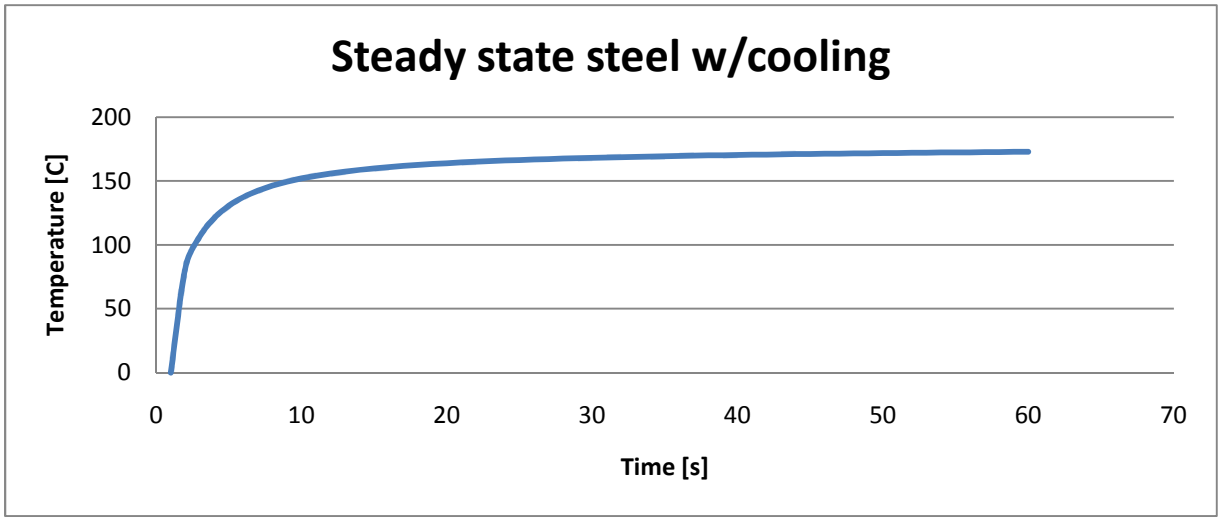

Figure 3.16 Temperature ahead of wire with water cooling conventional steel

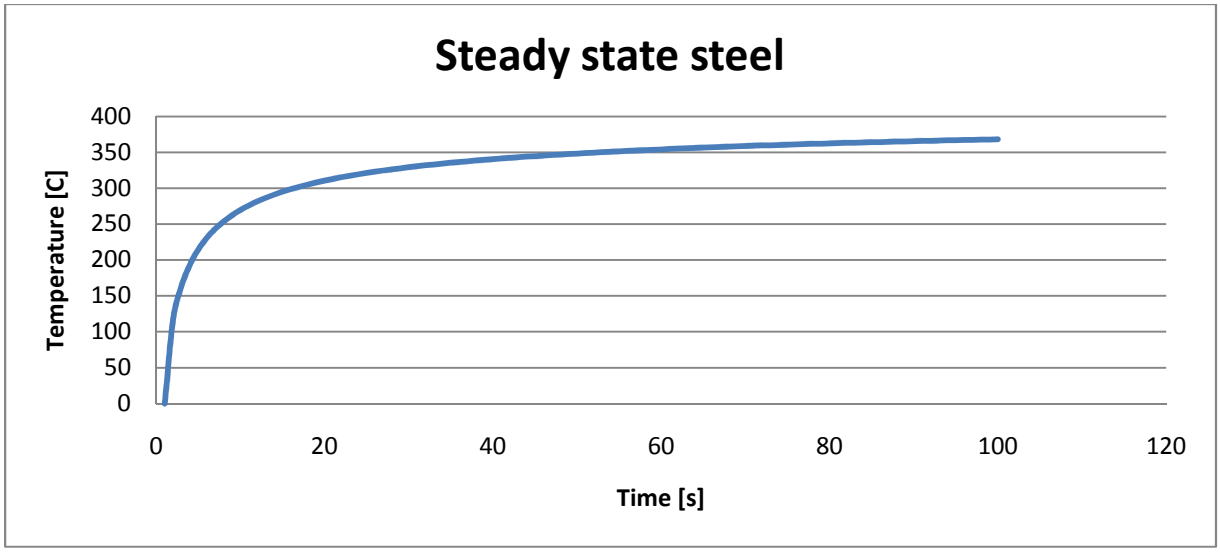

Figure 3.17 Temperature ahead of wire without cooling conventional steel

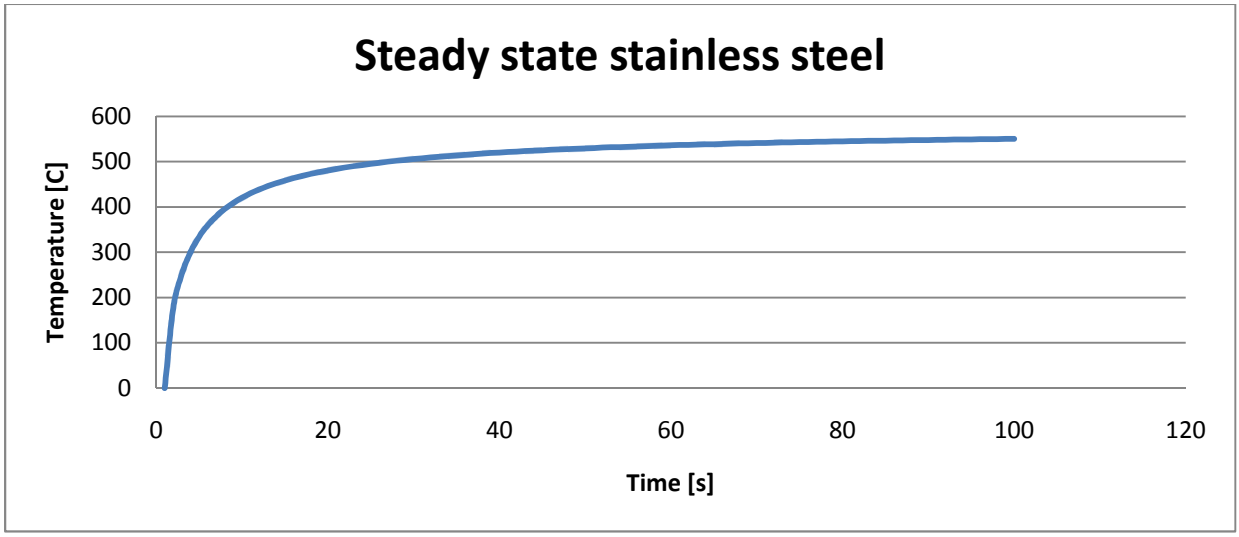

Figure 3.18 Temperature ahead of wire without cooling stainless steel

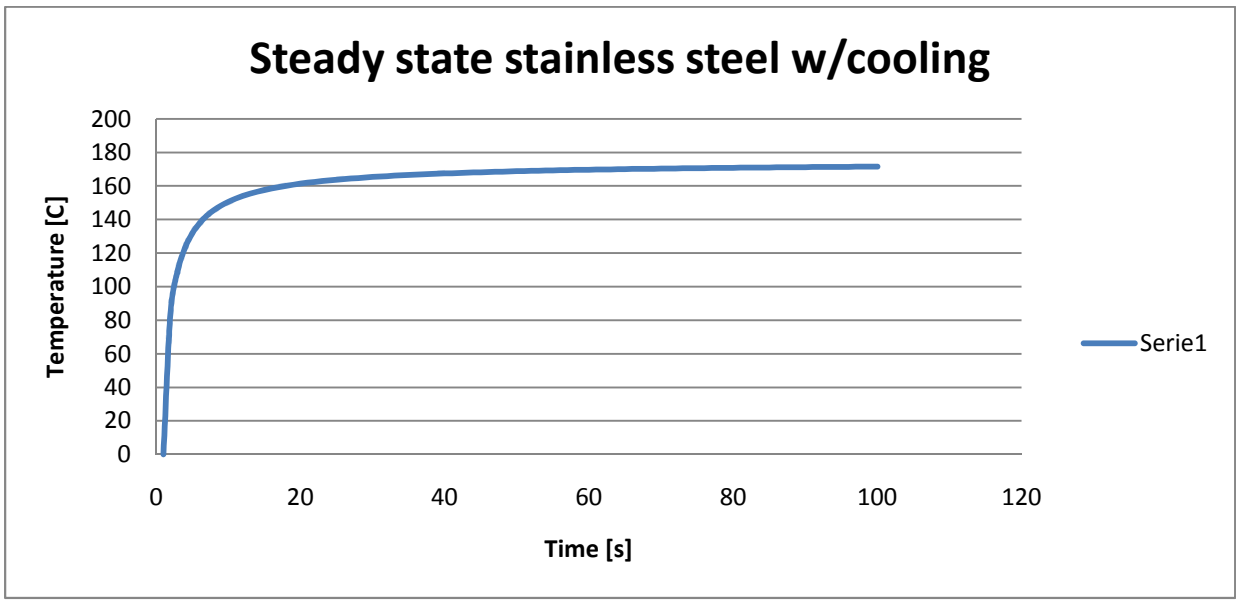

Figure 3.19 Temperature ahead of wire with water cooling stainless steel

Comparing figure 3.18 and 3.19 it's evident that the effect of cooling is significant, for stainless steel the steady state temperature decreases to below 30% of the steady state temperature for stainless steel. For conventional steel there is a reduction of approximately 50%, hence the effect is not that extreme, but still significant.

The reason for the difference in cooling effect is assumed to be the materials thermal diffusivity. Stainless steel will have a significantly lower value for this parameter, thus the heat is not conducted into the steel that easily. This will then create a higher temperature gradient between the work piece and the coolant, which will imply a more rapid heat transfer.

When comparing figure 3.19 and 3.17 the results are quite interesting since they both seem to converge against the same temperature.

At the introduction to chapter 3 it was stated that stainless steel would have approximately 75% of the material removal rate for cutting steel. In section 3.4.1 it was stated that the reduced material removal rate could not be supported by the results from table 2. The results in figure 3.19 are obtained by applying a reduced material removal rate and since the chip formation energies are quite similar the statement seems to be plausible.

3.6.2 Effects of shearing fluids

There are two main groups of shearing fluids; coolants and lubricators. The coolant water is presented in the previous chapter.

The main purpose for lubricators is to reduce friction. The potential in the reduction of friction is quite extensive for a cutting process. The chip formation consists of 33% friction in the interface between the grain and chip. This will also have a significant effect on the temperature rise due to cutting.

The rubbing forces will also be greatly affected by lubricating fluids, the effects of rubbing and wear flats is presented in the next chapter. In addition the lubricating fluid will also have a cooling effect as it is applied continuously and hence will transport heat in form of convection.

There exist a large variety of lubricators for machining, often they are custom built to enhance specific features of an operation [24]. However, their main disadvantage is that they are pollutive. Hence applying such fluid in uncontrolled environments would propose an environmental hazard.

3.6.3 Effects of wear flats

With reference to equations (1-4) and (1-4) the effects from wear flats can be estimated. By using the same line of reasoning that is found in equation (1-7) an expression for the specific rubbing energy can be derived.

The equations mentioned above are based on surface grinding of subjects. However, the geometrical differences between surface grinding and diamond wire cutting does not have any effect on these equations.

Since the specific rubbing energy would be the ration between the rubbing power and the material removal rate and the rubbing energy would be the product of the tangential rubbing force and the wire speed the following expression can be derived:

$$u_{Rubbing} = \frac{F_{t,rubbing} v_{wire}}{MRR} \tag{3-49}$$

In this equation the variable MRR would represent the material removal rate in mm^3/s.

For cutting in steel the MRR is assumed to be 0,15 m^2/3600s which corresponds to 541 mm^3/s.

The rubbing force is then to be assessed. The friction factor for grinding in steel usually lies between 0,2-0,59 [8]. From conventional textbooks friction coefficients for steel against steel is 0,6 [23]. It should also be noted that the friction coefficient would decrease after initiation of the wear flat mechanism as the whole problem source is polishing of cutting grains. Steel surfaces which have a thin layer of lubricants in between the surfaces could have the friction coefficient reduced to 0,05 [23]. This indicates the huge advantages that can be obtained by using lubricating shearing fluids. For this analysis a friction coefficient of 0,4 is assumed.

Equation (1-7) is based on the average contact pressure over the grinding zone and multiplying it by the effective contact area. Since the forces are easily obtained by assessing the hydraulic cylinder in figure 1.21 assessing the pressure is unnecessary. The pulley block from the same figure indicates the

wire is cut 4 times. Based on the pressure from the cylinder, which is 180 bar, the wire force would be approximately 9,5 kN (13 mm wire diameter).

The contact width is estimated to be 5 mm. This is based on a geometrical analysis of the wire as the in-feed is set to be 0,4 mm. This is represented in figure 3.6

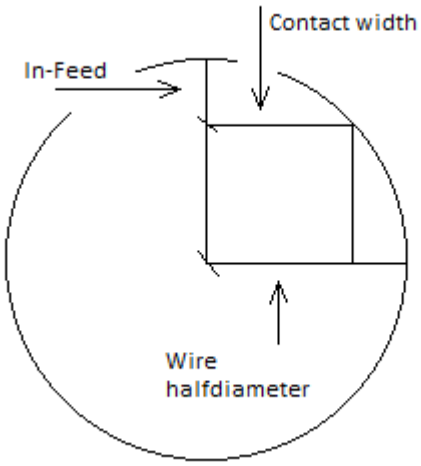

Figure 3.06 Geometrical representation of diamond wire cross-section.

By applying the above mentioned load the obtained results for forces and specific rubbing energies are shown in table 4. The calculation of the adiabatic temperature rise is based on equation (1-10) by setting the energy partition equal to 1 as there is actually no material removal performed by this mechanism. This also means that this is a theoretical value, and the real effect inflicted by wear flats will have to be assessed in combination with the procedure for energy partition in section 3.4.1.

Amount wear flat	Tangential rubbing force [N]	Specific energy [J/mm3]	Adiabatic temperature rise [C]
0,00	0,00	0,00	0,00
0,01	36,00	1,80	326,80
0,02	72,00	3,59	653,60
0,03	108,00	5,39	980,40
0,04	144,00	7,19	1307,19
0,05	180,00	8,98	1633,99
0,06	216,00	10,78	1960,79
0,07	252,00	12,58	2287,59
0,08	288,00	14,37	2614,39
0,09	324,00	16,17	2941,19
0,10	360,00	17,97	3267,99

Table 4 Effects of wear flats

According to Malkin and Guo the maximum amount for wear flats would be 8% [1]. At this partition it is assumed that the temperature rise would degrade the bonding material to that extent that the pull

out mechanism would initiate. For diamond wire it is seen that a wear flat amount of 2-3% would cause a temperature rise so intense that the work piece would start to melt.

Wear flats is not commonly known problem for diamond wire, at least not to that extend which is presented above. The reason for this is the superior hardness found in diamond grains. Thus, micro fracture and pull out mechanisms would be dominating at a much higher rate than for conventional grinding.

However, the effect of clogging is more or less identical to wear flats in terms of temperature rise. The rate of clogging is unknown, but it is assumed to be slow enough for the operator to take preventing measures before it escalates to be problematic.

3.7 Validation of model

Thermo graphical images have been captured for cutting in conventional steel with and without cooling. The test performed was initially meant as a decision foundation for acquiring an IR camera and the cameras ability to detect sparks was tested. Since the test was performed with another intention than measuring the surface temperatures and relating these to the material removal rate and consumed power the comparison between the proposed model and captured images will not provide a full validation. Figure 3.20 and 3.21 shows images of cutting in steel without cooling.

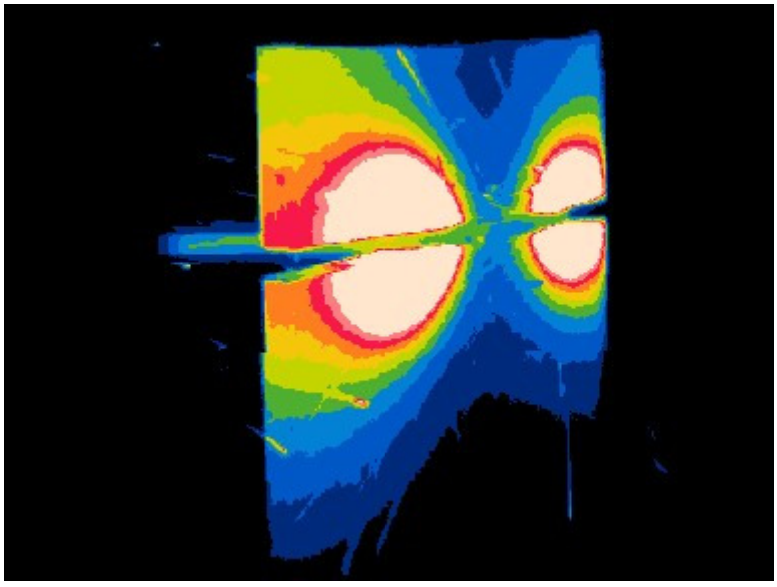

Figure 3.20 IR image of cutting of steel without cooling

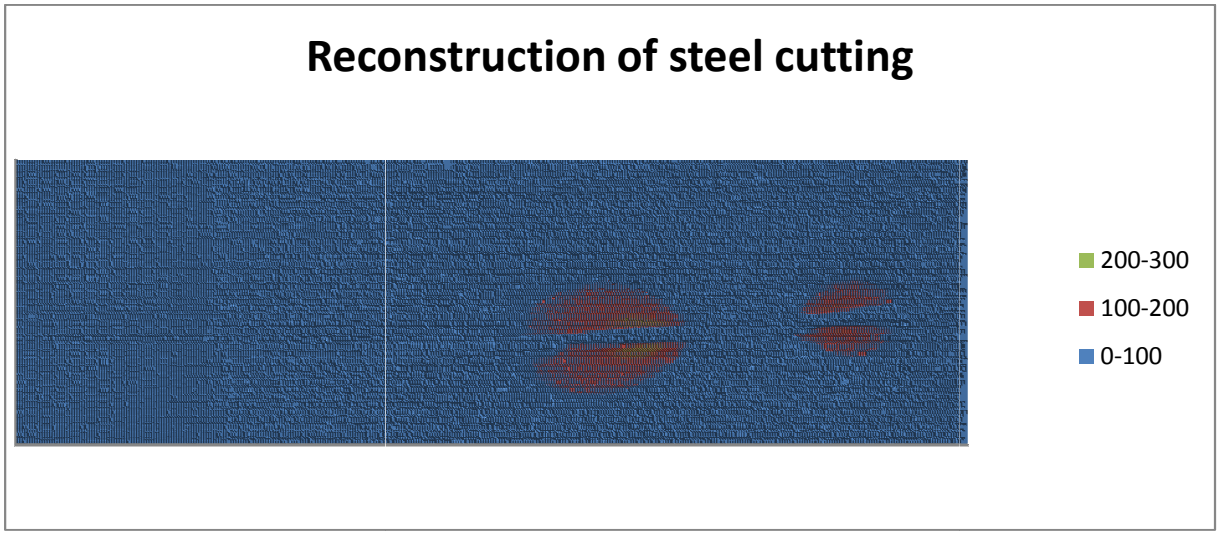

Figure 3.21 Reconstruction of IR image from figure 3.20

The reconstruction in excel is based on a set of temperature loads which was obtained from the thermo graphical camera. The maximum temperature was read to be 273 degrees Celsius and is located within the green spot in figure 3.21. This image can be compared to results from the numerical model as shown in figure 3.22. The numerical model does not represent the entire work piece as it is modeled by symmetry. The blue section at the bottom left corner represents the cut path.

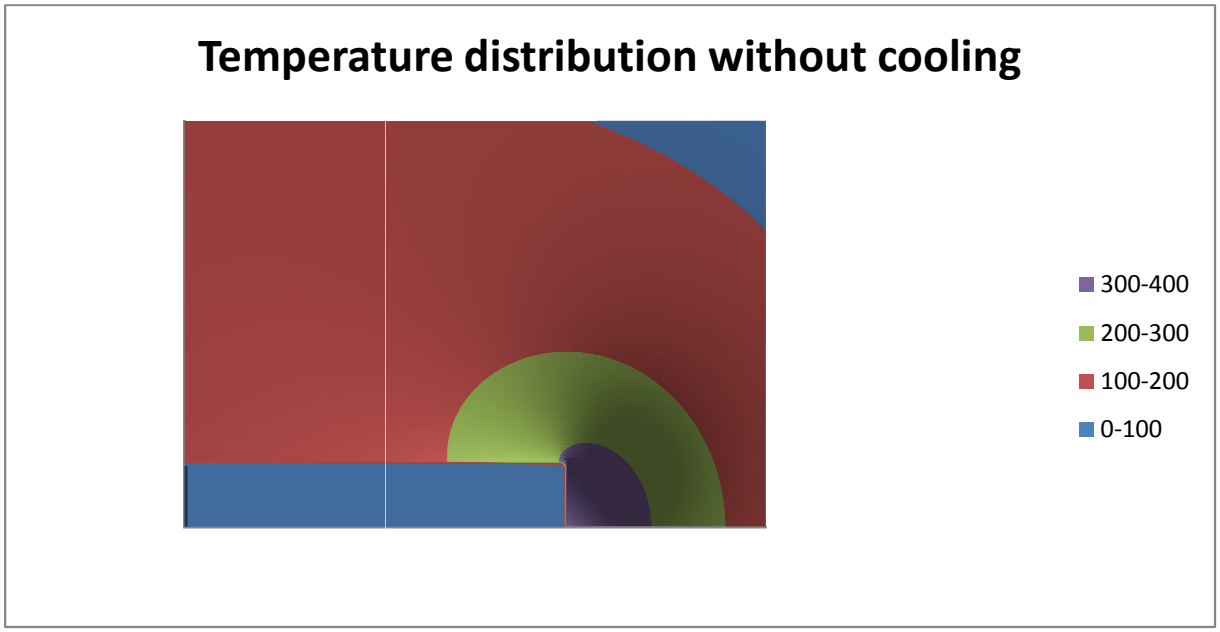

Figure 3.22 Temperature distribution cutting steel without cooling from numerical model

The contact length for the cut which is imaged in figure 3.20 is approximately 0,08 – 0,12m. It's seen that the temperature from figure 3.21 is slightly less than what is observed from the numerical model. This is to be expected as the numerical model is assumed constant in the z-direction and hence the convection effects from the free surface, which would cause a temperature decrease, is not included.

The maximum temperature ahead of the wire in figure 3.22 is not seen in figure 3.20 or figure 3.21. There could be several reasons for this to happen, the assumed reason is that the wire/work piece interaction does not occur in a plane perpendicular to the free surface as assumed in the model. This would cause the temperature to vary with the z-coordinate (assuming the z-axis to be normal to the plane presented in figure 3.22), which also would be a reasonable assumption as the spotted max temperatures in figure 3.21 is located in a small distance to the left of the wire.

For the same operation performed with cooling the results are divergent. The numerical model would give a result for around 170 degrees Celsius while the spotted max temperature would be 40 degrees Celsius. As mentioned above the convection effect from the free surface will affect the temperature spotted with the IR camera. In addition the heat convection coefficient is extremely larger for transfer to water than transfer to air. By doing a simple analysis with convection to the surface based on a mean temperature from the numerical model with cooling it was seen a temperature decrease from 170 to 80 degrees over 1 second. In addition to this convection effect the spotted maximum temperature was read from a point located on top of water flow. Thus, the assumed location of the maximum temperature from the numerical model was covered up. This was also the case for the performed test without water.

3.8 Summary

In this chapter the theory for transient thermal analysis has been presented and a numerical model has been built. It was shown that the analytical approach would not provide a plausible solution under the circumstances in this thesis, and the disadvantages for the FDM approach with a forward difference was presented to some extent, thus implying the requirement for another method of analysis.

From the validation section it's seen that the model fits rather well for simulating cutting without cooling. When cooling is applied it seems the results obtained are quite divergent. This does not imply that the model at its core is dysfunctional, rather that the modeling of applied convection has failed. The field of force convection is subject to extensive research [7, 10], and the amount of mathematical formulation found in the literature is staggering. Thus assuming a probable solution when accounting for convection with a single coefficient, would be naive. Despite this, the model has been proven to overestimate the temperatures, which might not be devastating as the aim with this thermal analysis is to determine the upper limits. If the model exceeds the limits which are set, it could be shown that a reasonable reduction in temperature is probable.

4 Existing research

4.1 Hot surfaces

Available literature and standards are quite consistent regarding the recognition of hot surfaces as an ignition source. However, the requirements in relevant standards set the requirement of highest allowable surface temperature to be equal to the auto ignition temperature of the hazardous atmosphere. By reviewing relevant literature, it is found that the surface temperature capable of ignition a hazardous atmosphere is dependent on several factors.

Drysdale defines the term ignition as the process which a rapid exothermic reaction is initiated and then propagates and causes the material to undergo change while producing extreme temperatures. This exothermic reaction would be the oxidation of the flammable substance. In nature there will always be oxidation in normal ambient surroundings, thus substances will always generate heat. Simultaneously as the heat is generated, heat will also be lost to the surroundings by convection. Both the heat generation rate and the heat loss rate increases with temperature but, their dependence on the temperature varies. This is shown in figure 4.1

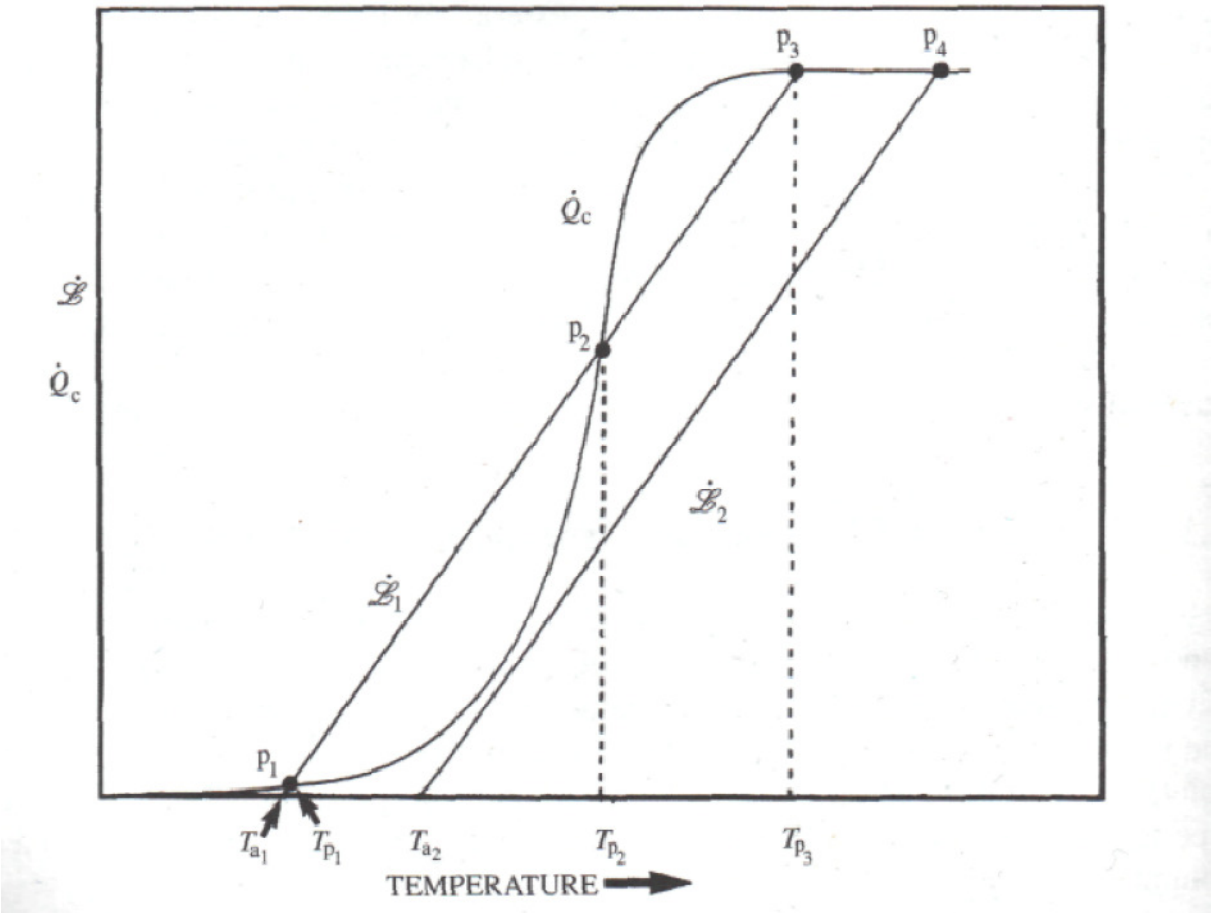

Figure 4.01 Rate of heat generation ($\dot{Q}_c$) and heat loss ($\dot{L}$) as function of temperature [F16]

The scenario known as combustion will arise when the temperature in figure 4.1 reaches the point p2. At this point the heat generation will be larger than the heat loss and thus, the process will be self-sustainable and propagate as a flame.

The point p2 will be the auto ignition temperature, as seen from figure 4.1 (which is exaggerated) the external effects will be very important when determining the actual auto ignition temperature.

Auto ignition temperatures can be obtained from various text books and engineering tables, these temperatures are determined by conducting experiments on stoichiometric mixtures of substantial volume. The auto ignition temperatures are then determined as the lowest uniform temperature creating ignition of the mixture [13]. When obtaining the auto ignition temperatures it was also observed a small time delay before ignition. This induction time reduced as the temperature of the mixture increased. For the auto ignition temperature the induction time was observed to be in the order of 1 second or more. This also indicates that determining the induction time for mixtures with uniform temperatures exceeding the auto ignition temperatures would be extremely difficult, and this is assumed to be the reason for the omission of this parameter in the literature.

Connecting the theory of auto ignition temperature to ignition by hot surfaces as done in the standards then would be an overestimation of the hot surfaces' ignition potential. Drysdale introduces the quenching distance. This parameter describes the minimum distance between the flame and a non-burning barrier. This might be surprising, but by evaluating the theories as presented by figure 4.1 in a scenario of a flame "from" a wall or similar it would be logical to draw the following conclusions:

- At the initial stages the surface in question would work as a barrier for the flames' propagation
- Assuming that the barrier is heat conductive, it will transport heat through its mass but not flames
- The heat loss to the barrier will then cause the temperature to decrease below the auto ignition temperature and thus, no flame propagation at the mixture layer close to the surface

The size of the quenching distance is in the order of 1-2 mm [13].

Drysdale thus determines the temperature requirement for ignition by hot surfaces to be the auto ignition temperature at a distance from the surface equal to the quenching distance.

Determining the maximum surface temperatures thus is a combination of size of surface (Drysdale has found the surface temperature for an area of approx. 50 mm^2 to be close to 1400 degrees Celsius for igniting 6% methane in air, auto ignition temperature for 6% methane in air is approx 550 degrees Celsius) the flow of mixture past the hot surface and the fraction of flammable substance dissolved in air.

The influence from the size of surface is proven by Proust et al. in their effort to simulate hot spots from impacts. The results obtained showed a necessary ignition temperature to be 50-80% higher for an area of approximately 10 mm^2 than for an area of 100 mm^2 [32].

Thus determining the maximum surface temperature involves a lot of complicated physics. The American Petroleum Institute has chosen to follow the following practice when determining the maximum surface temperature:

From API Recommended practice 2216 [27]:

- *The identification of the heated surface as the cause of ignition can often lead to an incorrect analysis of the real source of ignition. In general, ignition of hydrocarbons by a hot surface should not be assumed unless the surface temperature is approximately 360ºF (182 ºC) above the accepted minimum ignition temperature of the hydrocarbon involved.*

The latter requirement would be in strong contrast to the European adopted practices. However, the American standards are released from trustworthy sources and hence it indicates the possibility to declare a piece of equipment with higher surface temperatures than stated in European standards.

4.2 Mechanically generated sparks

In abrasive processes there will be a spark stream while executing the process. This spark stream is actually glowing chips that fly in the air. Initially these chips will have the same temperature as the surface of the work piece, but as they fly through the air they will react with the oxygen and generating temperatures even higher than the melting point of the work piece material [33, 1]. Malkin and Guo have also stated that no spark stream is observed when grinding in an oxygen free atmosphere.

Even though spark temperatures of grinding St 37 steel has been proven to be in the range of 1500-2000 degrees Celsius [33], no documentation exists for the actual spark being the ignition source when grinding in hazardous areas.

Impacts between solid bodies will, as abrasive processes, create sparks of significant temperatures. Sparks from impacts have the characteristics of being larger, and containing a higher temperature. The test set up seen in [33] consisted of the following test materials:

- Titanium
- Mild steel, St 37
- Alloy steel
- Rusty steel
- Rotating grinding wheel
- Concrete

The hazardous atmosphere tested in this experiment consisted of agricultural dusts, where dried corn starch is the substance having the lowest minimum ignition energy (< 4,5 mJ) and auto ignition temperature (330 degrees C). Results showed that the only combinations able to ignite this atmosphere were:

Titanium against:

- Rusty, mild steel
- Concrete
- Sandstone

All experiments conducted with an average impact-energy of approximately 20 J.

Thus steel impact on concrete, which would create spark temperatures of 2730 degrees Celsius, failed to ignite the explosive atmosphere along with the other remaining combinations, including rotating grinding wheel on steel.

The research from Proust et al. is of a slightly different kind. Their main focus was the hot spot generated in the body from either impact or friction and secondary the effects of sparks. The results obtained in this study are quite interesting when compared against that of Pedersen et al. regarding spark temperature.

The experimental set up for Proust et al. consisted of a machine which rubs to pieces of material against each other and creating sparks. Thus the premises are quite different which also is displayed in the results. While Pedersen et al. obtained spark temperatures of 1500-2000 degrees while grinding, Proust et al. obtained spark temperatures below 100 degrees Celsius [32]. The reasons for the temperatures are evident due to the experimental set up. However, it seems unreasonable that the different materials would cause the vast difference. Hence, it seems natural to assume that there exists a relation between spark producing process and the spark temperature.

The exothermic reaction of sparks is also investigated by Proust et al. to some extent. Fragments from either impacts or rubbing action managed to trigger an ignition.

Spark emission from abrasive waterjet cutting has been studied by Miller [30]. This study consisted of a proposed reason for the emitted sparks failure to ignite explosive projectiles while cutting. The explosives regarded in this study were TNT and PETN. Both substances are regarded as extremely unstable, PETN has an auto ignition temperature of 190 degrees C [I8].

Miller concludes that the spark emission from the collisions between abrasives and hard work pieces, like steel, creates small sparks which appear not to have melted. However, these sparks are too small and have insufficient energy to ignite explosive atmospheres. In addition, the cooling water will participate in the failure of ignition.

It should be noted that Miller give a faulty impression of the explosion limits of hydrogen/air mixtures both in terms of electrical spark discharge and mechanical impact energies in this study.

4.3 Summary

In this chapter the published research on ignition of explosive atmospheres has been presented. It's seen that auto ignition of gas mixtures are a rather complicated phenomenon, and the requirements set in the ATEX Directive regarding hot surface temperatures easily can be challenged.

Ignition by mechanical spark discharge seems to be rather unusual for impacts between conventional steel, concrete and alloy steel. However, collisions between titanium and steel, concrete or sandstone is proven to be capable of igniting dried corn starch dust atmosphere. It should be emphasized that neither of the discussed research have obtained ignition by the spark stream from a grinding process.

5 Results

5.1 Temperature distributions from model.

The obtained results from the model created in chapter 3 are presented by a graphical presentation of the temperature distributions at the boundaries. The graphs are coded according to figure 5.1.

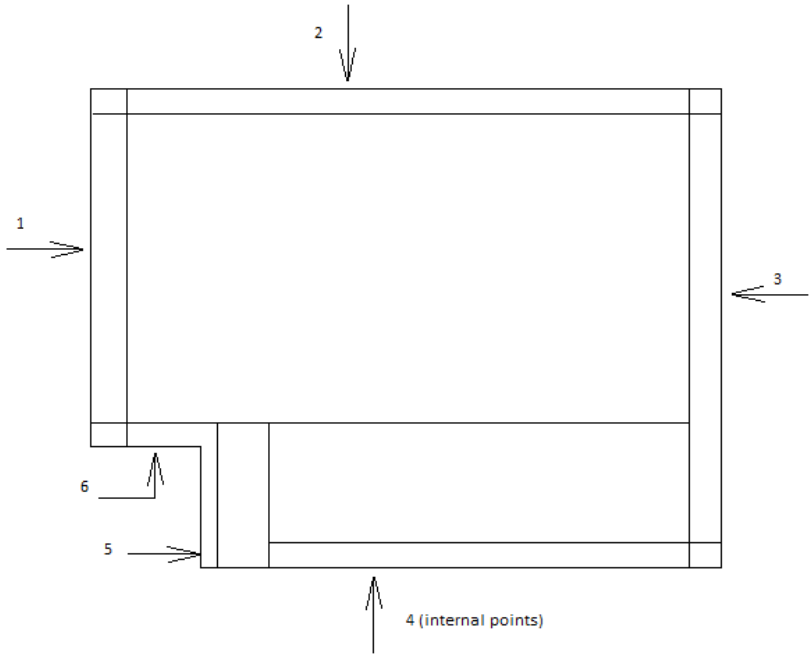

Figure 5.01 Presentation of surface lines

The simulation for cutting steel was performed with an increment size of 0,4 mm and 0,3 mm for stainless steel. Cutting of steel would then have a volumetric material removal rate of 540 mm^3/s while the material removal rate for stainless steel would be 75% of the material removal rate for steel. This is discussed under section 3.7. The temperatures will be presented against the increment distance. For line number 1 the increment number would be 1 in the upper left corner and increasing towards the intersection with line 6. For line 6 increment 1 would be at the intersection between line 6 and line 1. This logic is adapted to all of the lines around the work piece. All of the lines are surface areas except for line 4 which represent the internal line of symmetry.

The simulation has been set to simulate 100 seconds of cutting, and for all instances the temperature ahead of the wire has converged. This implies that the heat generation has reached its peak, when assuming no effects from the remaining depth of material. The effects of remaining material are addressed in chapter 3.5.

5.1.1 Temperature distribution for cutting steel without cooling

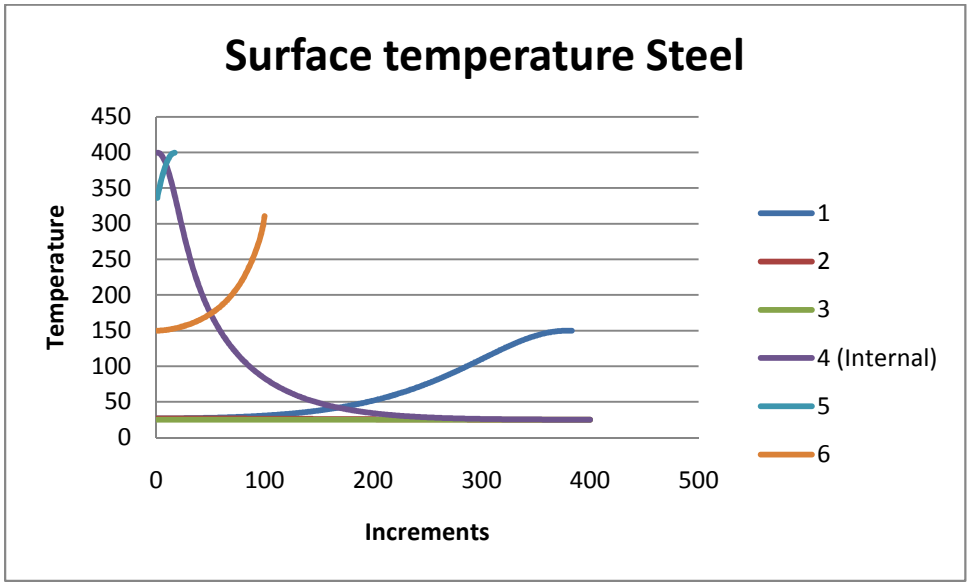

Figure 5.02 Temperature distribution for cutting steel without cooling

5.1.2 Temperature distribution for cutting steel with cooling

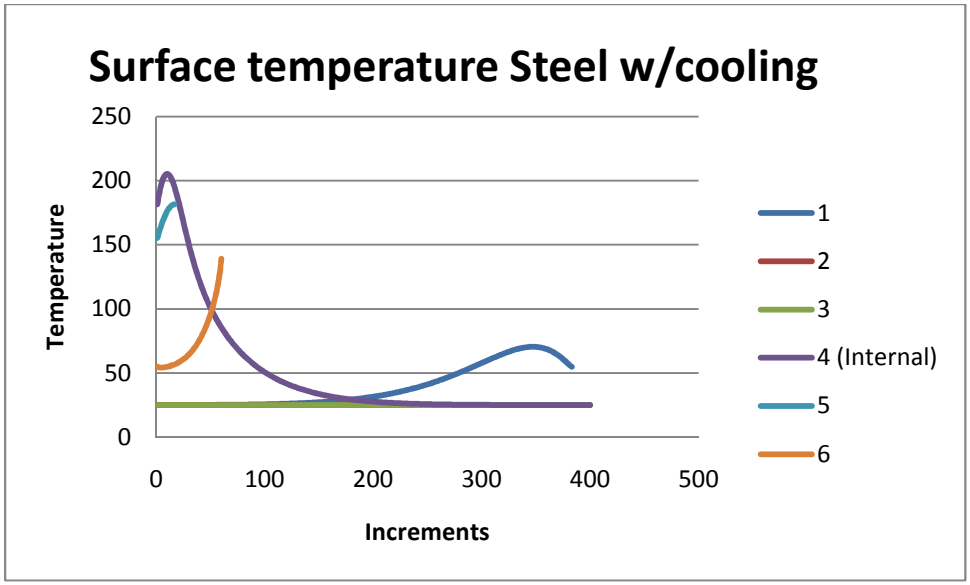

Figure 5.03 Temperature distribution for cutting steel with cooling

5.1.3 Temperature distribution for cutting stainless steel without cooling

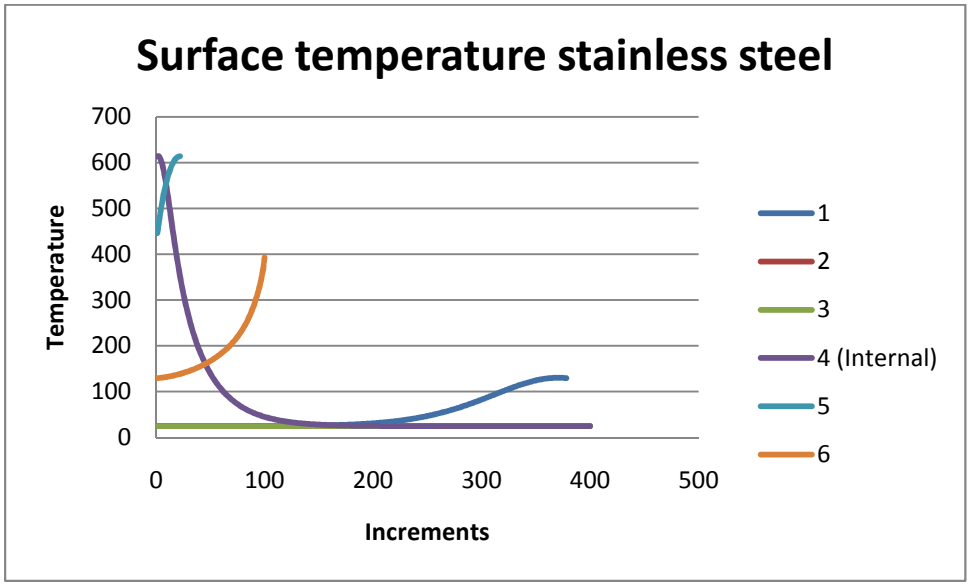

Figure 5.04 Temperature distribution for cutting stainless steel without cooling

5.1.4 Temperature distribution for cutting stainless steel with cooling

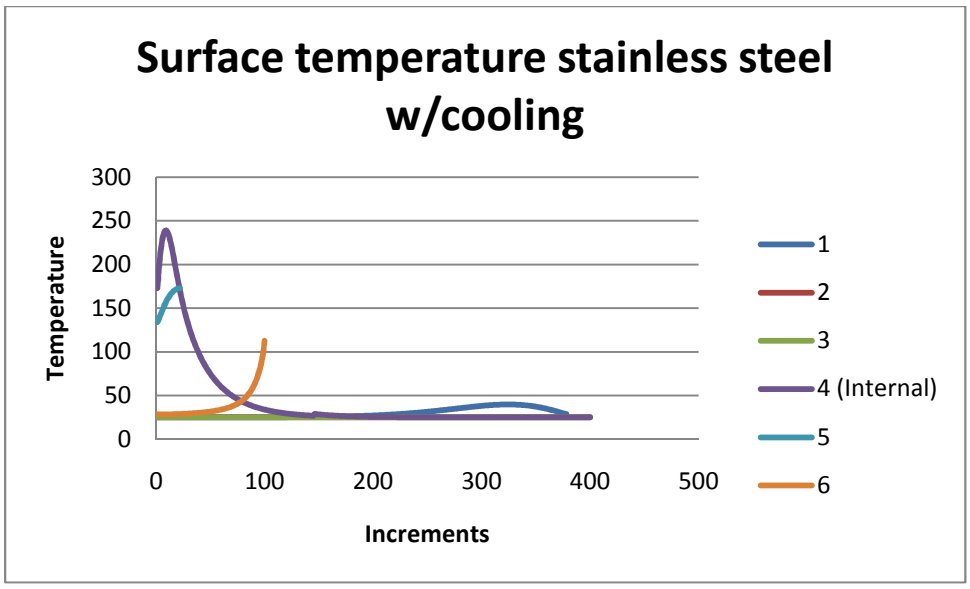

Figure 5.05 Temperature distribution for cutting stainless steel with cooling

5.2 Summary

It is seen from all of the figures in the previous section that the temperature will have the highest value ahead of the wire at an internal point. Off the surface temperatures it is seen that the models without cooling will not satisfy the ATEX requirements. However, by applying cooling the models will meet the requirements. Even though the models with cooling does have a faulty outcome, this flaw is assumed to homogeneous, and be founded on the improper applying of convection and thus overestimating the temperature.

Based on this it is natural to conclude that the model documents that the equipment meets the requirement of surface temperatures as stated in ATEX Directive and its Harmonized Standards.

The graphical representation of the temperatures, as shown in this section, is based on the 3-D presentations found in appendix D.

6 Conclusion

6.1 Summary

6.1.1Review of technology

Through this thesis a thorough review of the diamond wire technology is given in chapter 1. Available literature on the material removal process for diamond wire cutting was found to be extremely limited. Thus, the theory of material removal by conventional grinding was adapted as this also is an abrasive process.

A lot of effort was expended while trying to establish a relation which would describe the force needed to remove material. During this process it was experienced that grinding forces where determined experimentally for each specific set up. As a result of this another angle of attack was needed and thus, Malkin and Guo's theory of specific grinding energy related to the materials' melting energy was adopted.

Modeling on the basis of specific grinding energy was validated in section 3.8, proving that Malkin and Guo's theory fitted well to the technology of cutting by abrasive diamond wire.

6.1.2 Review of thermal analysis

The method used for thermal analysis in this thesis was the finite difference method with a forward difference. The FDM method have gained wide acceptance and seems to be the method of choice for thermal analysis. However, the forward difference proved to be very time consuming as it is significantly limited by the Fourier number. Despite this it was adopted due to its extreme user friendliness and low requirement on programming experience.

An analytical approach was also applied, but due to its complexity when handling non-homogeneous boundary conditions, especially convective borders, the approach had to be discarded.

6.1.3 Review of ATEX and ignition of explosive atmospheres

In chapter 2 the ATEX Directive and its harmonized standards were presented. By evaluating the characteristics of an explosive atmosphere it was found that the requirement regarding hot surfaces was overprotective.

The study of ignition of explosive atmospheres by mechanically generated sparks did not provide sufficient results for establishing a relation between the spark producing process and the ignition potential in the spark. It was seen that sparks from impacts between titanium and rusty steel provided a spark strong enough to ignite corn starch dust, and the spark temperatures in this case would be in the range of 2000-2900 degrees Celsius. In the same study it was seen that the spark temperature between steel and a grinding wheel produced sparks within the temperature range of 1600-1730, while other sources has found the temperatures of spark emission from rubbing hard steel against soft steel to contain temperatures below 100 degrees Celsius. Neither of the latter mentioned spark temperatures was capable of igniting dusts or gas mixtures. However, this clearly indicates that there exist a relation between the spark producing process and the spark temperature.

6.2 Concluding remarks

By combining the results from chapter 5 with the requirements it's seen that the diamond wire cutting process will not be an ignition hazard, in terms of hot surfaces, when sufficient cooling is

applied. However, the ATEX Directive demands that this requirement is obtained even in the case of malfunction to the system.

It's seen that when adequate cooling is not applied, the surface temperatures will create a potential ignition hazard according to the ATEX Directive. Thus an additional barrier needs to be provided. Alternatively it would be possible to perform full scale tests in a premixed atmosphere, according to the results obtained in chapter 2, this would most likely provide positive results.

The second requirement investigated under this thesis, the requirement of no spark emission in a hazardous atmosphere cannot be met without applying preventive measures nor can the ignition potential in emitted sparks be determined without full scale tests. Thus a conclusion founded on the work performed in this thesis cannot be performed.

To obtain conformity with requirements in the ATEX Directive, preventive measures need to be applied. From the authors' point of view, there are two sides to attack this problem from. Either the ignition source potential is reduced by removing sparks or removing the spark emission in an explosive atmosphere. Since no options for reducing the ignition potential in sparks were found, the option of removing the sparks in an explosive atmosphere would be the best choice.

ATEX Directive demands that there should be no spark emission in an explosive atmosphere, an explosive atmosphere would not be equivalent to a hazardous area as an area can be hazardous but not explosive. Thus, it would be possible to equip the diamond wire saw with a control system which would stop the process in case of gas detection.

Thus normal operation is secured by utilizing water coolants and gas detector connected to the power source of the wire saw. To obtain secure operation if these measures should fail another set of preventive measures need to be applied. For the cooling water it would be possible to install a temperature sensor on the wire. By measuring this temperature it would be possible to determine whether there is a problem with sufficient cooling and by connecting the sensor to the control system of the power source it could shut down the power source in case of overheating. In the case of failure of the gas detector installed, as mentioned earlier, it is assumed that the requirements would be fulfilled by installing another gas detector which would be independent of the other.

The preventive measures will then consist of:

- Cooling water
- Temperature sensor to shut down the equipment in the case of overheating
- Gas detector to shut down equipment in case of gas detection
- A second gas detector in case of malfunction of the other detector

By applying the above mentioned measures it is assumed that the equipment will fulfill the requirement of the ATEX Directive. Off course, this is under the assumptions that both the HPU and sawing machine will fulfill the requirements.

6.3 Recommendations for further progress in an evaluation process

It's seen from this thesis that the ignition potential in mechanically generated sparks is not easily determined. To account for this a full scale test in an explosive atmosphere with applied cooling is recommended. The results of this test will determine whether it will necessary to apply the gas detectors.

6.4 Further research

Through the work conducted in this thesis some interesting features were found. The adoption of the chip formation energy theory seemed to describe the process of wire cutting quite well. However, the validation can only be regarded as partial as testing against measured values were only performed against one single type of work piece. In addition the effects of convection were not successfully implemented.

For final validation an experiment, similar to described in appendix F should be conducted. In addition the model used in this thesis proved to be rather time-consuming and hence implying that either FEM or FDM with a backward difference would be a better method of analysis. For FEM non-linearity can be included and thus providing even better results.

The assumed vital phenomenon to be studied for achieving proper results with cooling would be convection. The available theory within this field is quite extensive even though specialist claim that the effects only can be estimated with a +/- 20 % tolerance [Holman et al.]. Also, the actual contact zone for the cooling fluid would be of importance.

For the energy levels in mechanically generated sparks it is assumed that evaluating the chemistry of the phenomenon would produce estimates which might be usable. For the initial stage, the spark would have the same temperature as the surface. When it flies through the air it will oxidize and release energy, in form of temperature. It is assumed that there exists theory of estimation of energy release during exothermic reactions. Thus, the field of chemistry would be the recommended field for further research on the energy level in sparks.

References

Figures

[F1] Abrasive water jet:
http://www.flowwaterjet.com/en/waterjet-technology/abrasive-waterjet.aspx

[F2] Grinding grain
Principles of modern grinding technology [2], p. 342

[F3] Sketch of conventional cutting by turning
Cutting tool technology [5], p 52

[F4] Orientation of shear zones
Cutting tool technology [5], p 55

[F5] Stages of grinding
Principles of modern grinding technology [1], p.16

[F6] Sketch of wear flat in abrasive processes
Principles of modern grinding technology [1], p.125

[F7] Force components in grinding and wear flats
Principles of modern grinding technology [1], p.123

[F8] Sketch of critical cut depth
Principles of modern grinding technology [1], p.130

[F9] Specific cutting energy VS volumetric removal rate per unit width for plunge grinding
Principles of modern grinding technology [1], p.128

[F10] Rake angle conventional machining
Principles of modern manufacturing [3], p.487

[F11] Minimum specific energy VS specific melting energy
Minimum Energy in Abrasive Processes [16]

[F12] Bond failure
Principles of modern grinding technology [1], p.83

[F13] Flow chart HPU
http://www.bb-armr.com/support/611XHPU/611X%20HPU%20Series%20Manual-RevC.pdf

[F14] Diamond wire sketches provided by Beerenberg Corporation

[F15] Evaluation process
Course material “Seminar om gass og støveksplosjoner 12-14 april 2011”

[F16] Heat generation and heat loss as function of temperature
An Introduction to Fire Dynamics 2nd edition [13], p 194

Bibliography

[1] Malkin and Guo, Grinding technology 2nd edition, Industrial Press; 2008

[2]W. Brian Rowe, Principles of modern grinding Technology, William Andrew; 2009

[3] Mikell P. Groover, Fundamentals of modern manufacturing 3rd edition, John Wiley and sons; 2007

[4] J. Paulo Davim –editor, Machining Fundamentals and Recent advances, Springer; 2008

[5] Graham Smith, Cutting tool technology, Springer; 2008

[6] Schmitz and Smith, Machining Dynamics, Springer; 2009

[7] J.P. Holman, Heat Transfer 7th edition, McGraw-Hill; 1992

[8] Lichun and Jizai, A study of grinding force mathematical model, Annals of the CIRP Vol 29/1; 1980

[9] Eastop and McConkey, Applied Thermodynamics 5th edition, Pearson; 1993

[10] Incropera, DeWitt, Bergman and Lavine, Fundamentals of heat and mass transfer 6th edition, John Wiley and sons; 2007

[11] Boyce and DiPrima, Elementary Differential Equations and Boundary Value Problems 8th edition, John Wiley and sons; 2005

[12] Rao, Mechanical Vibrations 4th edition, Pearson; 2004 (Matlab guidance)

[13] Drysdale, An Introduction to Fire Dynamics 2nd edition, John Wiley and sons; 1999

[14] Cook, Malkus, Plesha and Witt, Concepts and Applications of Finite Element Analysis 4th edition, John Wiley and sons; 2002

[15] Lillestøl, Hunderi and Lien, Generell Fysikk for universiteter og høgskoler –bind 2 Varmelære og elektromagnetisme, Universitetsforlaget; 2001

[16] Malkin and Joseph, Minimum Energy in Abrasive Processes, Wear 32 15-23, Elsevier; 1975

[17] Malkin and Guo, Energy partition and cooling during grinding, Journal of manufacturing processes Vol 2/No 3; 2000

[18] Innovative technology summary report, Diamond Wire Cutting of the Tokamak Fusion Test Reactor Vacuum Vessel, Report prepared for the U.S. Department of energy in 2000. Available from [I2]

[19] Husqvarna product catalogue, provided by Beerenberg Corporation

[20] Doman and Bauer, Finite element modeling approaches in grinding, International Journal of Machine Tools and Manufacture 49; 2009

[21] Chiu and Malkin, Computer simulation for cylindrical plunge grinding, Annals of the CIRP Vol 42/1; 2009

[22] Tönshoff, Peters, Inasaki and Paul, Modeling and simulation of grinding processes, Annals of the CIRP Vol 41/2; 1992

[23] Lillestøl, Hunderi and Lien, Generell Fysikk for universiteter og høgskoler – bind 1 Mekanikk, Universitetsforlaget; 2001

[24] Shubkin and Rudnick, Synthetic Lubricants and High-Performance Functional Fluids 2nd Edition, Marcel Dekker; 1999

[25] Te-Te ex guide, Course material from Cooper Crouse-Hinds, available for ordering from www.te-te.no

[26] Directive 94/9/EC of the European Parliament and the Council
Available from:
http://ec.europa.eu/enterprise/sectors/mechanical/documents/legislation/atex/index_en.htm

[27] Geir H. Pedersen, Mekanisk Utstyr og Sikkerhetssystemer, presentation from course in gas and dust explosions

[28] NS-EN 1127-1:2007, Explosive atmospheres – Explosion prevention and protection Part 1: Basic concepts and methodology, Standard Norge; 2008

[29] NS-EN 13463-1:2009, Non-electrical equipment for use in potentially explosive atmospheres Part 1: Basic method and requirements, Standard Norge; 2009

[30] Paul L. Miller, Formation of sparks from abrasive waterjet cutting and their effects on condensed explosives, [I6]; 1994

[31] Odd Thomassen and Jens Kristian Holen, SLIPEVERKTØY – klassifisert som "kaldt arbeid", [I7]; Unknown

[32] Proust, Hawksworth, Rogers, Beyer, Lakic, Raveau, Hervé, Pina, Petitfrére and Lefebvre, Development of a method for predicting the ignition of explosive atmospheres by mechanical friction and impacts (MECHEX), Journal of Loss Prevention in the Process Industries 20; 2007

[33] Pedersen and Eckhoff, Initiation of grain dust explosions by heat generated during single impact between solid bodies; Fire safety journal 12; 1987

Internet resources

[I1] Cutting in the mining industry:
http://findarticles.com/p/articles/mi_qa3983/is_200612/ai_n17196346/pg_3/?tag=mantle_skin;content

[I2] Diamond cutting in the nuclear industry
http://www.em.doe.gov/EM20Pages/pdfs/pubs/itsrs/itsr2389.pdf

[I3] Heat convection coefficients
http://www.engineeringtoolbox.com/overall-heat-transfer-coefficient-d_434.html

[I4] ATEX homepage
http://ec.europa.eu/enterprise/sectors/mechanical/atex/index_en.htm

[I5] Wikipedia on ATEX
http://en.wikipedia.org/wiki/ATEX_directive

[I6] Sparks from abrasive waterjet
http://www.dtic.mil/cgi-bin/GetTRDoc?Location=U2&doc=GetTRDoc.pdf&AD=ADA507520

[I7] SLIPEVERKTØY – klassifisert som “kaldt arbeid”
http://www.safety-tools.net/Documents/statoil.pdf

[I8] Wikipedia on PETN
http://en.wikipedia.org/wiki/Pentaerythritol_tetranitrate

Appendix A – Calculation of melting energies

Material	Diffusivity	Melting point (K)	density Kg/m3	Heat of fusion J/kg	melting energy J/mm3	chip formation J/mm3
Steel	0,000018	1800	7854	270000	10396339800	13,86
Stainless steel 304	0,00000395	1670	7900	225000	9570060000	12,76
Titanium	0,00000932	1953	4500	419000	6487650000	8,65
Aluminium pure	0,0000971	933	2702	398000	2745772400	3,66

	Temperature (K)									
Conductivity	100	200	300	400	600	800	1000	1200	1500
Steel	134	94	80	69,5	54,7	43,3	32,8	28,3	32,1
Stainless steel 316	9,2	12,6	14,9	16,6	19,8	22,6	25,4	28	31,7
Titanium	30,5	24,5	21,9	20,4	19,4	19,7	20,7	22	24,5
Aluminium pure	302	237	237	240	231				

	Temperature (K)								
Heat capacity	100	200	300	400	600	800	1000	1200	1500
Steel	216	384	447	490	574	680	975	609	654
Stainless steel 316	272	402	477	515	557	582	611	640	682
Titanium	300	465	522	551	591	633	675	620	686
Aluminium pure	482	798	875	949	1033	1146			

Appendix B – Drawings and diagrams

B.1 Sawing machine

Sawing machine from user manual Tyrolit Hydrostress SB 35

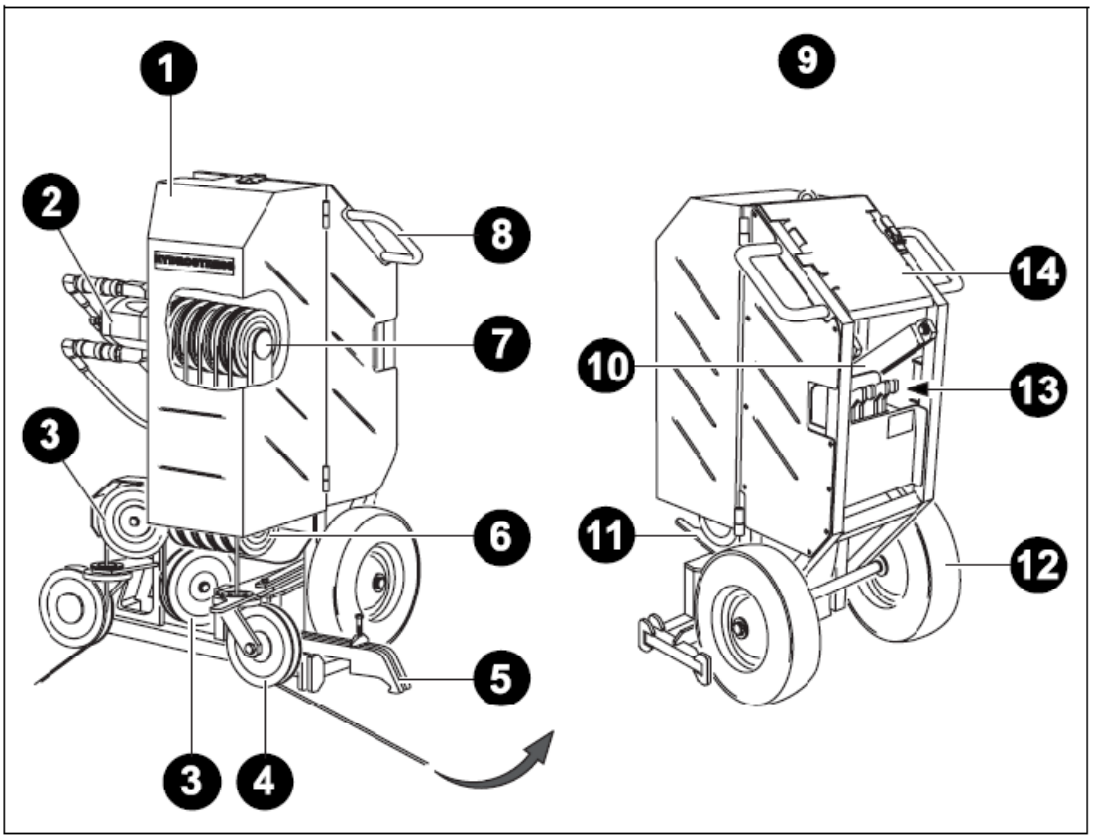

The most important modules

1. Protective hood
2. Drive motor
3. Deflection pulley
4. Swivelling pulley
5. Clamping shackle
6. Lower deflection pulleys
7. Drive pulleys
8. Chassis handle
9. Crane hook
10. Rocker
11. Pulley guide for wire storage
12. Wheel
13. Storage area for clamping shackles
14. Hinged working table

B.2 HPU

HPU flowchart from user manual, Hydrostress RD-S RC Power Unit

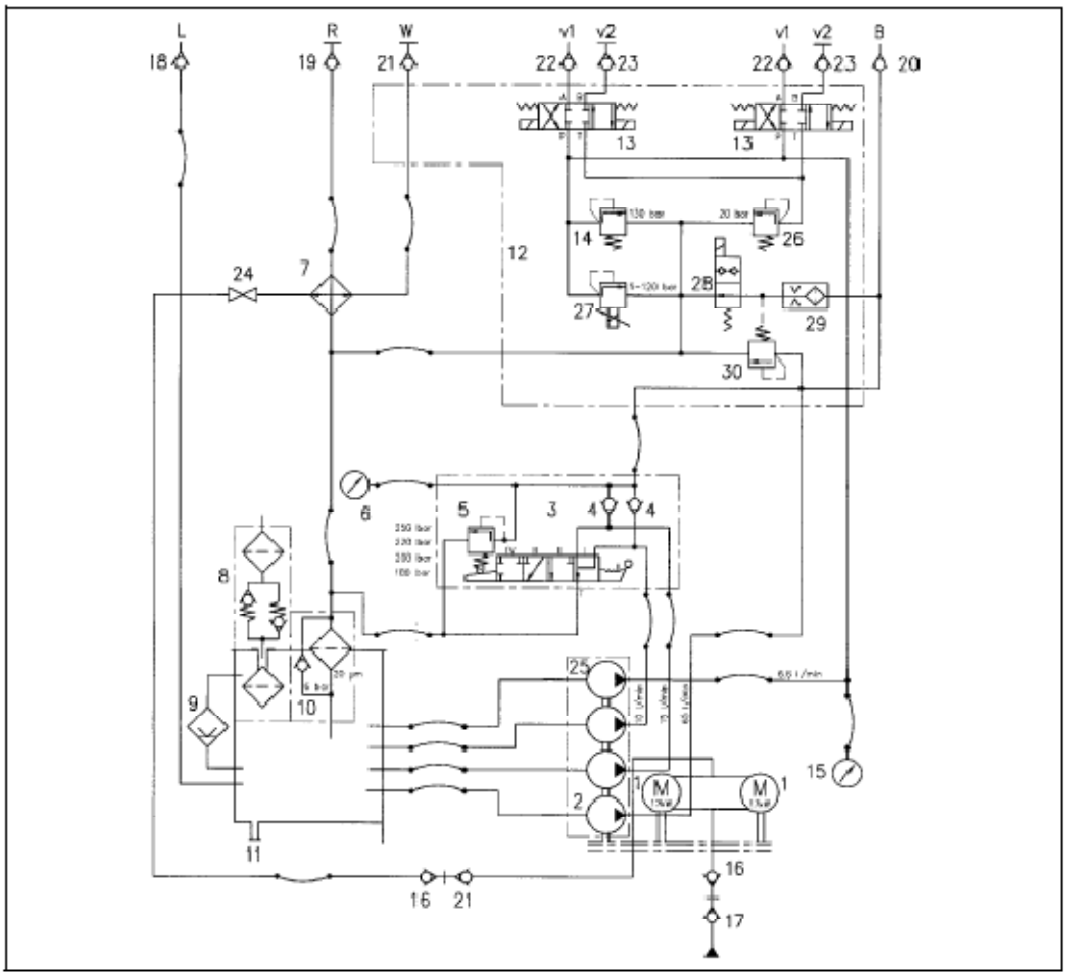

1. Electric motors
2. Pump assembly
3. Control valve
4. Check valve
5. Pressure relief valve
6. Main circuit pressure gauge
7. Oil cooler
8. Tank cover
9. Oil level
10. Oil filter
11. Screw plug
12. Control block
13. 4/3 way valve
14. Pressure relief valve
15. Feed pressure gauge
16. Nipple
17. Coupling
18. Leakage oil nippel
19. Main circuit coupling
20. Main circuit nipple
21. Coupling water
22. Feed nipple
23. Feed coupling
24. Water valve
25. Radial piston pump
26. Pressure valve
27. Proportional valve
28. Seat valve
29. Bijour nozzle
30. Pressure balance

Appendix C – Matlab programs

C.1 Convergence of steady state temperatures

```
clear all
close all
clc
Ti=1502
alfa=0.00000395;
dt=0.002;
dx=0.0003;
T=zeros(200);
IT=zeros(200);
T(:,:)=25;
Fo=alfa*dt/dx^2;
t=dt*100;
W=zeros(34,200);
for k=1:2
for i=73:123
    T(i,99)=Ti;
    T(i,100)=Ti;
    T(i,101)=Ti;
end
for q=1:500

   for i=2:199
       for n=2:199
           IT(i,n)=Fo*(T(i+1,n)+T(i-1,n)+T(i,n+1)+T(i,n-1))+(1-4*Fo)*T(i,n);
       end
   end
   T=IT;
   T(1,:)=25;
   T(200,:)=25;
   T(:,1)=25;
   T(:,200)=25;

end
for m=1:51
    W(m,k+1)=T(72+m,101);
end
end
```

C.2 FDM from textbook

```
clc
close all
clear all
increments=100;
length=0.15;
dx=length/increments
kappa=7.5*10^-6          %diffusitvity
lambda=18.75             %conductivity
h=125                    %heat convection coeff
dt=0.1
span=40000;              %time span
Fo=kappa*dt/dx^2
Tsurr=25;
T0=[800 800 800 800 800 800];
Tint=800
T=zeros(span,increments+2);
for bound=1:span

    T(bound,1)=(bound-1)*dt;
end
for n=2:increments+2
    T(1,n)=Tint;
end
for g=2:span
    for j=3:increments+1
        T(g,j)=Fo*(T(g-1,j+1)+T(g-1,j-1)+T(g-1,j)*(1/Fo-2));

    end

T(g,increments+2)=Fo*(T(g-1,increments+1)+T(g-1,increments+1)+T(g-1,increments+2
)*(1/Fo-2));
    T(g,2)=(T(g,3)+(h*dx*Tsurr/lambda))/(1+(h*dx/lambda));
end
    ET=zeros(60,7);
    for A=0:59
        ET(A+1,1)=T(((A)*600)+1,1);
        ET(A+1,2)=T(((A)*600)+1,2);
        ET(A+1,3)=T(((A)*600)+1,22);
        ET(A+1,4)=T(((A)*600)+1,42);
        ET(A+1,5)=T(((A)*600)+1,62);
        ET(A+1,6)=T(((A)*600)+1,82);
        ET(A+1,7)=T(((A)*600)+1,102);
    end
    for b=1:60
        ET(b,1)=ET(b,1)/60;
    end
```

C.3 Analytical with convection

```
clc
close all
clear all
h=125 ;              %heat convection coefficient
lc=0.15;             %characteristic length equals the halflength of wall
k=18.75 ;            %Thermal conductivity
alfa=7.5*10^-6;      %thermal diffusity
Bi=h*lc/k            %Biot number
Tsurr=25;            %surrounding temperature
Tint=800;            %initial temperature
x=1;
t=0;
dim=100;
span=1000;
ZETA=zeros(dim,1);
zetam = [0.8603
    3.4256
    6.4373
    9.5293
    12.6452
    15.77
    18.9024
    22.0364
    25.17244
    28.3096
    31.4477
    34.5864
    37.7256
    40.8651
    44.0050
    47.1450
    50.2853
    53.4257
    56.5663
    59.7070
    62.8477
    65.988
    69.1295
    72.2704
    75.4114
    78.5525];
for m=1:25
    ZETA(m,1)=zetam(m,1);
end

for N=5:dim
    ZETA(N,1)=ZETA(N-1,1)+3.1415;
end
ZETA;
F=0;
T=zeros(span,7);
for i=0:5
    x=(0.03*i)/lc;
    for g=0:span
    t=(g)*60;F=0;
    for n=1:dim

   zetax=ZETA(n);
    thetax=4*sin(zetax)/(2*zetax+sin(2*zetax))*
                                    exp(-1*zetax^2*alfa*t/lc^2)*cos(zetax*x);
    F=F+thetax;

    end

    T(g+1,7-i)=F*(Tint-Tsurr)+Tsurr;
    T(g+1,1)=g;
    end


 end

 T
 A=T(:,1);
 T1=T(:,2);
 T2=T(:,3);
 T3=T(:,4);
 T4=T(:,5);
 T5=T(:,6);
 plot(A,T1,A,T2,A,T3,A,T4,A,T5);
```

C.4 Analytical approach

```
clc
clear all
close all
Text=25;            %External temperature
Ti=1200;            %Initial temperature
alfa=18.8*10^-6;    %Thermal diffusivity
L=0.3;              %Length of work piece
increments=1000;    %Number of distane increments
dx=L/increments;

%Establishing temperature and Fourier matrices

T=zeros(62,increments);
IT=zeros(increments+1,2);
C=zeros(201,201);

%Establishing initial condition vector

for x=0:increments
    IT(x+1,1)=x;
end
IT(:,2)=Text;
IT(1,2)=Ti;
IT(1,2)=1200;
IT(1,2)=1200;
IT(1,2)=1200;
IT(1,2)=1200;
IT(1,2)=1200;


%Establishing steady state condition

for x=0:increments
    ST(x+1,1)=x;
    ST(x+1,2)=Ti;
 ST(increments+1,2)=Text;

end

%Establishing Fourier coefficients

Cn=zeros(1000,2);
for n=1:10000
     cn=0;
    for x=0:increments

     cn=cn+(IT(x+1,2)-ST(x+1,2))*sin(n*pi*x/increments)*dx;

    end
    Cn(n,1)=n;
    Cn(n,2)=2/L*cn;
end

%Calculating temperature distribution

for t=0:2

for x=0:increments
    B=0;
    for n=1:10000
        B=B+Cn(n,2)*exp(-1*(n^2)*pi^2*alfa*0.5*t/L^2)*sin(n*pi*x/increments);
        C(n,x+1)=B;
    end
    T(t+1,x+2)=(ST(x+1,2))+B;
end
end

%Moving boundary
```

```
for y=2:100
    %updating remaining length
    l=L-(L/increments)*(y-1);
    dx=l/(increments+1-y);
    %updating inital conditions
    pres=T(y+1,:)';
    IT=zeros(increments+1-y,2);
    for i=0:increments+1-y
        IT(i+1,2)=pres(i+y+1);
        IT(i+1,1)=i+1;
        IT(1,2)=Ti;
    end
    %updating Steady state condition
    ST=zeros(increments+1-y,2)
    for i=0:increments+1-y
        ST(i+1,1)=i/(increments+1-y);
        ST(i+1,2)=Ti;
        ST(increments+2-y,2)=Text;
        %ST(i+1,2)=(Text-Ti)*i/(increments+1-y)+Ti;
    end
    %updating fourier coefficient
    for n=1:1000
     cn=0;
    for x=0:increments+1-y

     cn=cn+(IT(x+1,2)-ST(x+1,2))*sin(n*pi*x/(increments+1-y))*dx;

    end
    Cn(n,1)=n;
    Cn(n,2)=2/l*cn;
    end

    %Calculation of temperature distribution

for t=1

for x=0:increments+1-y
    B=0;
    for n=1:increments-y
        B=B+Cn(n,2)*exp(-1*(n^2)*pi^2*alfa*t/L^2)*sin(n*pi*x/(increments+1-y));
        C(n,x+1)=B;
    end
    T(y+2,x+y+1)=(ST(x+1,2))+B;
end
end
end
```

C.5 FDM convection

```
clear all
close all
clc
Ti=1891
Text=25
alfa=0.0000185;
s=200;          %size of work piece in increments
dt=0.0001;
dx=0.0004;
T=zeros(s);
IT=zeros(s);
ww=0.013;       %Diamond wire width
w1=17;          %Half diameter of diamond wire width in icrements
(0,5*ww/dx)(Rounded up to next integer)
T(:,:)=25;
Fo=alfa*dt/dx^2;
W=zeros(34,s);
h=125;          %Heat transfer coefficient
ko=75.5;        %Heat conduction

%Applying moving border

for k=1:s-2
for i=0.5*s-w1:0.5*s+w1
    T(i,k)=Ti;
    T(i,k+1)=Ti;
end

%Calculation convective lines

for q=1:10000
   for i=2:s-1

IT(1,i)=Fo*(2*h*dx*Text/ko+2*T(2,i)+T(1,i-1)+T(1,i+1)+(dx^2/(alfa*dt)-2*(h*dx/ko
)-4)*T(1,i));

IT(s,i)=Fo*(2*h*dx*Text/ko+2*T(s-1,i)+T(s,i-1)+T(s,i+1)+(dx^2/(alfa*dt)-2*(h*dx/
ko)-4)*T(s,i));

IT(i,1)=Fo*(2*h*dx*Text/ko+2*T(i,2)+T(i-1,1)+T(i+1,1)+(dx^2/(alfa*dt)-2*(h*dx/ko
)-4)*T(i,1));

IT(i,s)=Fo*(2*h*dx*Text/ko+2*T(i,s-1)+T(i-1,s)+T(i+1,s)+(dx^2/(alfa*dt)-2*(h*dx/
ko)-4)*T(i,s));
   end

   %Calculating interior points

   for i=2:s-1
       for n=2:s-1
           IT(i,n)=Fo*(T(i+1,n)+T(i-1,n)+T(i,n+1)+T(i,n-1))+(1-4*Fo)*T(i,n);

       end
   end

   T=IT;

   %Calculating convective corners


T(1,1)=Fo*(2*h*dx*Text/ko+2*T(2,1)+2*T(1,2)+(dx^2/(alfa*dt)-2*(h*dx/ko)-4)*T(1,1
));

T(1,s)=Fo*(2*h*dx*Text/ko+2*T(1,s-1)+2*T(2,s)+(dx^2/(alfa*dt)-2*(h*dx/ko)-4)*T(1
,s));

T(s,1)=Fo*(2*h*dx*Text/ko+2*T(s-1,1)+2*T(s,2)+(dx^2/(alfa*dt)-2*(h*dx/ko)-4)*T(s
,1));


T(s,s)=Fo*(2*h*dx*Text/ko+2*T(s-1,s)+2*T(s,s-1)+(dx^2/(alfa*dt)-2*(h*dx/ko)-4)*T
(s,s));
end
for m=1:34
    W(m,k+1)=T(0.5*s-w1-1+m,k+2);
end
end
W;
```

C.6 FDM convection final

```
            for n=k+2:s-1                   %Bottom line

IT(0.5*s,n)=Fo*(2*T(0.5*s-1,n)+T(0.5*s,n+1)+T(0.5*s,n-1))+(1-4*Fo)*T(0.5*s,n);


            end


   for i=2:k+1                          %moving convective border along sides

IT(0.5*s-w1,i)=Fo*(2*h1*dx*Text/ko+2*T(0.5*s-w1-1,i)+T(0.5*s-w1,i-1)+T(0.5*s-w1,
i+1)+(dx^2/(alfa*dt)-2*(h1*dx/ko)-4)*T(0.5*s-w1,i));


   end
   for i=0.5*s-w1:0.5*s-1       %moving convective border behind the wire

IT(i,k+1)=Fo*(2*h1*dx*Text/ko+2*T(i,k+2)+T(i-1,k+1)+T(i+1,k+1)+(dx^2/(alfa*dt)-2
*(h1*dx/ko)-4)*T(i,k+1));


       IT(i+1,k)=0;

   end
                                   %Bottom left corner of cut path

IT(0.5*s,k+1)=Fo*(2*h1*dx*Text/ko+2*T(0.5*s,k+2)+2*T(0.5*s-1,k+1)+(dx^2/(alfa*dt
)-2*(h1*dx/ko)-4)*T(0.5*s,k+1));


   %CORNER POINTS
   %Left top corner

IT(1,1)=Fo*(2*h*dx*Text/ko+2*T(2,1)+2*T(1,2)+(dx^2/(alfa*dt)-2*(h*dx/ko)-4)*T(1,
1));


 %Right top corner

IT(1,s)=Fo*(2*h*dx*Text/ko+2*T(1,s-1)+2*T(2,s)+(dx^2/(alfa*dt)-2*(h*dx/ko)-4)*T(
1,s));


 %Left bottom corner (Moving boundary)

IT(0.5*s-w1,1)=Fo*(2*h*dx*Text/ko+2*T(0.5*s-w1-1,1)+2*T(0.5*s-w1,2)+(dx^2/(alfa*
dt)-2*(h*dx/ko)-4)*T(0.5*s-w1,1));


 %Right bottom corner

IT(0.5*s,s)=Fo*(2*h*dx*Text/ko+2*T(0.5*s-1,s)+2*T(0.5*s,s-1)+(dx^2/(alfa*dt)-2*(
h*dx/ko)-4)*T(0.5*s,s));


  T=IT;
end
for m=1:22
    w(m,k+1)=T(0.5*s-w1-1+m,k+2);
end
end
```

Appendix D – Temperatures distributions 3-D presentation

D.1 Steel without cooling view 1

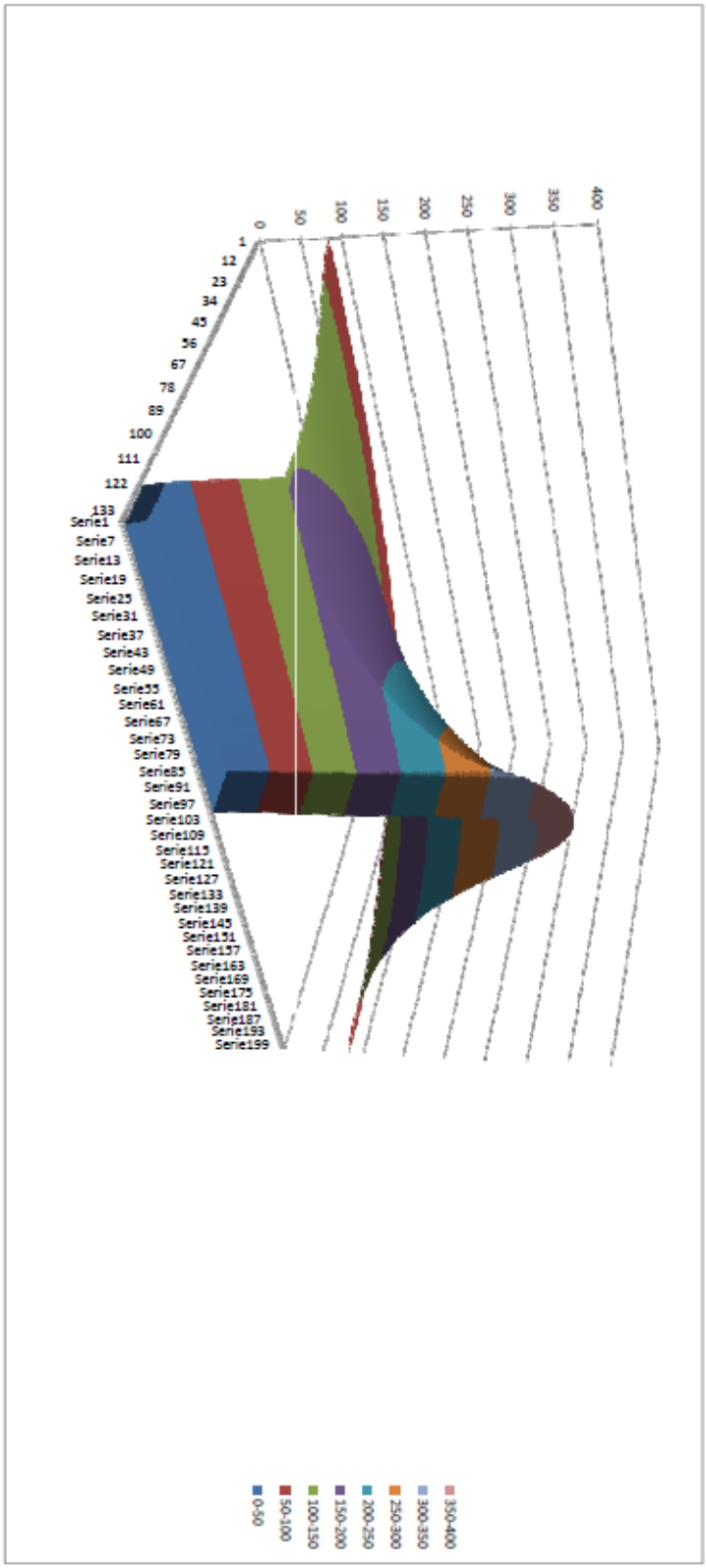

D.2 Steel without cooling view 2

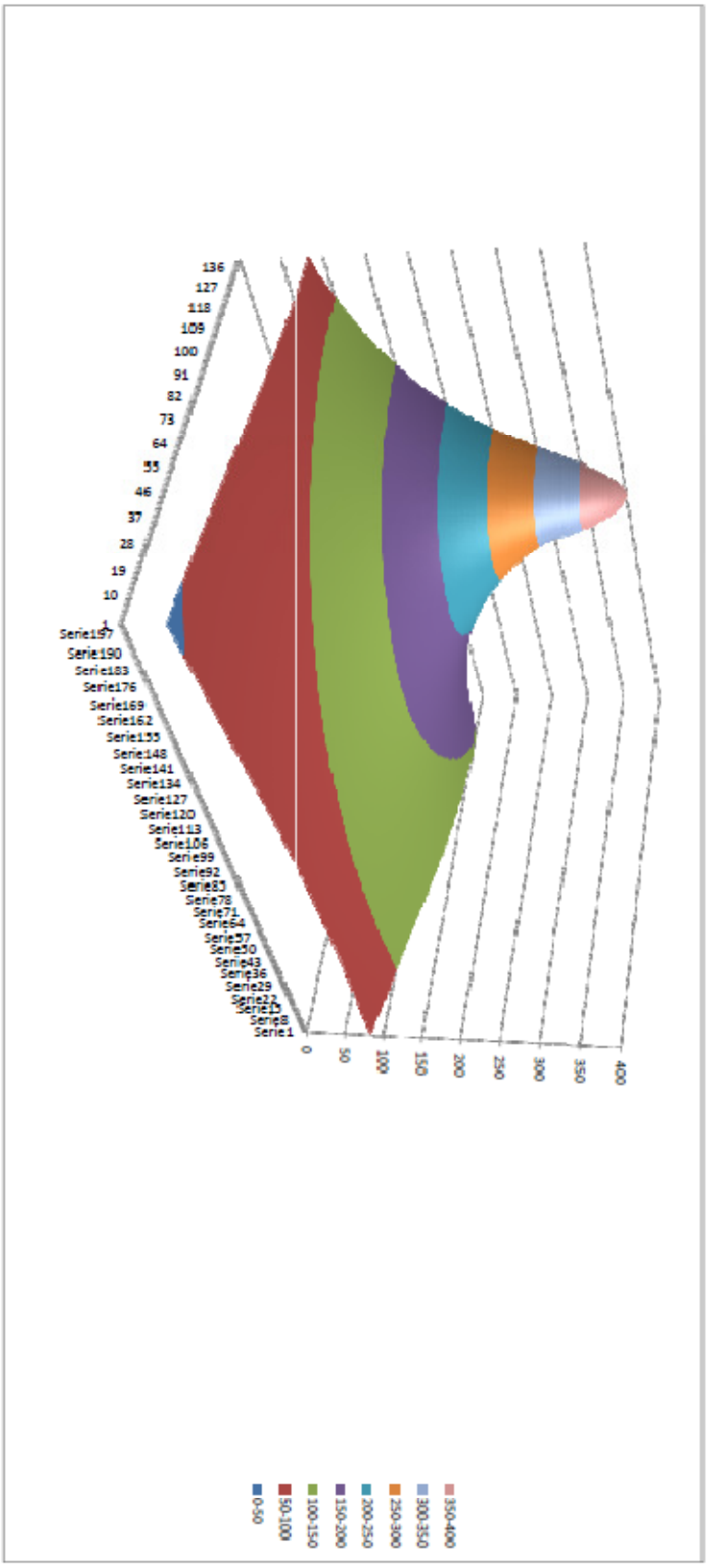

D.3 Steel with cooling view 1

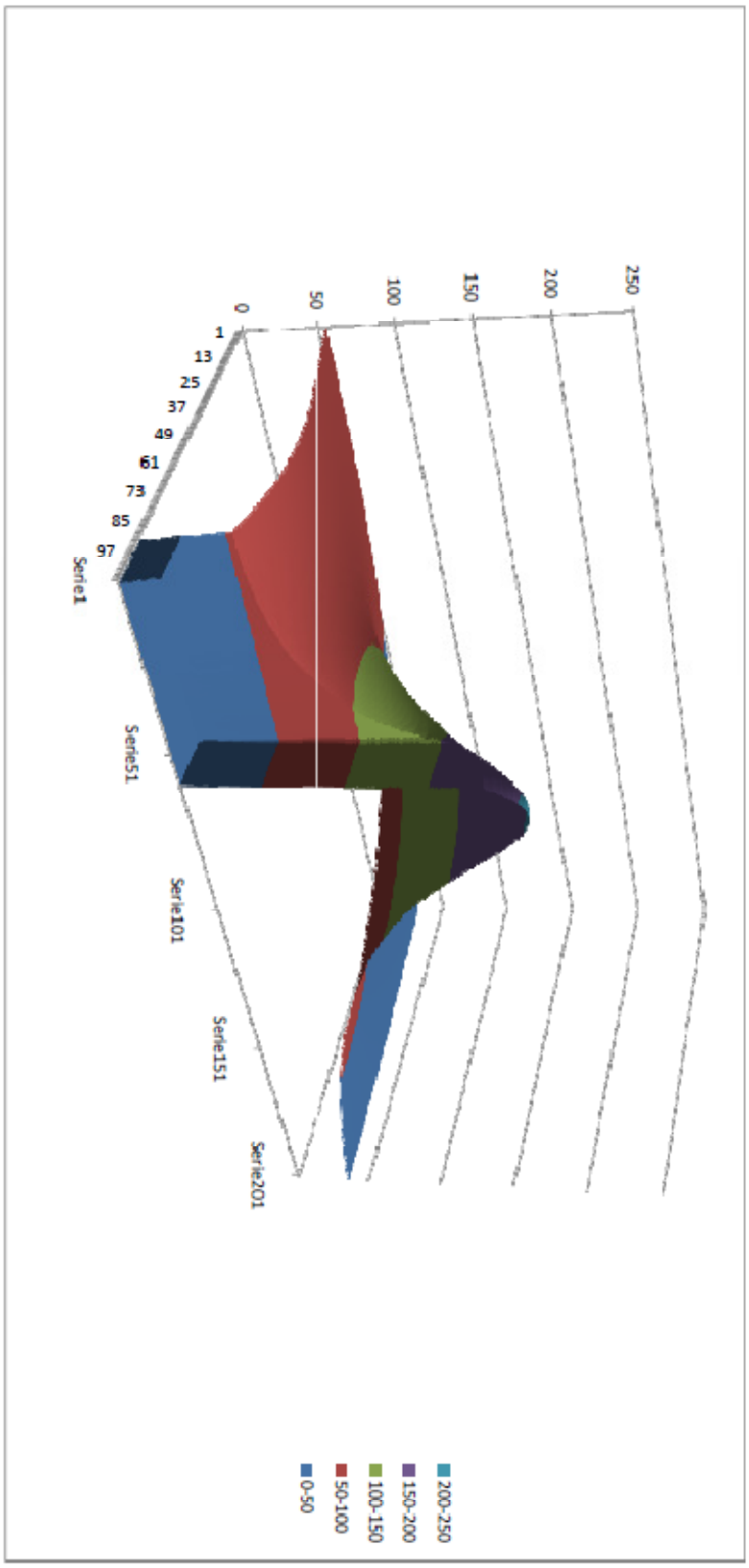

D.4 Steel with cooling view 2

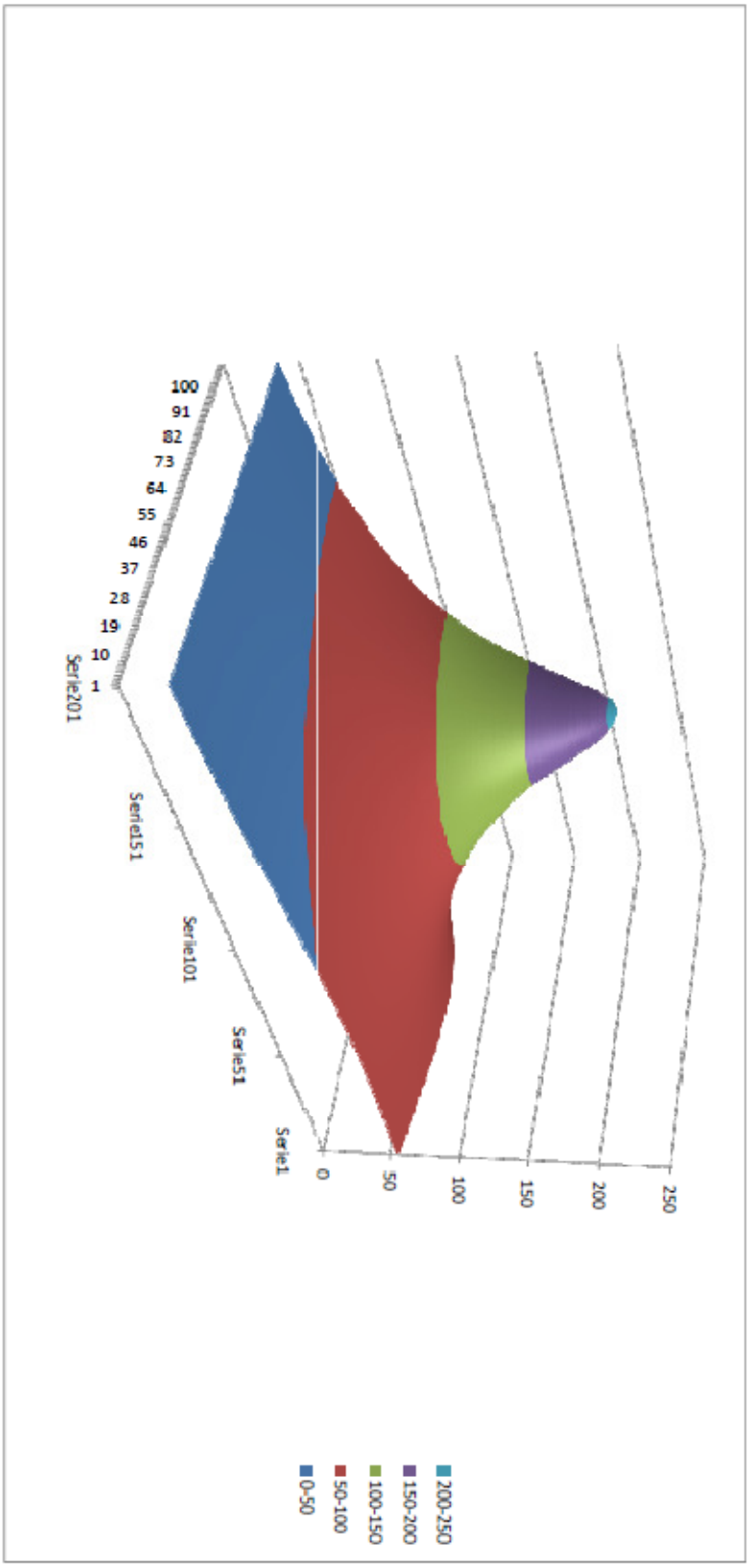

D.5 Stainless steel without cooling view 1

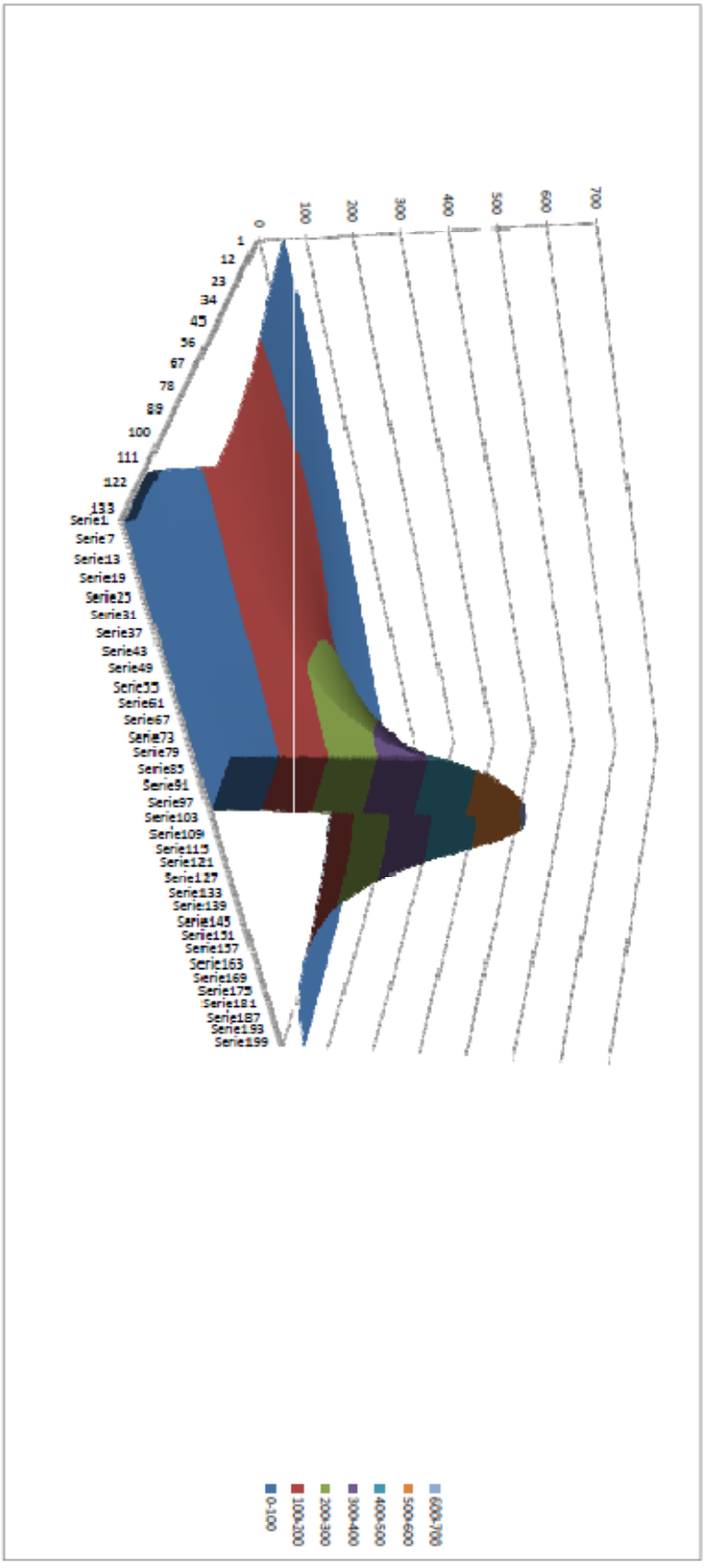

D.6 Stainless steel without cooling view 2

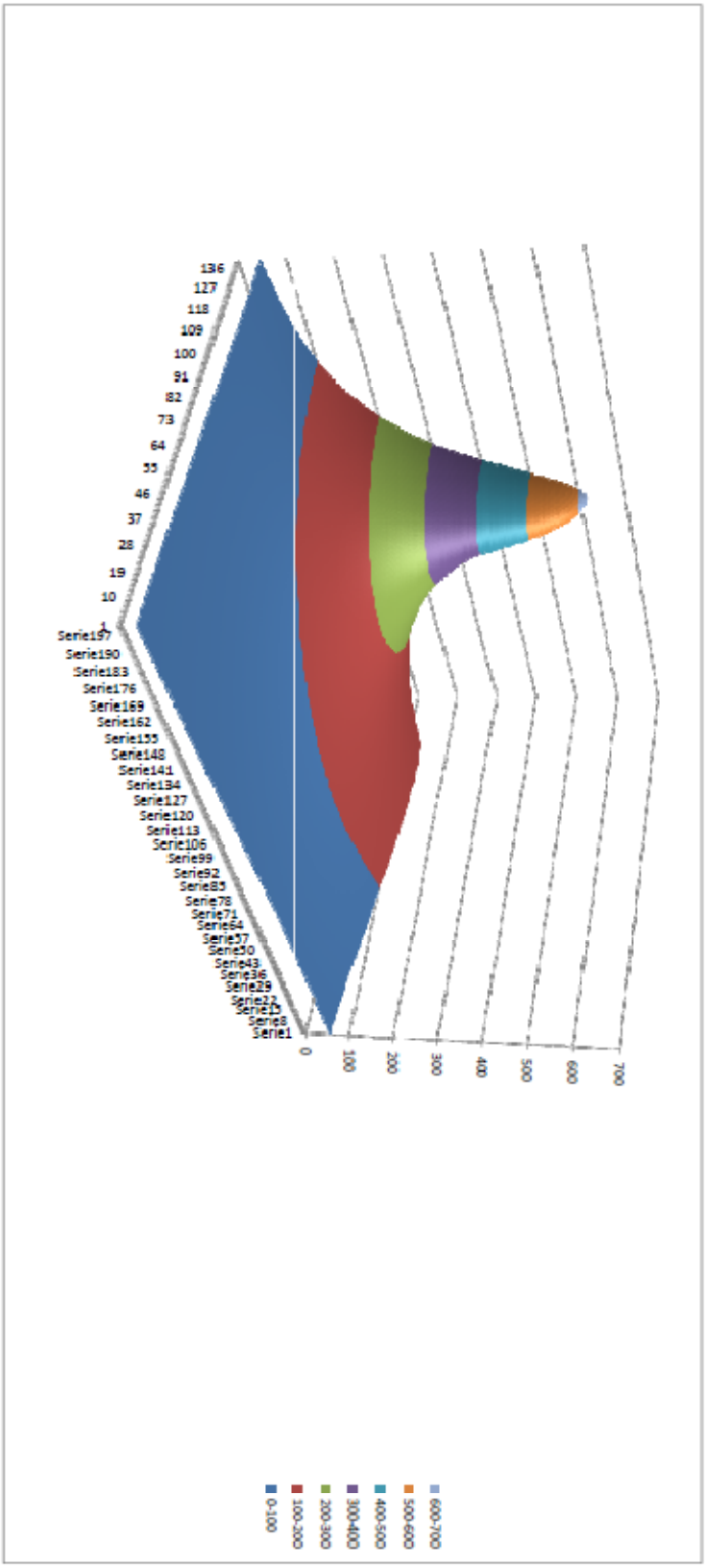

D.7 Stainless steel with cooling view 1

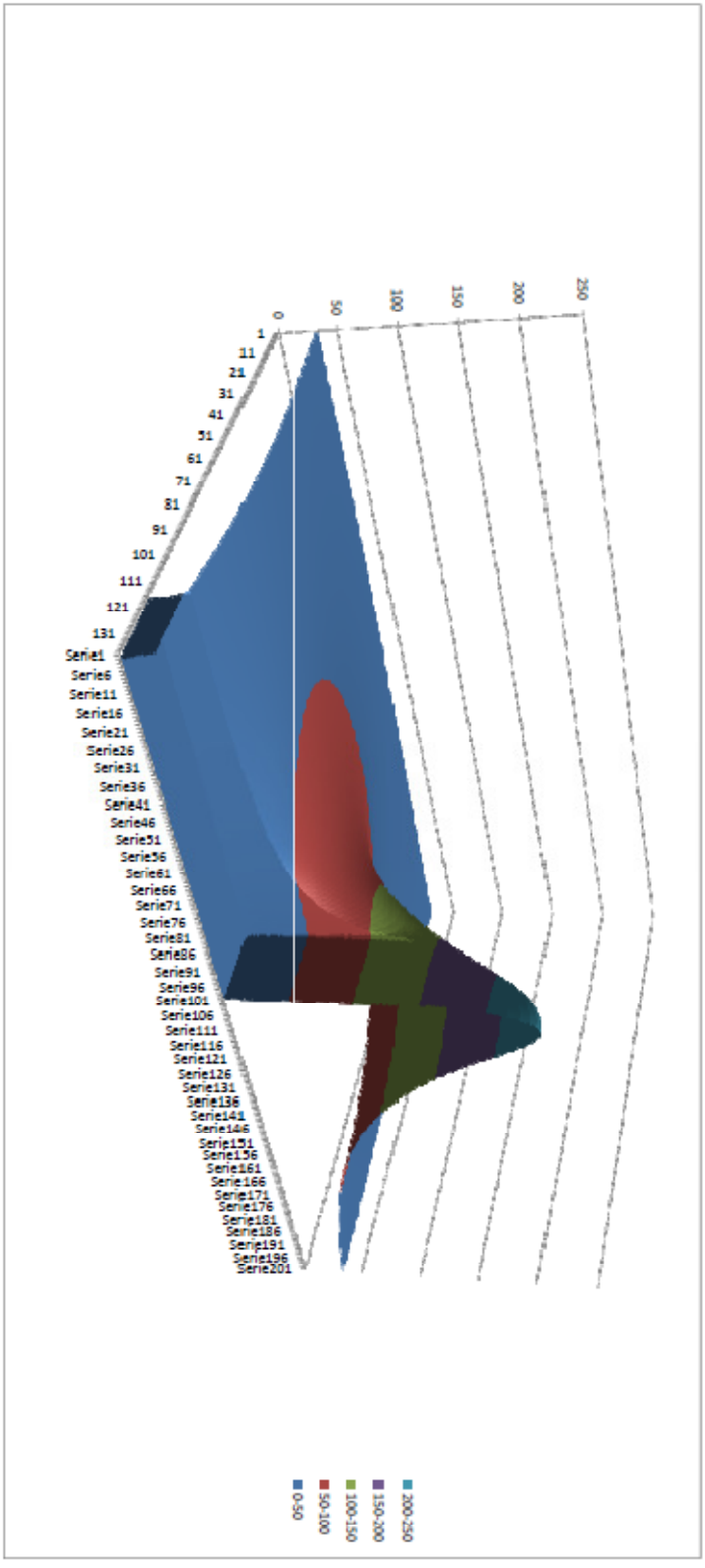

D.8 Stainless steel with cooling view 2

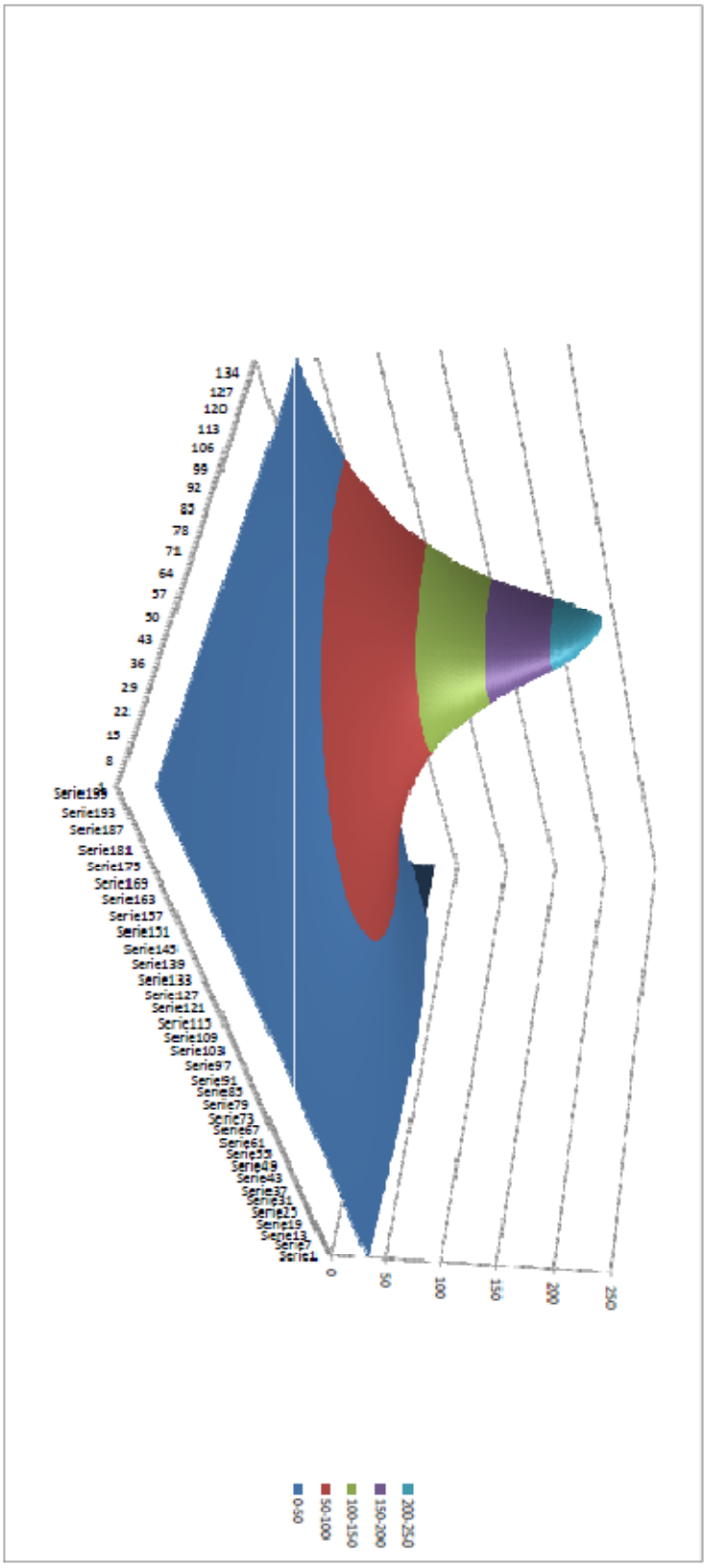

D.9 Titanium without cooling view 1

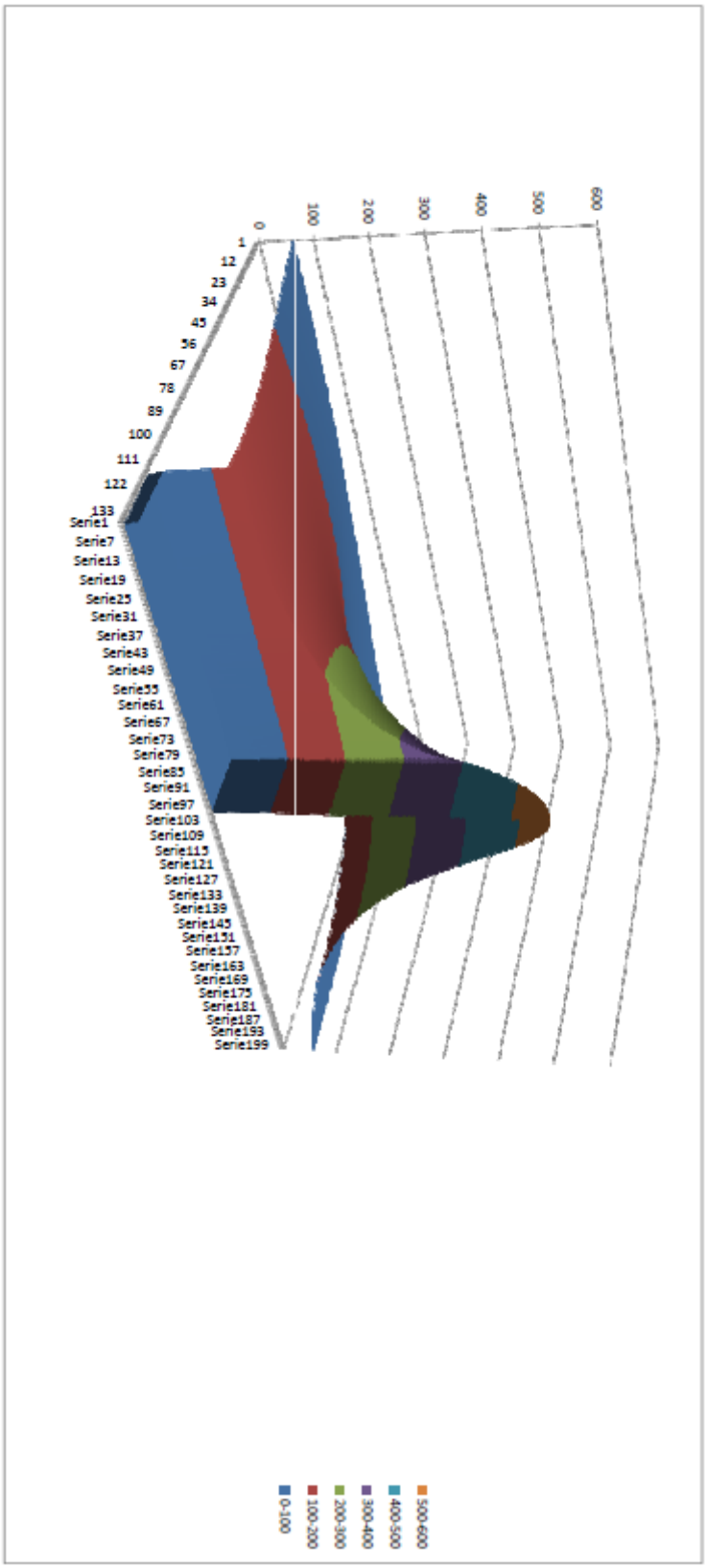

D.10 Titanium without cooling view 2

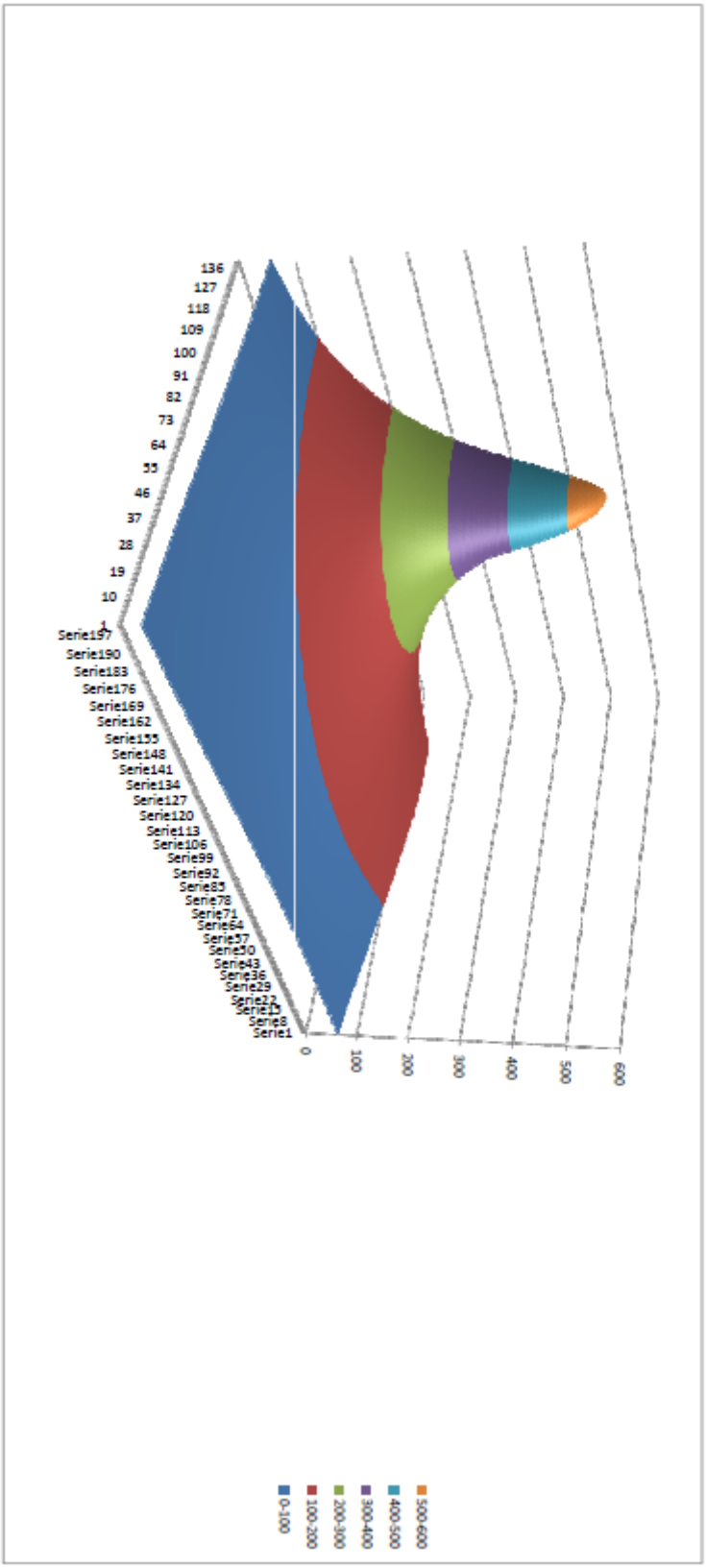

D.11 Titanium with cooling view 1

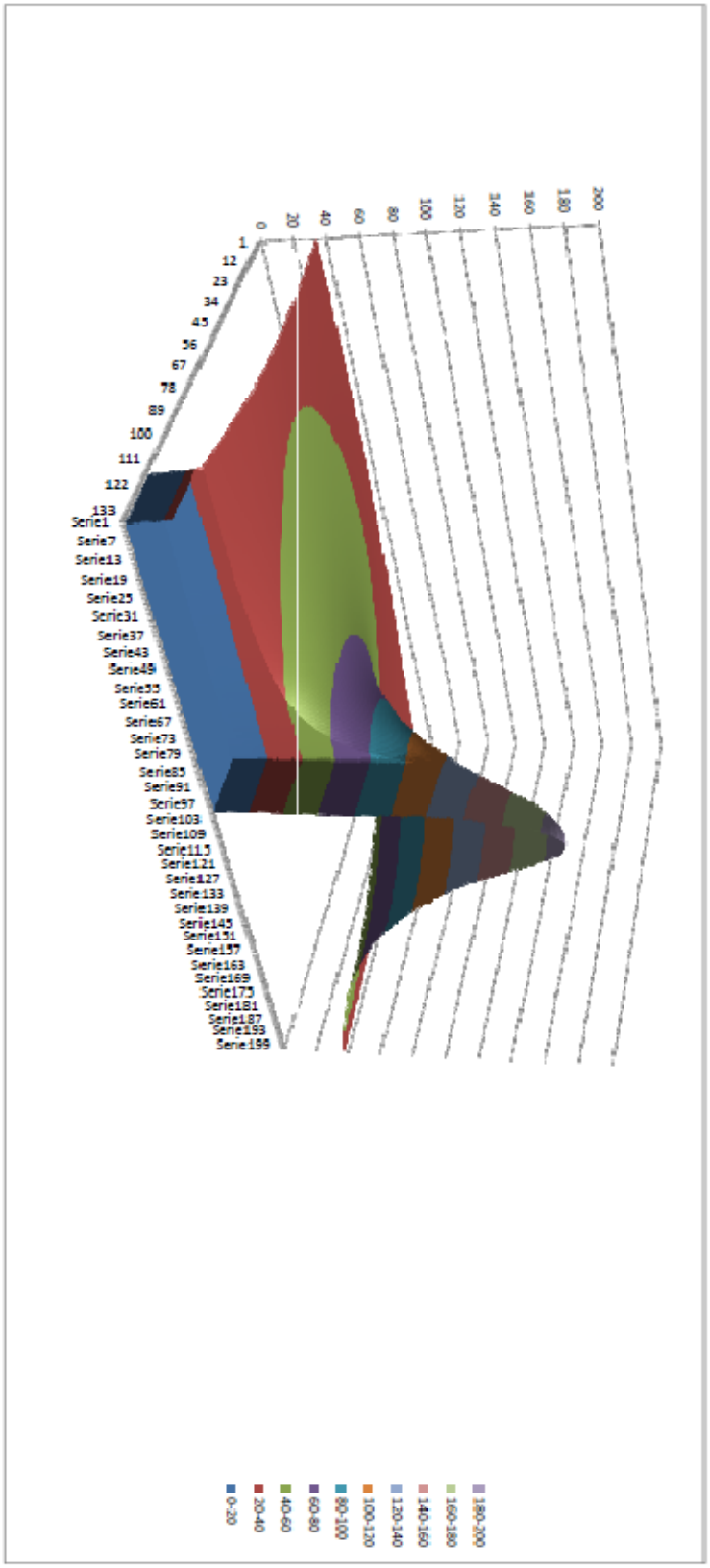

D.12 Titanium with cooling view 2

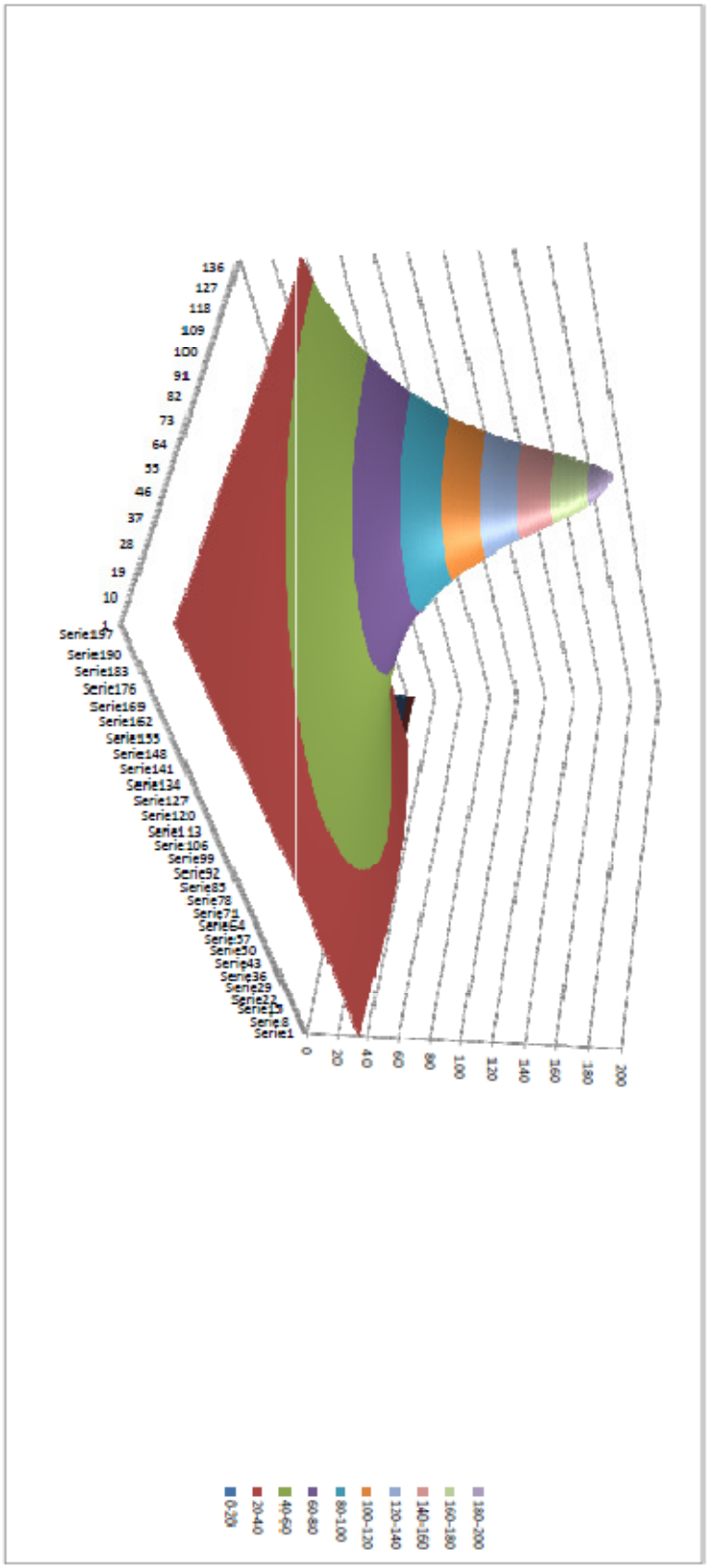

Appendix E – Synopsis report of 16.02.2011

Synopsis report - "Utilization of synthetic diamonds for cutting purposes in explosive environments"

Definitions

Hazardous zone – Area where the presence of hydrocarbons is possible
DW – Diamond Wire

Problem definition

When performing modifications, such as cutting, on process equipment or structural members in a hazardous zone it is usual to take extraordinary measures to reduce the potential for an accident. An accident is here referred to as a situation of fire or explosion caused by ignition of hydrocarbons by sparks from the modification activities.

For a hydrocarbon processing plant, offshore or onshore, the possibility of presence of hydrocarbons in the atmosphere will be possible as long as the plant is in operation. Therefore a process plant will be characterized as a hazardous zone when it's operating. This is due to the high possibility for leaks in valves, flanges and other connections.

As a result of a process plant being a hazardous zone there is a strict control of all sources of ignition. This means that all activities that will generate a source of ignition will be assessed individually to ensure that correct measures are being implemented to compensate for the addition of ignition source.

These extraordinary measures are usually rather expensive. Reducing the risk of a potential accident can be obtained by either remove the presence of hydrocarbons or remove the source of ignition.

Cutting activities are conventionally characterized as "Hot Work", which means it generates a source of ignition. The main objective of this thesis is to document that cutting by DW will not produce high energy sparks, and hence document that cutting by DW can be characterized as "Cold Work".

Objectives

The main object of the thesis is to establish a relationship between the energy used by the cutting machine and the energy absorbed by the work piece, tool and chip. This energy balance will be used to analyze the parameters affecting the energy level in the chip. Results from this analysis will be compared to current standards.

To obtain the main objective there will be several sub objectives, these are:

- Define a spark, in terms of energy level and origin
- Define explosive environments and sources of ignition
- Define the characteristics of current standards
- Define the forces in a regular cut and the parameters affecting the forces
- Establish analytical tools for energy levels in chip, work piece and cutting tool

Method

To obtain the above mentioned objectives there will be performed an extensive literature research. There has been performed a lot of research on the field of cutting and grinding, however this research is mainly focused on the mechanics of the operation, tool life and methods of optimizing. Also, published research is mainly concerned with cutting methods like lathe, grinding and milling. Hence the field of spark discharge from cutting with DW is a rather unexplored field.

The thesis will be a combination of studies from three different areas, general cut theory, cutting technology and the characteristics of an explosive environment.

First off the operation of cutting will be assessed to determine the forces acting in the cut. The study of cutting will also assess the energy consumption in a cutting process, the effects from different materials and shapes of the work piece.

Cutting technology will be assessed in terms of studying the different techniques available and their characteristics. Since the available literature is mostly concerned with other techniques than DW it's of high importance to establish analytical tools for DW. These tools will be derived from the published research on the other techniques. With the proper tools established the energy consumption to the cut will be analyzed. The focus of this analysis will be a thermal analysis of the cutting tool, the work piece and the chips. This analysis will be performed both to DW cutting and cutting by grinding. The reason for this comparison is that cutting by grinding is well known for discharging high energy sparks. The results from the analysis should conclude with the parameters affecting the energy level in the chip, such as cutting speed, cutting depth, work piece material etc.

The latter part of the thesis will be focused on explosive environments. The characteristics of such an environment will be assessed to define an ignition source. This is of importance to document that DW cutting can be characterized as Cold Work. Under this part there will also be a study of the current standards regarding ignition control in explosive environments.

Appendix F – Preliminary study for experiment

Determining the surface temperatures in a Diamond Abrasive wire cutting process

Objectives

Published research on the field of abrasive cutting is mainly concerned with surface grinding as seen at the end of production lines for industries with high production rates. One example for these industries is the automotive industry, where the number of parts for each product is high as well as the total number of products also are of significant order. As any enterprise, its goal is to maintain high quality at a lowest possible cost. Hence the background for their research is to determine the optimum grinding parameters to obtain proper surface roughness, minimum tool wear, no surface burns at the same time as obtaining a high removal rate.

Diamond abrasive wire cutting processes can be related to conventional grinding processes since the mechanics of the removal process are quite similar and the tool, abrasive grains, is more or less identical. Apart from this the similarities between the wire technology and the conventional disc technology are few. The major difference is the geometry of the tool holder, e.g. the geometrical difference between a wire and a disc. All the differences and their assumed effect on the parameters will be discussed later.

As mentioned earlier, there is at this time only empirical relationships for the grinding forces and grinding energy. Thus an application of the proposed relationship seems effortless since they are highly dependent on both work piece properties and tool properties. This combined with the geometry difference implies an uncertainty magnitude so vast that any produced results would be regarded as unusable.

For estimation of the surface temperatures in conventional grinding the technique of moving heat source has been applied. This method is dependent on the heat flux and the geometry of the cut. Heat flux is then highly dependent on the energy consumed in the cut. It's assumed that this technique also can be applied to wire technology.

The main objective is to determine the surface temperature during cutting. This will be obtained by performing a series of cuts while monitoring the temperatures with a thermographical camera and monitoring the energy consumed by the machine.

The details to be tested are the following,

- Trends that imply a different temperature development for different materials and its relation to the different alloys
- The effects of different tool and tool holders (diamond density, size)
- The trends in energy consumption for different materials regarding toughness and yield strength
- The effect of a cooling cutting fluid, e.g. water

The experimental setup

Equipment:

- Wire cutting machine
- HPU
- Diamond abrasive wire (x number of different wires)
- Thermographical camera
- Power analyzer
- Conventional laptop computer w/sufficient software
- A range of test specimen

Each cut will be performed four times at the identical set up for calibration purposes. A proper plan for the entire experiment will be presented.

Calibrating the thermographical camera

All objects which contain a temperature over absolute zero will radiate heat. This radiation will have a longer wave length and lower frequency than normal visible light. An infrared camera will detect this radiation and process it, thus presenting a thermal image based on the electromagnetic radiation.

The relationship between the radiation and the surface temperature is dependent on the surface ability to emit energy, in terms of radiation. This parameter is referred to as the surface emissivity and is the ratio between the energy radiation from the relevant surface and the energy radiation from a perfect blackbody at the same temperature.

Blackbody is an ideal body which absorbs all electromagnetic radiation. Since all electromagnetic light is absorbed, the visible light will not be reflected and hence the object will appear black. A real blackbody, as described here, does not exist in nature. Graphite, with an emissivity higher than 0.95 may be regarded as a blackbody.

REFERENCEWIKIPEDIA, BLACKBODY, RADIATION AND EMISSIVITY

Determination of emissivity

The main experiment is to determine the surface temperature in cutting with diamond wire, in this experiment there will be several materials interacting. These are:

- Abrasive Wire
- Test specimen steel
- Test specimen concrete

All of these materials have different emissivity which needs to be determined experimentally to able to calculate the correct surface temperatures at a later stage.

The experimental set up for this emissivity experiment is:

- Kettle with water
- Cooking plate
- Thermographical camera
- Test specimen

By heating the water to the boiling point a thermographical photo was taken showing the boiling water. Since this was performed under normal conditions the water would boil at 100 degrees Celsius. By adjusting the emissivity factor for the camera a temperature of 100 degrees Celsius was obtained with an emissivity factor of 0.93. By searching the internet a couple of sources stated the emissivity factor of water would be 0.94. It is assumed the pollution in the water could have an influence on the result.

The test specimen used in this emissivity experiment was rusted steel (QUALITY). The surface on one side of the specimen was polished clean with an angle grinder, while the other side was kept rusted. By using pincers the test specimen was lowered into the boiling water, the pincers would rest on two metal pieces at the bottom of the kettle to prohibit contact between the kettle bottom and the test specimen.

After being submerged in boiling water for approximately 15 minutes the test specimen was taken out of the water and photographed with a thermographical camera. By using the same method as mentioned above for water, the following results were obtained:

Specimen	Obtained temperature, Celsius	Emissivity
Polished steel	**100**	**0,27**
Rusty steel	**100**	**0,79**
Diamond wire coating	**100**	**0,61**
Diamond wire grains	**100**	**0,43**
Water	**100**	**0,93**

The results above agree whit the emissivity's listed in the user manual for the termographical camera for polished steel and oxidized steel. The rest of the materials are not listed in the user manual and hence is not available for comparison. The www.engineeringtoolbox.com has also been consulted with the same results as for the user manual.

Measurement of consumed energy

There are several ways to measure the amount of energy converted during a process. For this specific experiment it's of interest to measure the energy which has been consumed during a cutting process. The energy is being converted in multiple phases first form electrical energy to hydraulic energy, then from hydraulic energy to cutting energy, then from cutting energy to heat energy.

To obtain the quantities going into the processes it's possible to measure the effect at either the electrical stage or the hydraulic stage and integrate these amounts over the time domain. The equipment for these techniques is quite different and the complexity of the set up is quite different as well.

Measurement of consumed energy by power analyzer

By utilization of a power analyzer it's possible to read the consumed effect by the electrical system and logging this data against the time domain in a computer. The logging interval is at 10 s minimum, but this should be sufficient since the load of a cutting process is more or less constant. This would however create some uncertainties in the initial conditions, but a 10 second interval could easily be neglected for a longer operation. If the operation is rather short an interpolation would correct for

some of the lost data. However, sufficient correction with respect to the logging intervals should be investigated.

The key benefit from this technique is its simple installation, as it is installed on the main power lines to the hydraulic power source, and the logging directly to a computer feature. The disadvantage is that the uncertainty elements in the hydraulic system are poorly identified.

Measurement of consumed energy by pressure drop

The analytical relationship for the power output for a hydraulic motor is the product of flowrate, pressure drop over the motor and the motors degree of efficiency. The hydraulic power source operates with both constant flow and pressure in four different stages. This then means that it's possible to measure the output effect by applying a pressure manometer at the return side of the motor and calculate the effect.

This method then eliminates the sources of uncertainty in the hydraulic power source to some degree. There will still be some uncertainties in the values for pressure and flow rate at the intake side of the motor, this being a result of pressure drop caused by inline items such as bends and fitting, any inline equipment and length of tubing and hoses.

Since the hydraulic power source consists of 4 hydraulic pumps this technique is dependent on four manometer readings and accompanying logging. There is also the possibility to apply the manometers at drive motor for the cutting machine and at the tension actuator, this would reduce the measuring points to two individual readings. However, the latter method would also imply additional measuring of the actuator's parameters.

Estimation of consumed energy by measuring pressure drop has its key benefits in accuracy. The disadvantage is the need for more instrumentation since there will be more sampling points.

The method best suited for this experiment would be by measuring the electrical power. This method will have a rather easy setup, and provide proper results at a conditional basis. These conditions are:

- The degree of efficiency for the hydraulic power source needs to be addressed. This could be done by measuring the pressure drop over the hydraulic motor in the cutting machine with no loading on the wire. The test should be performed over the different cutting speeds available and compared against the logged data from the power analyzer. This will provide an estimate of the degree of efficiency at low loading.
- Due to the rather large sampling rate, the experiment should be designed for operations that would last over a large period of time compared to the sampling period.
- The degree of efficiency for the hydraulic power source at high loading could be estimated by measuring the output whit a custom made break or generator of some kind. However, it is assumed that this particular hydraulic power source follows the same evolution as other hydraulic power units where the rate of efficiency increases, to some extent, by increasing loading. This would imply that the estimated degree of efficiency from low loading would represent a lower limit for the degree of efficiency.

Estimation of material removal rate

The material removal rate could easily be estimated by calculating the volume that will be removed by the wire and dividing this quantity by the time spent cutting. However, the accuracy of this measurement is not known since the probability for the wire to obtain a trajectory with millimeter precision is assumed to be quite low.

To obtain a second reference the work piece would be weighed before the cut and after the cut. By dividing this observation by the work piece density the removed volume is obtained. When dividing this quantity by the time spent cutting the material removal rate is obtained.

For the latter method there will be some uncertainties both in the weight and in the density. The sensitivities to these sources of error will be investigated and reduced.

The experiment

By logging the results for consumed energy, material removal rate and registered surface temperature the relation between the material removal rate, consumed energy and surface temperatures can be investigated.